GEOLOGICAL SURVEY OF CANADA
OPEN FILE 6583

Advanced numerical simulation of CO_2 hydrate formation in geological reservoirs by injection of CO_2 gas

M. Uddin and D. Coombe

2011

Natural Resources
Canada

Ressources naturelles
Canada

Canada

GEOLOGICAL SURVEY OF CANADA
OPEN FILE 6583

Advanced numerical simulation of CO_2 hydrate formation in geological reservoirs by injection of CO_2 gas

M. Uddin[1] and D. Coombe[2]

[1] Alberta Innovates-Technology Futures (formerly Alberta Research Council Inc.), 250 Karl Clark Road, Edmonton, AB, T6N 1E4
[2] Computer Modeling Group Ltd., 6223 Lakeview Dr SW, Calgary, AB, T3E 5S9

2011

Recommended citation:
Uddin, M. and Coombe, D., 2011. Advanced numerical simulation of CO_2 hydrate formation in geological reservoirs by injection of CO_2 gas; Geological Survey of Canada, Open File 6583, 95 p. doi:10.4095/288725

Publications in this series have not been edited; they are released as submitted by the author.

FOREWORD

This report contained herein was prepared for the Geological Survey of Canada (GSC), a branch of Natural Resources Canada (NRCan) by Dr. Mafiz Uddin of the Alberta Research Council (ARC), which is currently known as Alberta Innovates – Technology Futures. The research presented in the report was conducted under a formal Letter of Agreement between NRCan's Office of Energy Research and Development (OERD) and ARC, covering fiscal years 2005-06 and 2006-07. Primary funding for the study was provided by Canada's Climate Change Action Plan 2000 (CCAP 2000), with limited in-kind support provided by both the GSC and ARC. The ARC report is presented in its entirety, as delivered by ARC to GSC, without changes or editorial comment by the GSC Scientific Authority.

Scientific Authority: J. F. Wright
                       Geological Survey of Canada
                       Natural Resources Canada
                       9860 West Saanich Rd.
                       Sidney BC Canada
                       V8L 4B2

Email: *Fred.Wright@NRCan.gc.ca*

ADVANCED NUMERICAL SIMULATION OF CO$_2$ HYDRATE FORMATION IN GEOLOGICAL RESERVOIRS BY INJECTION OF CO$_2$ GAS

Mafiz Uddin
Dennis Coombe (Computer Modelling Group)

REPORT PREPARED FOR
GEOLOGICAL SURVEY OF CANADA
NATURAL RESOURCE OF CANADA
BY ALBERTA RESEARCH COUNCIL INC.

HEAVY OIL AND OIL SANDS
250 KARL CLARK ROAD
EDMONTON, ALBERTA   T6N 1E4
CANADA

CONFIDENTIAL

May, 2006

DISCLAIMER

This report was prepared as an account of work conducted at the Alberta Research Council Inc. (ARC) on behalf of the Geological Survey of Canada (GSC). All reasonable efforts were made to ensure that the work conforms to accepted scientific, engineering and environmental practices, but ARC makes no other representation and gives no other warranty with respect to the reliability, accuracy, validity or fitness of the information, analysis and conclusions contained in this Report. Any and all implied or statutory warranties of merchantability or fitness for any purpose are expressly excluded. Reference herein to any specified commercial product, process or service by trade-name trademark, manufacturer or otherwise does not constitute or imply an endorsement or recommendation by ARC.

ACKNOWLEDGEMENT

EXECUTIVE SUMMARY

This study numerically investigates a possible sequestration of CO_2 as stable gas hydrate in reservoir geological formations. ARC's unified gas hydrate model coupled with a thermal reservoir simulator (CMG STARS) was applied to simulate CO_2 hydrate formation in four generic reservoir geological formations and Mallik natural gas hydrate formation. The four generic reservoirs can be described as, **Reservoir I: similar to Mallik silt with porosity 0.30 and permeability 100 mD, Reservoir II: similar to Mallik sand with porosity 0.35 and permeability 1000 mD, Reservoir III: conventional sandstone with porosity 0.25 and permeability 20 mD, and Reservoir IV: similar to tight gas formation with porosity 0.25 and permeability 10 mD.** The Mallik gas hydrate bearing formation can be described as several layers of variable thickness with permeability varied from 1 mD to 1000 mD.

The report describes numerical methodology, model input data, and reservoir simulation results, including an enhancement to model the effects of ice formation and decay. The numerical investigation showed that the gas hydrate model effectively captured the spatial and temporal dynamics of CO_2 hydrate formation in geological reservoirs by injection of CO_2 gas. Practical limitations to CO_2 hydrate formation by gas injection were identified and potential improvements to the process were suggested.

TABLE OF CONTENTS

Advanced Numerical Simulation of CO_2 Hydrate Formation
In Geological Reservoirs by Injection of CO_2 Gas   [iv]
May, 2006

ALBERTA
RESEARCH
COUNCIL

LIST OF TABLES

LIST OF FIGURES

Advanced Numerical Simulation of CO_2 Hydrate Formation
In Geological Reservoirs by Injection of CO_2 Gas   [vi]
May, 2006

ALBERTA
RESEARCH
COUNCIL

Advanced Numerical Simulation of CO_2 Hydrate Formation
In Geological Reservoirs by Injection of CO_2 Gas   [vii]
May, 2006

ALBERTA
RESEARCH
COUNCIL

Advanced Numerical Simulation of CO₂ Hydrate Formation
In Geological Reservoirs by Injection of CO₂ Gas   [ix]
May, 2006

ALBERTA
RESEARCH
COUNCIL

ADVANCED NUMERICAL SIMULATION OF CO_2 HYDRATE FORMATION IN GEOLOGICAL RESERVOIRS BY INJECTION OF CO_2 GAS

MAFIZ UDDIN AND DENNIS COOMBE

1.0 INTRODUCTION

Background - Gas hydrates are ice-like solids composed of gas molecules and water. Gas hydrates form when relatively small guest molecules (such as carbon dioxide *(CO_2)* and methane *(CH_4)*) come into contact with water under low-temperature, high-pressure conditions, both above and below the freezing point of water. Depending on the types of gas present, several crystal structures of gas hydrate are known to occur (such as Structure I, Structure II and Structure H), each with different physical and stability properties (Sloan, 1998; Sloan, 2003).

In natural environments, the pressure-temperature conditions favouring gas hydrate formation could occur offshore in shallow depths below the ocean floor and onshore beneath the permafrost. Areas offshore of Canada's west coast and a number of onshore Arctic locations are know to contain some of the most concentrated CH_4 hydrate deposits in the world. One large CH_4 hydrate deposit is located in the Mallik field, Mackenzie Delta on the coast of the Beaufort Sea, in Canada's Northwest Territories. In addition, geological reservoirs with favorable pressure - temperature conditions for CO_2 hydrate formation exist offshore of Canada's east and west coasts, widespread in numerous arctic settings, and several spots of the deeper Great Lakes geological settings. In these geological formations, CO_2 hydrate formation can be induced by injecting CO_2 gas into the formation water.

Geologic Sequestration - Possible sequestration of CO_2 as a stable gas hydrate in geological formations affords a huge potential for offsetting industrial-sourced green house gas *(GHG)* emissions to the atmosphere, and thus could be a significant factor for mitigating future climate change. Large scale injection of CO_2 into depleted natural gas hydrate reservoirs and into deep saline aquifers is one of the most promising methods of geological storage of CO_2. The greatest operational challenge to the formation of CO_2 hydrate by gas injection into natural geologic reservoirs is the maintenance of the bulk contact between the gaseous and aqueous phases, assuming that temperature and pressure stability conditions for continued hydrate formation prevail.

Before implementation of GHG geological storage, a series of questions need to be addressed, the most important of which relate to the short- and long term fate of the injected CO_2. In this aspect, fundamental research and development is needed to understand the physics and chemistry of CO_2 hydrate formation in porous media. A numerical study of CO_2 injection operations under actual field conditions provides the opportunity to learn about the fate of the injected gases, and represents a unique opportunity to investigate the feasibility of CO_2 geological storage.

Key Variables - In porous media, several variables and processes play a vital role in gas hydrate stability in geological formations. The key variables are reservoir properties (geological formation, permeability and porosity), reservoir conditions (saturation and pore water chemistry) and well operating constraints (well head pressure and fluid production-injection rates). Several other processes such as well bore, overburden and underburden heat flux significantly affect the spatial and temporal dynamics of gas hydrate distribution. Under the Mallik gas hydrate research program, numerous laboratory, field and numerical studies have been conducted on the kinetics, stability, dissociation and formation processes (as reviewed by Dallimore and Collett, 2005; Dallimore, *et al.,* 2005). Several studies published laboratory gas hydrate data such as hydrate stability, kinetics and thermal conductivity (Adisasmito, *et al.,* 1991; Hong and Pooladi-Darvish, 2003; Kim *et al.,* 1987; Malegaonkar *et al.,* 1997; Reid *et al.,* 1977[2]; Seo *et al.,* 2002; Sweigert *et al.,* 1946; Wright *et el.,* 2005a, 2005b).

In the CO_2 hydrate project, one of the main challenges is how to incorporate and predict the role of spatial variation of the reservoir properties (permeability and porosity) on CO_2 hydrate formation. Well log data in the Mallik gas hydrate research project showed that the properties like permeability may vary by three or more orders of magnitude in a reservoir. However, the variation of these properties is not completely disordered in space; different sediment types exhibit different characteristics but with a degree of order within each sediment. These data may show some structure which may be described as layers with recognizable but variable thickness.

For any stochastically random distribution of permeability, it is possible to calculate some spatial distribution parameters such as autocorrelation and autocovariance. Then with the aid of geostatistics, a relationship can be established between the magnitude and spatial correlation of permeability heterogeneity and the time dependent behaviour of gas hydrate saturation in the geological reservoir. In this aspect, the concept of geostatistics in reservoir description to describe a heterogeneous medium has been applied successfully in the field of contaminant hydrogeology. In the literature, there are several schemes to assign random permeability fields in numerical models (Schwartz, 1977; Mantoglu and Wilson, 1982). Each method has its own advantages and disadvantages. More recently at ARC, a simple geostatistical program has been developed which is capable of generating permeability and porosity for numerical grid cells with predefined statistical properties (such as mean, variance and correlation length).

Numerical Study - Previously, ARC with the support of GSC performed a preliminary CO_2 hydrate simulation in a simplified geological reservoir considering different porosity and permeability (Uddin, M. 2004). The preliminary simulation investigated the spatial and temporal dynamics of reservoir pressure, temperature and gas hydrate saturation under varied initial and operating conditions. The numerical investigation described a unified gas hydrate kinetic model that when coupled with a multi-phase and multi-component thermal reservoir simulator could simulate the sequestration of CO_2 as stable gas hydrate in deep geological formations. More recently, significant improvements have been made to the original gas hydrate model to include the handling of boundary heat flux and ice formation and melting processes. The current version of the unified gas hydrate model is capable of handling mixed CO_2 and CH_4 hydrates dissociation and formation processes in three phases (such as aqueous, gaseous and solid) and unlimited components of a hydro-geochemical environment (Uddin, M. 2006).

Advanced Numerical Simulation of CO_2 Hydrate Formation
In Geological Reservoirs by Injection of CO_2 Gas   [2]
May, 2006

ALBERTA
RESEARCH
COUNCIL

Objective – The main objective of this project was to conduct a detailed gas hydrate simulations under different geologic settings. There are two primary simulation components of this study: (1) the formation of CO_2 hydrate in four generic geological reservoirs by injecting CO_2 gas and (2) the dissociation of Mallik CH_4 hydrate by depressurization and CO_2 hydrate formation in the CH_4 hydrate dissociated reservoir by injecting warm CO_2 gas.

The numerical simulations are evaluated to address several key issues such as reservoir properties (porosity and permeability), boundary heat flux, well operating constraints (injection and production) and ice modeling. In addition, some preliminary simulation results are included on possible short and long term roles of geochemical and geo-mechanical aspect in field scale modeling

Advanced Numerical Simulation of CO_2 Hydrate Formation
In Geological Reservoirs by Injection of CO_2 Gas   [3]
May, 2006

ALBERTA
RESEARCH
COUNCIL

2.0   HYDRATE MODELLING

2.1   MODEL STRUCTURE

A six component kinetic model was developed to simulate gas hydrate formation and decomposition in a geological reservoir. The components are water *(H₂O)* in the aqueous and gas phases, methane *(CH₄)* and carbon dioxide *(CO₂)* in the aqueous, gaseous and solid phases, CH₄ hydrate *(CH₄.nH₂O)*, CO₂ hydrate *(CO₂.nH₂O)* and ice in the solid phase. The kinetic model can be organized into a component-phase chart as in Table 1.

Gas hydrate formation and decomposition processes in this six component system can be represented by the following two kinetic reactions,

$$CH_4(g) + nH_2O(w) \leftrightarrow CH_4 \cdot nH_2O(s) \pm Heat$$
$$CO_2(g) + nH_2O(w) \leftrightarrow CO_2 \cdot nH_2O(s) \pm Heat$$
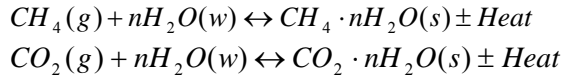
Gas hydrate formation is an exothermic process (releasing heat) whereas hydrate decomposition to gas and water is an endothermic process (taking heat). Two simple rate equations were proposed for the hydrate formation (forward kinetic) and the hydrate decomposition (backward kinetic) using gas hydrate stability curves (Uddin *et al.*, 2004). This approach is also used in the current report and generalized to handle the formation and decay of ice as well.

2.2   KINETICS AND THERMAL PROPERTIES

The gas hydrate equilibrium or stability data, component basic properties (for example, molecular mass, critical pressure and critical temperature), fluid enthalpies, thermal conductivity and rock-fluid properties are vitally important in modeling the dynamics of hydrate formation and decomposition in a geological reservoir. A number of published laboratory experimental data on the kinetics of CH₄ and CO₂ hydrates were compiled. The necessary input parameters were obtained from the literature data with some approximation (Tables 2 and 3). Figures 1 to 6 illustrate the relevant hydrate stability curves and the corresponding equilibrium partitioning behaviour.

Hydrate and Ice Stability

Gas hydrate equilibrium or stability in porous media primarily depends upon pressure, temperature, coexisting phase composition (such as gas composition, pore water chemistry), and sediment characteristics (for example, grain size, pore geometry, mineralogy).

Three-phase equilibrium *(Lᵥ-H-V)* data of water-rich liquid, hydrate and vapor of pure CH₄ and CO₂ components are taken from Adisasmito *et al.* (1991). Three-phase equilibrium *(Ice-H-V)*

Advanced Numerical Simulation of CO₂ Hydrate Formation
In Geological Reservoirs by Injection of CO₂ Gas   [4]
May, 2006

ALBERTA
RESEARCH
COUNCIL

data of ice, hydrate and vapor are taken from North *et al.* (1998) and Moridis *et al.* (2003). This data can be summarized in the form of average curves shown in Figures 1, 2, 4 and 5.

In the present gas hydrate model, the phase equilibrium is specified using phase equilibrium *K* values. This *K* values at a given pressure, *p*, and temperature, *T*, can be defined as, $K(p, T) = p_{(L-H-V)}/p$, where, $p_{(L-H-V)}$ is the experimentally measured three-phase (*Liquid-Hydrate-Vapor, L-H-V*) equilibrium data. *K* value tables as functions of pressure and temperature were obtained from the measured three-phase equilibrium data. This data can again be summarized in the form of average curves expressed by a three-parameter *K* value correlation as, $K = (k_1/p)exp(k_2/(T-k_3))$, where, k_1, k_2 and k_3 are the fitting parameters. The CH_4 and CO_2 hydrates equilibrium *K* values predicted from laboratory data and the best fitted curves are shown in Figures 3 and 6.

Component Properties

Basic component properties such as molecular mass, molar density, compressibility, critical pressure and critical temperature were obtained from the literature and reports. The necessary hydrate kinetic parameters are summarized in Tables 2 and 3. Several key issues can be emphasized about handling of the basic parameters in the present modeling approach: (1) the mass density determines the hydrostatic head of each phase, and may affect fluid phase distributions and pressure responses after stability curves are crossed, (2) critical pressure and temperature are required parameters, used in the calculations of gas density compressibility factor $Z (=nV/RT)$, and vaporization enthalpy.

The additional properties for ice were set as those for methane hydrates (mass density 919.7 kg/m^3; ice heat capacity 1600 J/kg-K) except that reaction enthalpy for ice formation was set to the ice latent heat of 333.6 kJ/kg (or 6009.8 J/gmole).

Fluid Enthalpies

In hydrate modeling, the following three quantities are required for each condensable component: (1) heat capacity in a liquid phase, (2) heat capacity in the gas phase and (3) enthalpy of vaporization as a function of temperature. However, only two of these three quantities are independent, since at any given temperature, enthalpy of vaporization is the difference between enthalpy in the liquid phase and enthalpy in the gas phase. In the simulator, three enthalpy datum options are available, allowing a choice of which two of the above three quantities to enter as data. In the present simulation, the four-parameter gas heat capacity correlation along with vaporization enthalpy was used. The gas phase heat capacity $c_{pg}(T)$ and vaporization enthalpy $h_{VAP}(T)$ for the condensable components were defined as, $c_{pg}(T) = c_1+c_2T+c_3T^2+c_4T^3$, and $h_{VAP}(T) = h_{VR}(T_{cr}-T)^{Ev}$, where, c_1, c_2, c_3 and c_4 are the heat capacity coefficients, *T* is temperature, T_{cr} is critical temperature, *Ev* is an exponent assumed to be 0.38 and h_{VR} is enthalpy coefficient. The heat capacity and enthalpy coefficients data were obtained from the CMG STARS manual.

Advanced Numerical Simulation of CO₂ Hydrate Formation
In Geological Reservoirs by Injection of CO₂ Gas   [5]
May, 2006

ALBERTA
RESEARCH
COUNCIL

Thermal Conductivity

For the calculation of heat flow between two blocks, the thermal conductivity is evaluated in both blocks and then mixed with a harmonic weighting scheme. This method is consistent for all cases of block size, flow directions and conductivity values. Wright *et al. (*2005b) estimated total thermal conductivity of 2.7 *W/mK* for the Mallik hydrate bearing formation of porosity of 0.35, hydrate saturation of 0.80 and water saturation of 0.20. The effect of heat transfer was investigated by using three rock thermal conductivities of 1.5 *W/mK*, 3.92 *W/mK* and 8.0 *W/mK* in one of the investigative generic reservoir. The thermal conductivity and heat capacity values are summarized in Table 4.

2.3 ROCK-FLUID PROPERTIES

In this study, we have examined selected laboratory reports, but the limited scope of our project precluded a full analysis of all of the historic lab core data from different geological formations.

The relative permeability and capillary pressure data were obtained from analytical functions suggested by van Genuchten, 1980 and Parker *et al.*, 1987. The presence of hydrate phase was incorporated into these functions. The chosen curves for water relative permeability *(k_{rw})* and gas relative permeability *(k_{rg})* are summarized as follows:

$$k_{rw} = k_{rwro}\, \overline{S}_w^{1/2} \left[1 - (1 - \overline{S}_w^{1/m})^m \right]^2 \quad \text{..(1)}$$

$$k_{rg} = k_{rgo}\, \overline{S}_g^{1/2} \left(1 - \overline{S}_{wH}^{1/m} \right)^{2m} \quad \text{..(2)}$$

Where, the normalized water, hydrate and gas saturations can be defined as,

$$\overline{S}_w = \frac{S_w - S_{wr}}{1 - S_{wr} - S_{gr}} \quad \text{..(3a)}$$

$$\overline{S}_{wH} = \frac{S_w + S_H - S_{wr}}{1 - S_{wr} - S_{gr}} \quad \text{..(3b)}$$

$$\overline{S}_g = \frac{1 - S_w - S_H - S_{gr}}{1 - S_{wr} - S_{gr}} \quad \text{..(3c)}$$

Here, S_{wr} is the irreducible water saturation and S_{gr} is the residual gas saturation. In addition, the grid cell saturations hold an auxiliary relation as, $S_g + S_w + S_H = 1$.

Not surprisingly, relative permeability curves can be significantly different for Mallik silt, Mallik sand and sandstone formations. Based on the well log data, one could even use different curves for the Mallik geological formations (i.e., silt and sand layers), but we have not done so; our model utilizes only one rock type. We have retained the parameters, *m = 0.45, S_{wr} = 0.3, S_{gr}*

Advanced Numerical Simulation of CO₂ Hydrate Formation
In Geological Reservoirs by Injection of CO₂ Gas   [6]
May, 2006

ALBERTA
RESEARCH
COUNCIL

= 0.05, k_{rwo} = 0.5 and k_{rgo} = 1.0, for water – gas relative permeability throughout our simulation study. The relative permeability exponents and end-points are summarized in Table 5.

Water-gas capillary pressure curves can be fit to the data, using the following form:

$$p_c = p_{co} \left[\overline{S}_w^{-1/m} - 1 \right]^{1-m}$$ ....(4)

The gas phase pressure (p_g) and the water phase pressure (p_w) in a grid cell also hold an auxiliary relation as, $p_c (S_w) = p_g - p_w$. The capillary pressure curve used as initial assumptions in our study for the reservoir geological formations is also defined with the parameters given in Table 5.

Advanced Numerical Simulation of CO₂ Hydrate Formation
In Geological Reservoirs by Injection of CO₂ Gas   [7]
May, 2006

ALBERTA
RESEARCH
COUNCIL

3.0   FIELD MODELLING

3.1   RESERVOIR CHARACTERIZATION

Geological heterogeneity plays an important role in gas hydrate formation and decomposition processes in the porous media because of spreading and dissipation of injected and produced fluids. To capture some of the geologic features, reservoir properties such as formation permeability, porosity, residual phase saturation, phase relative permeability, and phase capillary pressure are allowed to vary spatially in the numerical simulation.

In this study, ARC's geo-statistical program can be used to incorporate predefined permeability and porosity distribution in the gas hydrate simulation grid cells. The permeability distribution can be assumed to be log normally distributed with mild heterogeneity. The porosity is assumed to have a random normal distribution.

3.2   WELL BORE MODELING

A mechanistic model coupled with CMG STARS was used to model fluid and heat flow in the wellbore and between a wellbore and a reservoir / overburden. For the horizontal section of the wellbore, a numerical method termed the Discretized Wellbore is used, where the mass and energy conservation equations are solved together with reservoir equations for each wellbore section (perforation). Pipeflow correlations to handle laminar and turbulent flow are available. More details of this method can be found in Oballa *et al.* (1997).

For the vertical section of the wellbore, from the surface to the entry point into the perforated reservoir wellbore, the pressure drop along the wellbore and radial heatloss from the wellbore is calculated semi-analytically. The basic approach was developed by Fontanilla and Aziz (1982) but has been generalized for both injector and producer wells and to include both rate and pressure operating conditions. Pressure drop depends on friction, gravity and kinetic energy. Radial wellbore heatloss is a product of an overall heat transfer coefficient and a difference between fluid and formation temperature. The overall heat transfer coefficient is calculated from the input data. It depends on resistivity in the fluid film, tubing wall, insulation, annular space, casing wall and cement. This semi-analytic model can be coupled at the perforated entry point to either a simple (steady state) horizontal well model option, where frictional effects are ignored, or to the more mechanistically correct Discretized Well model just described.

3.3   OVERBURDEN - UNDERBURDEN MODELING

Overburden and underburden heat losses consist of heat flow between a boundary grid block and a semi-infinite portion of formation adjacent to that block.   The heat loss rate and its derivative with respect to temperature can be calculated, and used directly in the energy

Advanced Numerical Simulation of CO₂ Hydrate Formation
In Geological Reservoirs by Injection of CO₂ Gas   [8]
May, 2006

ALBERTA
RESEARCH
COUNCIL

conservation equation. In the present approach, the only data required are heat capacity and thermal conductivity of the base and cap rock, both of which are quite standard data.

A simple semi-analytical method for predicting cap and base rock heat losses in gas hydrate simulations was applied. This method was developed by Vinsome and Westerveld (1980) and is available in the STARS simulator. The minimum temperature difference between block temperature and the initial temperature of the formation adjacent to the reservoir was set at 0.10 ^{o}C. The semi-analytical heat loss calculation was only performed when the difference was greater than 0.10 ^{o}C.

3.4   PROTOTYPE ICE FORMATION MODEL

As a test of the ice formation model, a simple single vertical well radial model was employed based on Case Study I from Uddin *et al.* (2004) that was earlier used as a first test of methane and carbon dioxide hydrate formation and decomposition kinetic modelling approach. This model consists of a 10 m hydrate zone overlaying a 10 m hydrate free zone, in a reservoir with a constant porosity of 0.28 and a permeability of 20 mD. The cylindrical grid employed uses 97 grid cells radially and 20 grid cells vertically. Basic parameters can be found in Tables 2-4 of that report, which are equivalent to the majority of the fluid and rock parameters found in Tables 2-6 of this report as well. However, in order to accentuate the possible formation of ice during pressure depletion of the methane hydrate, the initial temperature was reset to 6 degree C (279.15 K). The initial pressure was maintained at 6,913 kPa.

Figure 7 compares the predicted gas production for this model with and without the possibility of ice formation. These are seen to be basically identical. Also compared is the average change in methane hydrate decomposition, which shows minor deviations as ice begins to form, but that that a significant hydrate composition remains. Ice forms as the reservoir temperature drops below zero (around 390 days), since hydrate decomposition is an endothermic process. The predicted average ice concentration is seen to fluctuate.

The distribution by about 500 days is found to be variable in the same zone as the co-existing methane hydrate. This is contrasted with the methane hydrate distribution which is relatively uniform, except at the upper and lower boundaries of the hydrate accumulation, where there is an increased melting (i.e., lower hydrate concentration levels). Over time, the simulation predicts that the ice distribution becomes more erratic but with region of very high ice levels. The fluid saturations reflect this effect, as the water saturation distribution also becomes erratic. The ice is formed from water uptake, and the more the non-mobile ice level rises, the lower is the fluid permeability to redistribute fluids.

Advanced Numerical Simulation of CO₂ Hydrate Formation
In Geological Reservoirs by Injection of CO₂ Gas   [9]
May, 2006

ALBERTA
RESEARCH
COUNCIL

4.0   CASE STUDIES

4.1   GENERIC RESERVOIRS

In consultation with the Geological Survey of Canada (GSC), four different geological formations of 20 *m* thickness were selected to investigate CO_2 hydrate formation. All these reservoirs were assumed to be extended from 1005 to 1025 m in depth. **The first reservoir (reservoir I) is similar to hydrate-free Mallik silt with mean porosity 0.30 and mean absolute permeability 100 mD. The second reservoir (reservoir II) is similar to hydrate-free Mallik sand with mean porosity 0.35 and mean permeability 1000 mD. The third reservoir (reservoir III) is similar to a conventional sandstone reservoir with mean porosity 0.25 and mean permeability 20 mD. The fourth reservoir (reservoir IV) is similar to tight gas reservoir with mean porosity 0.25 and mean permeability 10 mD.** The basic reservoir parameters and initial conditions are given in Table 6. The reservoir initial conditions were assumed to be the same for all four example problems. The key initial values are: pressure of 3000 kPa, temperature of 6 degrees C, water saturation of 75% and CH_4 gas saturation of 25%. It is important to note that these generic reservoirs are CH_4 hydrate dissociated reservoirs where 25% CH_4 gas saturation remains. Figure 8 shows a schematic of the process trajectory over the hydrate stability curve studied with the generic reservoir modelling.

Setup Numerical Domain – In the numerical representation, impermeable flow boundaries were assumed to confine a 20 m gas hydrate formation reservoir. Schematic diagrams of the simulated domain with a simplified description of the initial and boundary conditions are depicted in Figures 9 and 10. This represents a half pattern rectangular *(200 m x 4 m x 20 m)* simulation domain with a horizontal well configuration. The perforation length of the well is extended horizontally at the bottom of the reservoir. We considered 4 m length of perforation length and 200 m length perpendicular to the perforation length. The CO_2 gas at a temperature of 6 degree C was injected for 600 days with a maximum bottom hole pressure of 5000 kPa. This operating constraint maintains pressure-temperature conditions below the CH_4 hydrate stability curves. The numerical simulations at three CO_2 gas injection rates of 200, 300 and 400 m^3/day were assumed to be uniform along the 4 m length. A sample calculation in Figure 9 showed that an injection rate of 200 m^3/day would be equivalent to 40,000 m^3/day injection rate in an actual field operation with a 400 m horizontal perforation length. Figure 11 shows the wellbore data used for the vertical section of the well, solved semi-analytically.

The numerical domain was discretized into 200 cells in the *x*-direction *(1 m cell)*, 4 cells in the *y*-direction *(1 m cell)* and 40 cells vertical the *z*-direction *(0.5 m cell)*, resulting in a total of 32,000 active blocks. The smaller dimension was used in order to capture a very steep transient pressure, temperature and gas hydrate concentration fronts. Using the currently available ARC geo-statistical program, porosity and permeability values were assigned in every grid cell with predefined statistics (mean, variance and correlation). Figures 12, 15, 18 and 21 show the porosity with normally distributed and log-normally distributed permeability values for each of the four generic reservoirs.

4.2 MALLIK FORMATION (5L-38)

The Mallik gas hydrate field is located in the Mackenzie Delta on the coast of the Beaufort Sea, in Canada's Northwest Territories. Several articles have described aspects of the Mallik site hydrate deposit, including Ohara *et al.* (2000), Moridis *et al.* (2004a), (2004b). The production research well, JAPEX/JNOC/GSC *et al.* Mallik 5L-38 showed three gas hydrate zones. These zones can be summarized as:

Upper Zone: The upper zone extending from 892 to 930 *m*, occurs entirely within the Mackenzie Bay Sequence. Gas hydrate saturations range from 50 to 85%. This zone was excluded from our present numerical simulations.

Middle Zone: The middle zone extending from 942 to 993 *m*, is a complex interbedded section comprising a series of 5 to 10 *m* thick gas hydrate bearing sand units separated by 0.5 to 1 *m* thick gas-hydrate-free silt layers. Gas hydrate saturations range from 40 to 80%. In the scope of this report, this zone was also excluded from our present numerical simulations.

Lower Zone: The lower zone extending from 1060 to 1120 *m*, consists of two thick hydrate occurrences with many similarities to the upper gas hydrate bearing sand. Gas hydrate saturations are very high, ranging from 80% to 90%. Core observations confirm that the gas hydrate occurs primarily as pore-filling material in clean sand with low silt content. In this zone, the top 8 *m* (1070-1078 *m*) has more variable gas hydrate saturations and a more complex inter-bedded character. Sediments in this upper section consist of inter-bedded silty sand and sandy silt, with silt and clay contents in the 10 to 50 % range.

The lower contact of gas hydrate zone, at a depth of 1107 *m*, marks an abrupt change from gas hydrate bearing sand to gas hydrate free sand. The pressure and temperature at the base of the hydrate stability zone are 12,962 *kPa* and 12.2 ^0C, respectively. Wright *et al.* (2005a) predicted that the pressure and temperature conditions for the base of the gas hydrate stability zone at 1107 *m* are consistent with in situ pore-water salinities of 45 *ppt* (parts per thousand).

In the field, small scale production tests were conducted by using pressure-drawdown experiments. During each test, the formation behaviour parameters, including pressure, temperature, flow of gas and flow of water were measured in response to depressurization. The depressurization production test also included small-scale geo-mechanical testing with fracture-initiation studies and analysis of how fracturing affects gas production from gas hydrate. A thermal-stimulation production test of longer duration was carried out by circulating warm fluids into the high gas hydrate saturation zone. The flow gas from dissociating gas hydrate was separated at the surface from the circulating fluids to allow quantification of flow volumes, gas chemistry, and possible changes in fluid chemistry.

In this project, gas hydrate simulation is targeted in the depressurization test extended from 1060 to 1120 m in depth. In the scope of this work, numerical history matches of the above observed variables were not performed. Figure 28 shows a schematic of the process trajectory over the hydrate stability curve studied with the generic reservoir modelling.

ALBERTA
RESEARCH
COUNCIL

Setup Numerical Domain - A schematic diagram of the simulated domain with a simplified description of the initial and boundary conditions is depicted in Figures 29 and 30. In this study, a simple half pattern rectangular simulation domain was setup to model the lower gas hydrate bearing formation (*1060 – 1120 m)* with a horizontal well configuration. The well is located at the base of the bottom hydrate layer. In the numerical representation, impermeable flow boundaries were assumed to confine the 60 m thickness geological formation. Although the corresponding actual confining shale zones at the overburden and underburden elevations had low (but nonzero) intrinsic permeability, the assumption of impermeable boundaries was reasonable given the much larger intrinsic permeabilities of the gas hydrate zone.

5.0   RESULTS AND DISCUSSIONS

5.1   GENERIC GEOLOGICAL FORMATIONS

A detailed numerical investigation was conducted to study CO_2 hydrate formation in the four different geological formations. This study considered a rectangular numerical domain (*200 m x 4 m x 40 m*) with horizontal well configuration.   The reservoir properties (porosity and permeability), initial conditions (pressure, temperature and saturation), numerical domain setup (grid cells) and well operating conditions (injection and production rates and pressures) are discussed in Section 4.1.

Figures 12, 15, 18 and 21 show the grid cells porosity and permeability for one geo-statistical realization for each of the four reservoir types. With the limited scope of this work, we have chosen and incorporated only one realization of mild heterogeneity for all four generic reservoirs.   In this realization, porosity was assumed to be normally distributed and the permeability is log normally distributed with a mild heterogeneity. Detailed gas hydrate simulations in the generic reservoirs with several predefined realizations (low to strong heterogeneity) can be conducted to understand and establish a possible relationship between permeability heterogeneity and gas hydrate formation.

Pressure-Temperature Response – The overall flow system pressure-temperature responses at any given time primarily driven by two processes: hydrate kinetic rates (i.e., transfer of water and gas moles into hydrate crystals) and CO_2 injection rates (injection of CO_2 gas moles into the flow system).   In numerical computation, an excess pressure or deviation of grid cell pressure (i.e., pressure undershoot or overshoot) from the hydrate equilibrium pressure is the primary driver of gas hydrate kinetics (dissociation or formation rates). In the formation of hydrate, heat is released and the temperature of the grid cell increases. In terms of the volume changes, approximately 1 *mL* of water converts into 1.1 *mL* of hydrate crystal. At the same time, a large volume of gas moles physically get trapped in hydrate cavities. The trapped gas moles may have some spinning rotation within the cavities depending on the relative sizes of guest gas moles and host cavities.

Figures 13, 16, 19 and 22 show the average field (*200 m x 4 m x 40 m*) pressure, temperature and CO_2 hydrate concentrations over 60 day simulation periods for the four generic reservoirs. All of these numerical experiments were conducted at three constant gas injection rates (*200, 300 and 400 m³/day*) with a maximum bottom hole constraint of 5000 kPa. The spatial distributions of the above variables (pressure, temperature and hydrate concentration) were constantly monitored during the simulation periods. Spatial observations at the end of 360 days for the four generic reservoirs (reservoir I, II, III and IV) are shown in Figures 14, 17, 20 and 25.

The numerical simulations showed that the gas injection rates were starting to decline when the well pressure increased to the maximum bottom hole pressure constraint of 5000 kPa. This leads to a sharp break in the average field pressure curves. The results illustrate that reservoir properties (such as permeability and porosity) play a significant role in the growth and shape of pressure pulse and gas hydrate concentration plume. A very rapid dissipation of the pressure overshoot was observed for high permeability reservoir II (Figure 17). At the end of 360 days,

pressure contours are nearly horizontal for this high permeability reservoir II (Mallik sand). Conversely the pressure contours for all three reservoirs (reservoir I, III and IV) of relatively lower permeabilities are nearly vertical in Figures 14, 20 and 25. It is important to note that the pressure overshoot is the primary driver for gas hydrate formation.

Previously, Uddin, M. (2005) with the support of GSC, conducted a preliminary simulation to induce the formation of CO_2 hydrate by injecting CO_2 gas into these simplified geological settings. This earlier study considered a 200 m radius numerical domain with a vertical well configuration. One of the interesting observations of this earlier work was that at low injection rates, the average field pressure and temperature dropped significantly with the formation of CO_2 hydrates. This condition can occur when hydrate kinetics (reaction rates) consumed more gas moles compared to the injected gas moles in the flow system. This effect has to be high enough to overcome volume expansion due to the formation of gas hydrate crystals (typically, 1 *mL* water converted into 1.1 *mL* gas hydrate).

Gas Hydrate Concentration - The cumulative gas hydrate concentration curves at three injection rates (Figures 13, 16, 19 and 22) illustrate that the gas hydrate accumulation around the well bore may significantly increase with the gas injection rate. The formation of gas hydrate releases heat and increases the temperature of the flow system. This shows a higher temperature in the higher gas hydrate concentration area. The shape of the concentration plume corresponds to the temperature profile. The overburden and underburden heat flux leads to a developing gas hydrate concentration plume along the middle layer.

Figure 25 compares the average field hydrate concentration when the initial pore water salinity of 2.0 *ppt* with the gas hydrate concentration when no background salinity. The results illustrated that the pore water salinity have a significant effect on the gas hydrate formation and dissociation processes. It should be noted that in this study, the gas hydrate stability curves were shifted 1.0 ^0C per 20 *ppt* salinity based on the GSC laboratory investigation (Wright *at el.*, 2005a.)

Figures 26 and 27 show a comparison of the average gas hydrate concentration, pressure and temperature for all four generic reservoirs at injection rates of 200 m³/day and 400 m³/day, respectively. Table 7 summarizes the material balance statistics.

5.2   MALLIK CH4-HYDRATE BEARING FORMATION

The geology of the Mallik gas hydrate field has been extensively described in numerous publications (Dallimore and Collett, 1999, Jenner *et al.*, 1999, Dallimore and Collett, 2005). The gas hydrate bearing formation targeted in the depressurization test extended from 1060 to 1120 m in depth. Figure 29 shows a well log data characterizing rock types, porosity, permeability and gas hydrate saturation. The intrinsic permeability of the porous medium at different locations within the gas hydrate interval was measured in various core studies (as reviewed by Collett *et al.*, 2005).

The pressure in the gas hydrate interval matched very closely the hydrostatic – pressure distribution at the depth (Hancock *et al.*, 2005). The initial temperature profile was obtained

from the initial (pre test) DTS readings (Hennings *et al.*, 2005) along the profile of the gas hydrate interval. The average initial temperature of 12.6 degree C can be approximated corresponding to the prevailing pressure of 12,912 kPa. According to Wright *et al.*, 2005a, salinity estimates near the base of the gas hydrate stability zone ranged between 35 and 45 ppt (parts per thousand) based on chlorinity and temperature data.

Figure 34 shows the evolution of average pressure, temperature and hydrate content of the Mallik zone over approximately 20 day of production, based on a maximum fluid production rate of 100 m^3/day and a minimum bottom hole pressure constraint of 3000 kPa. With the observed rapid pressure decline, there is a related temperature decline and decomposition of the methane hydrate. The rapid pressure decline is associated with the assumed well completion in the high (*1000 md)* sand. This perforation location may not be where the actual Mallik field test was performed.

Figure 35 shows the associated production behaviour, which illustrates the rapid decay of well pressure to the specified minimum, and an associated spike in gas production from the dissociating hydrate. Associated with the pulse of gas and the the bottomhole pressure restriction, there is a decline in water production. The bottomhole pressure restriction basically limits the whole process such that a steady behaviour is approached before 20 days of production. It is noted that there was a mini-production test of this well as part of the Mallik test, but we have made no attempt to do a proper history match of the observed behaviour.

Figure 36 compares the predicted hydrate distributions at 2 and 10 days (i.e., before and after the large gas pulse produced by the hydrate decomposition). It is seen that the majority of the hydrate decomposition occurs in the zone with the highest hydrate saturation, although the other hydrate containing zones are decomposing somewhat as well. Figure 37 shows the corresponding pressure profiles. Obviously, the pressure decline is first seen near to the horizontal well, but over a short period of time the pressure profile becomes quite uniform throughout the reservoir. In contrast, the temperature profiles as shown in Figure 38 retain the layering associated with the hydrate accumulations. In particular, in zones where no hydrate originally existed, the pressure decline has no effect on the temperature evolution and the temperature remains high. In contrast, in zones containing hydrate, the pressure and temperature changes track each other because of the effect of the hydrate stability curve. Overall, there is an interplay between phase behaviour (hydrate stability curves) and flow which needs further detailed analysis. It is seen that the temperature is still very far from possible ice formation effects in this simulation.

5.3   MALLIK CH₄-HYDRATE WITH ICE

The Mallik reservoir scenario was also used to examine possible effects of ice formation during a methane hydrate decomposition process. For these early test runs, a staged, variable pressure decline schedule was employed and an initial gas saturation was assumed to exist as a result of previous methane hydrate dissociation. These assumptions were used to accentuate the possibility of ice formation. Figure 39 compares the gas production behaviour with and without possible ice formation. Using the supplied pressure decline protocol, the reservoir temperature

ALBERTA
RESEARCH
COUNCIL

dropped below zero around 360 days, and the results show a dramatic increase in gas production at this point.

Figures 40 and 41, which show the predicted ice and methane hydrate distributions at 500 days, give an indication of the origin of this observation. Here almost all of the methane hydrate has decomposed (except for a band of lower concentration hydrate) and has been replaced by a higher concentration of ice. As hydrate contains gas, but ice does not, more gas has been released to be produced. In the Mallik case, the ice distribution is seen to be less erratic at the time of observation than what was observed in the prototype ice formation simulations.

These preliminary "ice formation" runs illustrate the need for further evaluation and checking. They do demonstrate the extreme nonlinearity of the coupled phenomena which involve the crossing of several multi-phase boundaries with very different flow properties, and how various production strategies and reservoir characteristics can combine to give different "trajectories through these multiphase zones.

6.0   CONCLUSIONS AND RECOMMENDATIONS

ARC's multi-phase and multi-component gas hydrate model was used to simulate CO_2 hydrate formation in several geological reservoirs by injecting CO_2 gas under different operating conditions. The key investigative issues were reservoir properties (porosity and permeability), reservoir initial conditions (pressure, temperature and saturation), reservoir boundary conditions (well bore, over burden and underburden heat flux) and well operating conditions (CO_2 injection rate and well bottom hole pressure). The following specific conclusions can be obtained from this project:

(1) Reservoir properties – The pressure overshoot built up upon the injection of CO_2 gas was strongly dictated by the reservoir permeability. The pressure overshoot was significantly lower for the high permeability reservoir – II (porosity – 0.35 and permeability – 1000 mD).

(2) The gas hydrate simulations were conducted for one realization of the permeability heterogeneity. A slight distortion of the gas hydrate concentration was observed. This could be due to the permeability heterogeneity. Further conclusions need to evaluate numerical results for several geo-statistical realizations.

(3) A significant change in the shape and growth of the CO_2 hydrate concentration plume was observed. An early symmetric plume shape around the well bore gradually shifted into a laterally elongated shape in the centre of the flow system. This was primarily dictated by the gas hydration and boundary heat fluxes.

(4) The gas hydrate formation releases heat and temperature rises. A similar trend was observed in the shape and growth of gas hydrate concentration and temperature.

(5) The average reservoir pressure dropped when relatively less gas moles were reacted compared to the gas mole injection. The hydrate kinetics (kinetic rates) and CO_2 injection rates primarily control the overall reservoir pressure.

(6) The effect of impermeable boundaries (overburden-underburden) such as heat flux and flow were clearly noticeable on the gas hydrate formation. A sensitivity study is needed for any further conclusion.

(7) The nonhomogeneous initial distribution of hydrate found in the Mallik test case impacted on how and where the gas hydrate is produced. In particular, the location of the perforation could effect the well pressure decline performance and a proper engineering analysis of well operating conditions is required for optimal production performance.

(8) If the temperature/pressure conditions evolve such that ice formation does occur, this can increase the gas production associated hydrate decomposition. For CO_2 sequestration, however, ice formation is deleterious as this removes water for possible CO_2 hydrate formation.

The following follow-up work is recommended from this study:

I. Laboratory Gas Hydrates Experiment – A laboratory sand pack experiment can be setup to induce the formation of CO_2 hydrate by injection of CO_2 gas. Systematic laboratory tests, under controlled pressure/temperature/porous media conditions, are needed to evaluate gas hydrate

Advanced Numerical Simulation of CO_2 Hydrate Formation
In Geological Reservoirs by Injection of CO_2 Gas   [17]
May, 2006

ALBERTA
RESEARCH
COUNCIL

reaction rate coefficients (kinetics) and dispersion of the water phase components. The laboratory solvent dispersion in a layered porous media experiment conducted by Uddin and Bray (1998) could be evaluated for this proposed gas hydrate experiment.

II. Generic Reservoir Simulation – A further refinement of the numerical simulations is needed to evaluate the formation of CO_2 hydrate under an actual geological setting (such as reservoir heterogeneity, initial pressure, temperature, saturation).

> (1) Detailed gas hydrate simulations in the generic reservoirs with several predefined realizations (low to strong heterogeneity) can be conducted to understand and establish a possible relationship between permeability heterogeneity and gas hydrate formation.
> (2) The injection of CO_2 gas into a geological reservoir with 100% water saturation to induce the formation of CO_2 hydrate can be investigated. This may require some engineering challenges such as setup production well or formation dilation around the injector.

III. Mallik Gas Hydrate Simulation – Detailed CH_4 hydrate dissociation and CO_2 hydrate formation simulations can be performed under several horizontal and/or vertical well configurations and operating conditions.

> **(1)** perform numerical history matches for the available small scale thermal and pressure drawdown production data.
> **(2)** perform systematic single pattern multi-well gas hydrate simulations and optimize CO_2 sequestration. The proposed operating strategy in Figure 42 can be investigated.
> **(3)** perform Mallik field scale gas hydrate simulation considering the entire vertical and lateral geological settings.

IV. Geochemistry and Geomechanics – In CO_2 sequestration, geochemical and geo-mechanical options can be considered to evaluate the short and long term fate of the formation of CO_2 hydrate and distribution of CO_2 gas. A brief description of the geochemical and geomechanical models is given in the following sections.

Geochemistry
Carbon dioxide dissociates in formation water affecting solution pH and can be involved with complex carbonate and silicate reactions depending on pressures, temperatures and cation availability in the formation water and the mineral components. The geochemical reactions such as calcite synthesis reactions consume Ca^{++} and release H^+ to the formation water, both the dissolved Ca^{++} and the pH are rapidly lowered, the partial pressure of the CO_2 *(pCO₂)* builds up and affects the stability of CO_2 hydrates. The water chemistry data for several Alberta formations and Mallik gas hydrate formation were complied. These data are summarized in Table 7.

A preliminary geochemical simulation for one of the generic reservoirs was performed by decoupling the gas hydrate model. Figure A-I-1 shows the simulation domain with initial geochemistry data. The simulation illustrated the necessary geochemical processes under situations when CO_2 hydrate might not form. Figures A-I-2 and A-I-3 show the spatial evolution

of the CO_2 plume after 6 years, with the distribution of bicarbonate ion and acidic pH governed by the aqueous solution chemistry and the calcium ion production from calcite dissolution. The geochemical option could be coupled with the gas hydrate model in the CO_2 sequestration project.

Geomechanics

Hydrate stability to the mechanical forces induced by fluid injection and production practices needs to be explored more extensively. A geomechanics model is essential to solve force equilibrium of the geological formation and predict volumetric dilation/compression as a result of both elastic and plastic straining caused by fluid injection and production. The pore volume changes may be caused by a combination of compression/tension or by shear stresses. These changes in pore volume and the associated changes in transmissibilities are used in the reservoir model for calculating mass and energy balances in the reservoir.

During injection, the stress state at a location may reach a yield condition and begins to accumulate plastic strains. Shear dilatancy is a component of the resulting volumetric dilatation. Upon production, the material may be unloaded, resulting in the stress state dropping-off from the yield surface. During this period, the material may lose some of the reversible elastic strains. Figure A-II-1 illustrates the expected cyclical response.

A preliminary geomechanical simulation for one of the generic reservoirs was performed to investigate these effects, using the coupled geomechanics module available in STARS. The reservoir model is illustrated in Figure A-II-2, which is similar to earlier models except that a coarser grid discretization was employed. Figure A-II-3 shows the pressure and gas production/injection response associated with methane hydrate decomposition and production followed by CO_2 injection and CO_2 hydrate formation. The associated geomechanical responses of effective stress and porosity changes are illustrated in Figure A-II-4. Figures A-II-5 shows the spatial distribution of these quantities at the end of the production cycle.

7.0   REFERENCES

Adisasmito, S., Frank, R.J, and Sloan, E. D. Jr, "Hydrates of carbon dioxide and methane mixtures", Journal of Chem. Eng. Data, vol. 36, pp. 68-71, 1991.

Collett, T.S., Lewis, R.F., and Dallimore, S.R., "JAPEX/JNOC/GSC et al. Mallik 5L-38 gas hydrate production research well downhole well-log and core montages", *in* Scientific Results from the Mallik 2002 Gas Hydrate Production Research Well Program, Mackenzie Delta, Northwest Territories, Canada, (ed.) S.R. Dallimore and T.S. Collett; Geological Survey of Canada, Bulletin 585, 2005

Dallimore, S.R. and Collett, T.S., "Regional gas hydrate occurrences, permafrost conditions, and Cenozoic geology, Mackenzie Delta area", *in* Scientific Results from JAPEX/JNOC/GSC Mallik 2L-38 Gas Hydrate Research Well, Mackenzie Delta, Northwest Territories, Canada, (ed.) S.R. Dallimore, T. Uchida, and T.S. Collett; Geological Survey of Canada, Bulletin 544, p. 31-43, 1999.

Dallimore, S.R. and Collett, T.S. (ed.) "Scientific Results from the Mallik 2002 Gas Hydrate Production Research Well Program", Mackenzie Delta, Northwest Territories, Canada, (ed.) S.R. Dallimore and T.S. Collett; Geological Survey of Canada, Bulletin 585, 2005.

Dallimore, S.R., Medioli, B.E., Laframboise, R.R., and Giroux, D. (comp.), "Mallik 2002 Gas Hydrate Production Research Well Program, Mackenzie Delta, Northwest Territories: well data and interactive data viewer", Appendix A *in* Scientific Results from the Mallik 2002 Gas Hydrate Production Research Well Program, Mackenzie Delta, Northwest Territories, Canada, (ed.) S.R. Dallimore and T.S. Collett; Geological Survey of Canada, Bulletin 585, 2005a.

Dallimore, S.R., Taylor, A.E., Wright, J.F., Nixon, F.M., Collett, T.S., and Uchida, T., "Overview of the coring program for the JAPEX/JNOC/GSC et al. Malik 5L-38 gas hydrate production research well", *in* Scientific Results from the Mallik 2002 Gas Hydrate Production Research Well Program, Mackenzie Delta, Northwest Territories, Canada, (ed.) S.R. Dallimore and T.S. Collett; Geological Survey of Canada, Bulletin 585, 2005b.

Fontanilla, J.P., and Aziz, K, "Prediction of bottom-hole conditions for wet steam injection wells", Journal of Canadian. Petroleum Technology, vol. 21, #2, pp. 82-88, 1982.

Hancock, S.H., Collett, T.S., Dallimore, S.R., Satoh, T., Inoue, T., Huenges, E., Henninges, J., and Weatherill, B., "Overview of thermal-stimulation production-test results for the JAPEXJNOC/GSC et al. Mallik 5L-38 gas hydrate production research well", *in* Scientific Results from the Mallik 2002 Gas Hydrate Production Research Well Program, Mackenzie Delta, Northwest Territories, Canada, (ed.) S.R. Dallimore and T.S. Collett; Geological Survey of Canada, Bulletin 585, 2005a.

Advanced Numerical Simulation of CO$_2$ Hydrate Formation
In Geological Reservoirs by Injection of CO$_2$ Gas   [20]
May, 2006

ALBERTA
RESEARCH
COUNCIL

Hancock, S.H., Dallimore, S.R., Collett, T.S., Carle, D., Watherill, B., Satoh, T., and Inoue, T., "Overview of pressure-drawdown production-test results for the JAPEXJNOC/GSC et al. Mallik 5L-38 gas hydrate production research well", *in* Scientific Results from the Mallik 2002 Gas Hydrate Production Research Well Program, Mackenzie Delta, Northwest Territories, Canada, (ed.) S.R. Dallimore and T.S. Collett; Geological Survey of Canada, Bulletin 585, 2005b.

Henninges, J., Schrőtter, J., Erbas, K., and Huenges, E., "Temperature field of the Mallik gas hydrate occurrence-implications on phase changes and thermal properties", *in* Scientific Results from the Mallik 2002 Gas Hydrate Production Research Well Program, Mackenzie Delta, Northwest Territories, Canada, (ed.) S.R. Dallimore and T.S. Collett; Geological Survey of Canada, Bulletin 585.

Hong, H, and Pooladi-Darvish, M, "A Numerical study on gas production from formations containing gas hydrates", Paper 2003-060 presented at the Petroleum Society's Canadian International Petroleum Conference (CIPC) 2003, Calgary, Alberta, Canada, June 10 – 12, 2003.

Jenner, K.A., Dallimore, S.R., Clark, I.D., Paré, D., Medioli, B.E., "Sedimentology of gas hydrate host strata from the JAPEX/JNOC/GSC Mallik 2L-38 gas hydrate research well", *in* Scientific Results from the JAPEX/JNOC/GSC Mallik 2L-38 Gas Hydrate Research Well, Mackenzie Delta, Northwest Territories, Canada, (ed.) S.R. Dallimore, T. Uchida and T.S. Collett, Geological Survey of Canada, Bulletin, vol. 544, pp. 57-68.

Kim, H.C., Bishnoi, P.R., Heidemann, R.A, and Rizvi, S.S.H., "Kinetics of methane hydrate decomposition", Chemical Engineering Science, vol. 42, No. 7, pp. 1645-1653, 1987.

Malegaonkar, M.B, Dholabhi, P. D., and Bishnoi, P. R., "Kinetics of carbon dioxide and methane hydrate formation", The Canadian Journal of Chemical Engineering, Vol. 75, pp. 1090-1099, December 1997.

Mantoglou, A. and Wilson, J.L., "The turning bands method for simulation of random fields using line generation by a spectral method", Water Resour. Res., 18, pp. 1379-1394, 1982.

Moridis, G.J, "Numerical Studies of Gas Production from Methane Hydrates", SPE Journal, Vol. 8, #4, pp. 359-370, 2003.

Moridis, G.J., Collett, T.S., Dallimore, S.R., Satoh, T., Hancock, S., and Weatherill, B., "Numerical Studies of Gas Production from Several CH4 Hydrate Zones at the Mallik Site, Mackenzie Delta, Canada", Journal of Petroleum Science and Engineering, Vol. 43, pp. 219-238, 2004a.

Moridis, G.J, "Numerical Studies of Gas Production from Class2 and Class3 Hydrate Accumulations at the Mallk Site, Mackenzie Delta, Canada", SPE Reservoir Evaluation and Engineering, Vol. 7, pp. 175-183, 2004b.

Advanced Numerical Simulation of CO$_2$ Hydrate Formation
In Geological Reservoirs by Injection of CO$_2$ Gas   [21]
May, 2006

ALBERTA
RESEARCH
COUNCIL

North, W.J, Blackwell, V. R., and Morgan, J. J., "Studies of CO_2 Hydrate Formation and Dissolution", Environmental Science and Technology, Vol. 32, pp. 676-681, 1998.

Ohara, T, Dallimore, S.R., and Fercho, E., "JAPEX/JNOC/GSC MALLIK 2L-38 Gas Hydrate Research Well, Mackenzie Delta, N.W.T.: Overview of Field Operations", SPE paper 59795, presented at the 2000 SPE/CERI Gas Technology Symposium, Calgary, AB, April 3-5, 2000.

Parker, J.C., Lenhard, R.J., and Kuppusamy, T., "A parametric model for constitutive properties governing multiphase flow in porous media", Water Resources Research, Vol. 23, No. 4, pp. 618-624, 1987.

Seo, Y., Lee, H. and Uchida, T., "Methane and Carbon Dioxide Hydrate Phase Behavior in Small Porous Silica Gels: Three-Phase Equilibrium Determination and Thermodynamic Modeling", Langmuir 2002, vol. 18, pp. 9164-9170, 2002.

Reid, R.C., Prausnitz, J.M, and Sherwood, T.K., "The properties of gases and liquids", 3rd edition, McGraw-Hill, Inc., 1977.

Schwartz, F.W., "Macroscopic dispersion in porous media: The controlling factors", Water Resour. Res., 13, pp. 743-752, 1977.

Sloan, E.D., "Clathrates of natural gases", Marcel Dekker, New York, New York, 705 p., 1998.

Sloan, E.D., "Fundamental principles and applications of natural gas hydrates", Nature, v. 426, p. 353-359, 2003.

Swinkels, W.J.A.M. and Drenth, R.J.J., "Thermal Reservoir Simulation Model of Production from Naturally Occurring Gas Hydrate Accumulations", SPE Reservoir Eval. & Eng., vol. 3, No. 6, pp. 559-566, December 2000.

Sweigert, R.L., Weber, P., and Allen, R.L., "Thermodynamic properties of gases – carbon dioxide", Ind. Eng. Chem. 38, 185-200, 1946.

STARS 2004, Advanced Process and Thermal Reservoir Simulator, Computer Modelling Group Ltd., Office #200, 3512-33 Street N.W. Calgary, Alberta, Canada T2L 2A6.

Uddin, M. and Bray, D., "Study of transient transport processes in layered porous media", proceedings, presented at the 1998 CSCE Annual Conference, Halifax, Nova Scotia, June 10-13, 1998.

Uddin, M., Law, D. and Coombe, D., "Numerical simulation of carbon dioxide (CO_2) sequestration processes in gas hydrate reservoirs", CCTII Unconventional Gas Supply Report, Natural Resource of Canada, 2004.

Uddin, M., "Numerical simulation and Assessment of Alternative Strategies for Formation of CO_2 Hydrate in Geological Reservoirs", Report prepared for the Geological Survey of Canada, Natural Resource of Canada, April, 2005

Advanced Numerical Simulation of CO_2 Hydrate Formation
In Geological Reservoirs by Injection of CO_2 Gas   [22]
May, 2006

ALBERTA
RESEARCH
COUNCIL

Uddin, M., Coombe, D., Law, D. and Gunter, B., "Numerical studies of gas hydrate formation and decomposition in a geological reservoir", proceedings, presented at the 2006 SPE Gas Technology Symposium, Calgary, Alberta, Canada, May 15-17, 2006.

Van Genuchten, M.T., "A closed-form equation for predicting the hydraulic conductivity of unsaturated soils", Soil Science Society of America Journal, vol. 44, pp. 892-898, 1980.

Vinsome, P.K.W. and Westerveld, J., "A Simple Method for Predicting Cap and Base Rock Heat Losses in Thermal Reservoir Simulators", Journal of Canadian Petroleum Technology, vol. 19, #3, pp. 87-90, 1980

Wright, J.F., Dallimore, S.R., Nixon, F.M., and Duchesne, C., "In situ stability of gas hydrate in reservoir sediments of the JAPEX/JNOC/GSC et al. Mallik 5L-38 gas hydrate production research well", *in* Scientific Results from the Mallik Gas Hydrate Production Research Well Program, Mackenzie Delta, Northwest Territories, Canada, (ed) S.R. Dallimore and T.S. Collett; Geological Survey of Canada, Bulletin 585, 2005a.

Wright, J.F., Nixon, F.M., Dallimore, S.R., S.R., Henninges, J., and Côté, M.M., "Thermal conductivity of sediments within the gas-hydrate-bearing interval at the JAPEX/JNOC/GSC et al. Mallik 5L-38 gas hydrate production research well", *in* Scientific Results from the Mallik Gas Hydrate Production Research Well Program, Mackenzie Delta, Northwest Territories, Canada, (ed) S.R. Dallimore and T.S. Collett; Geological Survey of Canada, Bulletin 585, 2005b.

Advanced Numerical Simulation of CO_2 Hydrate Formation
In Geological Reservoirs by Injection of CO_2 Gas   [23]
May, 2006

ALBERTA
RESEARCH
COUNCIL

Table 1: Gas hydrate model - Components and phases

Component	Phase		
	Aqueous	Gaseous	Solid
H_2O	X		X
CH_4	X	X	X
CO_2	X	X	X
$CH_4.nH_2O$			X
$CO_2.nH_2O$			X
Ice			X

Note: Phase is a physical manifestation of one or more components. All physical properties are assigned to a model component in terms of the phases in which that component may be found.

Advanced Numerical Simulation of CO_2 Hydrate Formation
In Geological Reservoirs by Injection of CO_2 Gas   [24]
May, 2006

ALBERTA
RESEARCH
COUNCIL

Table 2: CO_2 and CH_4 hydrate kinetics properties (Structure I hydrate, all cavities are filled with CH_4 or CO_2 gas molecules)

Components	$CO_2.nH_2O$	$CH_4.nH_2O$
Molecular weight, M_m *(kg/gmole)*	147.500×10^{-3}	119.543×10^{-3}
Mass density, ρ *(kg/m³)*	1100	919.7
Volumetric mole density, ρ *(gmole/m³)*	7458	7696
[1] Intrinsic decay rate, k_d^0 *(gmole/(day.kPa.m²))*	1.071×10^{13}	1.071×10^{13}
[1] Intrinsic formation rate, k_F^0 *(gmole/(day.kPa.m²))*	3.024×10^4	2.506×10^5
[2] Specific area of hydrate particles, A_{SH} *(m²/m³)*	3.75×10^5	3.75×10^5
Activation energy, E *(J/gmole)*	81084.2	81084.2
Reaction enthalpy *(J/gmole)*	51857.9364	51857.9364
[3] Kinetic rate constants		
A *(gmole/m³)$^{-1}$/kPa.day)*	9.706×10^9	9.706×10^9
B *(1/kPa.day)*	2.043×10^5	2.043×10^5

(1) Hong and Pooladi-Darvish (2003) used this intrinsic, k_d^0, for CH_4 hydrate decomposition simulation. The kinetic parameter, k_F^0, was taken from Malegaonkar *et al.* (1997).

(2) Kim *et al.* (1987) determined this value for hydrate particles in a PVT cell.

(3) Kinetic rate constants for the ARC's gas hydrate model (Uddin *et al.,* 2006)

Advanced Numerical Simulation of CO_2 Hydrate Formation
In Geological Reservoirs by Injection of CO_2 Gas   [25]
May, 2006

ALBERTA
RESEARCH
COUNCIL

Table 3: Component properties at reference temperature and pressure ($T = 25$ *deg C*, and $p = 101$ *kPa*) (data sources – CMG STARS user's guide, 2004; Reid *et al.*, 1977)

Parameters	H_2O	CO_2	CH_4
Constant			
Molecular weight, M_m *(kg/gmole)*	18.015×10^{-3}	44.010×10^{-3}	16.043×10^{-3}
Molar density, ρ *(kg/m³)*	1000	350.6	300.37
Volumetric mole density, ρ *(gmole/m³)*	55502	7965	18723
Critical point			
- Temperature, T_{cr} *(deg C)*	374.2	31.05	-82.55
- Pressure, p_{cr} *(kPa)*	22048	7376	4600
Quadruple point or Freezing point			
- Temperature *(deg C)*	0.0	-56.61	-182.5
- Pressure *(kPa)*	0.612	517.80	101.3
Functional [(1)]			
Vapor heat capacity *(J/gmole-K)*	33.659	47.125	35.557
Liquid heat capacity *(J/gmole-K)*	-	-	-
Vaporization enthalpy at boiling point, h_{vap} *(J/gmole)*	40690	17166.09	8188.65

[(1)]   Temperature dependent parameters were defined by CMG STARS correlation options

Advanced Numerical Simulation of CO_2 Hydrate Formation
In Geological Reservoirs by Injection of CO_2 Gas   [26]
May, 2006

ALBERTA
RESEARCH
COUNCIL

Table 4: Other thermal properties

Components	Gas hydrate bearing formation
Rock/Phase	
Volumetric rock heat capacity ($J/m^3\ K$)	2.120×10^6
Hydrate heat capacity ($J/kg\ K$)	1600
Rock thermal conductivity (J/m-day-K)	3.387×10^5
Hydrate thermal conductivity (J/m-day-K)	3.395×10^4
Water thermal conductivity (J/m-day-K)	5.183×10^4
Gas thermal conductivity (J/m-day-K)	140.0
Heat Loss to Adjacent Formations	
Temp difference to trigger heat loss ($^0 C$)	0.10
Overburden heat capacity ($J/m^3\ K$)	2.120×10^6
Overburden thermal conductivity(J/m-day-K)	1.296×10^5
Under burden heat capacity ($J/m^3\ K$)	2.120×10^6
Under burden thermal conductivity(J/m-day-K)	1.296×10^5

Note: Total thermal conductivity was assumed to be 2.7 *W/mK* with estimated rock conductivity of 3.92 *W/mK*, hydrate of 0.393 *W/mK* and water of 0.6 *W/mK*. Wright *et al.* 2005b estimated total thermal conductivity of 2.7 *W/mK* for the Mallik hydrate bearing formation of porosity of 0.35, hydrate saturation of 0.80 and water saturation of 0.20.

Advanced Numerical Simulation of CO_2 Hydrate Formation
In Geological Reservoirs by Injection of CO_2 Gas   [27]
May, 2006

ALBERTA
RESEARCH
COUNCIL

Table 5: Parameters for relative permeability and capillary pressure (Parameters associated with the analytical functions, van Genuchten 1980 and Parker *et al.*, 1987)

Parameters	Generic Reservoirs	Mallik Site (5L-38)
Rel. Permeability		
m	0.45	0.45
S_{wr}	0.3	0.3
S_{gr}	0.05	0.05
k_{rwo}	0.5	0.5
k_{rgo}	1.0	1.0
Capillary Pressure		
p_{co} *(kPa)*	1.0	1.0

ALBERTA
RESEARCH
COUNCIL

Table 6: Generic reservoirs – Reservoir properties and initial conditions

Parameters	Reservoir I (Mallik silt)	Reservoir II (Mallik sand)	Reservoir III (Sandstone-1)	Reservoir IV (Sandstone-2)
Basic reservoir parameters				
Mean porosity $(-)$	0.30	0.35	0.25	0.25
Mean permeability (mD)	100	1000	20	10
Thermodynamic condition				
Pressure (kPa)	3000	3000	3000	3000
Temperature $(degree\ K)$	279.15	279.15	279.15	279.15
Other reservoir parameters				
Simulation domain (m^3)	200 x 20 x 4	200 x 20 x 4	200 x 20 x 4	200 x 20 x 4
Water saturation $(-)$	0.75	0.75	0.75	0.75
Gas saturation $(-)$	0.25	0.25	0.25	0.25
Hydrate saturation $(-)$	0.00	0.00	0.00	0.00
Rock density (kg/m^3)	2650	2650	2650	2650
Initial material in place				
Gas $(std\ m^3)$	7.873×10^4	9.185×10^4	6.561×10^4	6.561×10^4
Water $(std\ m^3)$	7.184×10^3	8.381×10^3	5.986×10^3	5.986×10^3
Hydrate $(std\ m^3)$	0.0	0.0	0.0	0.0

Note: Previously, numerical simulations were conducted for CO_2 hydrate formation in the reservoir(s) I, II and III (GSC report – Uddin, M. 2004). Reservoir – IV is included based on GSC request. These reservoirs were assumed to be CH_4 hydrate dissociated reservoirs with a cooler temperature *(6 degree C)* and lower pressure *(3 MPa)* and 25% saturation of CH_4 gas remaining.

Advanced Numerical Simulation of CO₂ Hydrate Formation
In Geological Reservoirs by Injection of CO₂ Gas   [29]
May, 2006

ALBERTA
RESEARCH
COUNCIL

Table 7: Material balance statistics at the end of 600 days – Generic Reservoirs (CO_2 gas injection rate, $q = 200\ m^3/day$)

| Res.	Component	Original Total	Current Total	Injection	Net Reaction	Net heat lost
I	CH_4 *(gmol)*	3.3192×10^6	3.3192×10^6	0.0	0.0	-
	CO_2 *(gmol)*	2.2866×10^2	3.2788×10^6	5.000×10^6	-1.7217×10^6	-
	H_2O *(gmol)*	3.9873×10^8	3.8883×10^8	0.0	-9.8998×10^6	-
	$CO_2.nH_2O$*(gmol)*	0.0	1.7217×10^6	-	8.7177×10^5	-
	Enegry *(J)*	-8.7609×10^{11}	-8.0722×10^{11}	-4.3291×10^9	8.9284×10^{10}	-1.6092×10^{10}
II	CH_4 *(gmol)*	3.8724×10^6	3.8724×10^6	0.0	0.0	-
	CO_2 *(gmol)*	2.2866×10^6	3.5810×10^6	5.0591×10^6	-1.4147×10^6	-
	H_2O *(gmol)*	4.6519×10^8	4.5704×10^8	0.0	-8.1348×10^6	-
	$CO_2.nH_2O$*(gmol)*	0.0	1.4147×10^6	-	7.1278×10^5	-
	Enegry *(J)*	-9.1228×10^{11}	-8.5289×10^{11}	-4.3802×10^9	7.3366×10^{10}	-9.0419×10^9
III	CH_4 *(gmol)*	2.7660×10^6	2.7660×10^6	0.0	0.0	-
	CO_2 *(gmol)*	2.2866×10^2	2.3587×10^6	3.9842×10^6	-1.6261×10^6	-
	H_2O *(gmol)*	3.3228×10^8	3.2292×10^8	0.0	-9.3505×10^6	-
	$CO_2.nH_2O$*(gmol)*	0.0	1.6261×10^6	-	8.4250×10^5	-
	Enegry *(J)*	-8.3989×10^{11}	-7.7866×10^{11}	-3.4496×10^9	8.4230×10^{10}	-1.9651×10^{10}
IV	CH_4 *(gmol)*	2.7660×10^6	2.7660×10^6	0.0	0.0	-
	CO_2 *(gmol)*	2.2866×10^2	2.1636×10^6	3.7768×10^6	-1.5952×10^6	-
	H_2O *(gmol)*	3.3228×10^8	3.2310×10^8	0.0	-9.1724×10^6	-
	$CO_2.nH_2O$*(gmol)*	0.0	1.5952×10^6	-	8.3463×10^5	-
	Enegry *(J)*	-8.1595×10^{11}	-7.5239×10^{11}	-3.2700×10^9	8.2723×10^{10}	-1.5895×10^{10}

Note: CO_2 injection rate, $q = 200\ m^3/day$, was starting to decline when the well pressure increased to the maximum bottom hole constraint of *5,000 kPa*.

Advanced Numerical Simulation of CO_2 Hydrate Formation
In Geological Reservoirs by Injection of CO_2 Gas   [30]
May, 2006

ALBERTA
RESEARCH
COUNCIL

Table 8: Hydro-geochemical parameters

Component	Alberta		Mallik Site (5L-38)
	Carbonate reservoir	Sandstone reservoir	
Formation water	*Conc. (mg/L)*	*Conc. (mg/L)*	*Conc. (mg/L)*
Na$^+$	20,000 - 45,000	30,000 - 45,000	2,300 – 19,000
Ca^{++}	3,000 - 10,000	2,000 - 7,000	40 – 2,800
Mg^{++}	750 – 2500	500 – 1750	24 – 4,900
Cl$^-$	(35/24)Na$^+$	(35/24)Na$^+$	(35/24)Na$^+$
HCO$_3^-$	100 - 1,000	100 - 1,000	?
pH	5.5 – 7.5	5.5 – 7.5	5.5 – 7.5
CO$_3^{--}$	(HCO$_3^{--}$/H$^+$)*10$^{-8.48}$	(HCO$_3^-$/H$^+$)*10$^{-8.48}$	?
SiO$_2$ (aq)	1.0x10^{-5}	1.0x10^{-5}	?
Total salinity *(part per thousand)*	1 - 200	1 - 200	1 – 50
Mineral	*Conc. (Vol. fraction)*	*Conc. (Vol. fraction)*	*Conc. (Vol. fraction)*
Calcite (CaCO$_3$)	20 - 100	0 - 10	0 – 10 (?)
Dolomite (Ca(MgCO$_3$)$_2$)	0 - 80	0 - 5	0 – 5 (?)
Feldspar	0 - 4	0 - 30	0 – 30 (?)
Kaolinite	0 - 10	0 - 20	0 – 20 (?)
INERT (Others)	0 - 10	0 - 100	0 – 100 (?)

Advanced Numerical Simulation of CO$_2$ Hydrate Formation
In Geological Reservoirs by Injection of CO$_2$ Gas   [31]
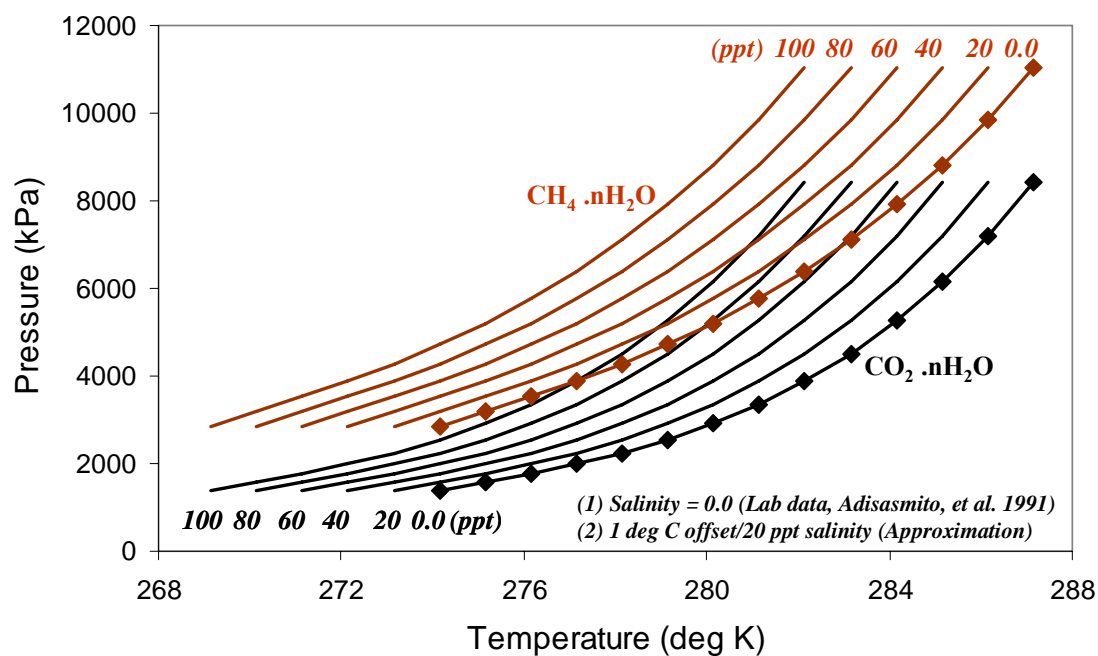May, 2006

ALBERTA
RESEARCH
COUNCIL

$$\text{Curve – II} \quad / \quad P = \frac{27.0716-0.3742(T)+0.00132(T^2)}{1-0.01102(T)+4.1573 \times 10^{-5}(T^2)-5.3182 \times 10^{-8}(T^3)}$$

$$\text{Curve – IV} \quad / \quad P = \frac{27.0716-0.3742(T)+0.00132(T^2)}{1-0.01102(T)+4.1573 \times 10^{-5}(T^2)-5.3182 \times 10^{-8}(T^3)}$$
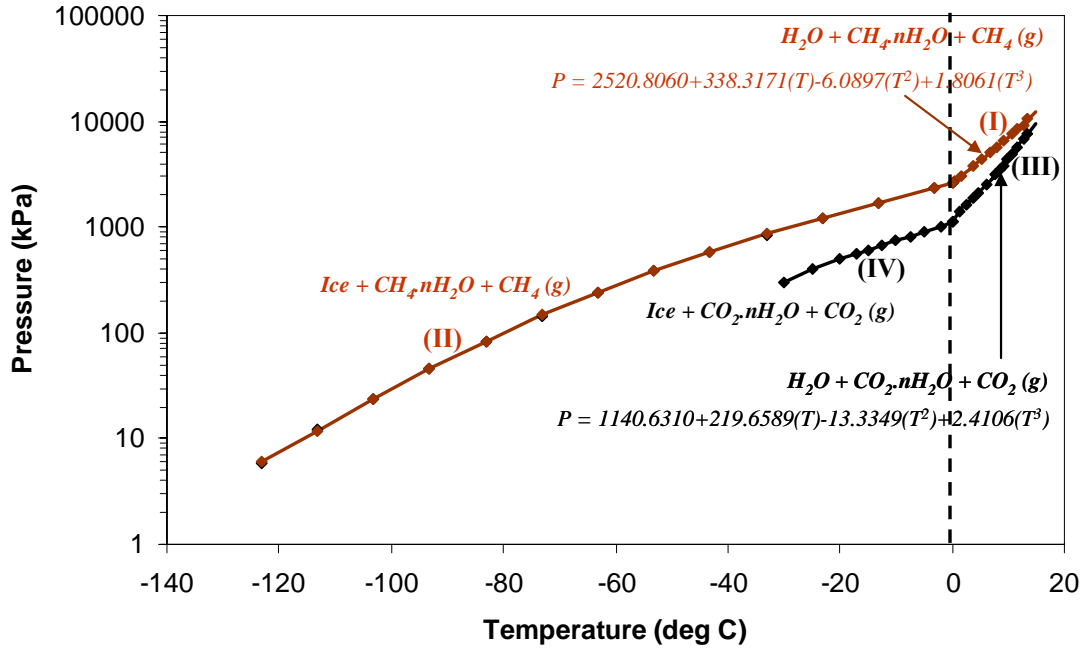
Note : Temperature (T) in degree K for the fitted curves (I, II, III and IV)

Figure 1: **CH$_4$- and CO$_2$ hydrates stability curves for above freezing point** *(water-hydrate-gas system)* **and below freezing point** *(ice-hydrate-gas system)* **(data sources: Adisasmito** *et al.* **1991, North** *et al.* **1998 and Moridis** *et al.* **2003)**

Advanced Numerical Simulation of CO₂ Hydrate Formation
In Geological Reservoirs by Injection of CO₂ Gas   [32]
May, 2006

ALBERTA
RESEARCH
COUNCIL

Figure 2: **CH$_4$ - and CO$_2$ hydrates stability curves for above freezing point** *(water-hydrate-gas system)* **(Pore-water salinity in parts per thousand** *(ppt)***) (Based on Wright** *et al.* **2005a, stability curves were shifted** *1 degree C* **per** *20 ppt* **salinity)**

Advanced Numerical Simulation of CO₂ Hydrate Formation
In Geological Reservoirs by Injection of CO₂ Gas   [33]
May, 2006

ALBERTA
RESEARCH
COUNCIL

Fitted Curves, K = (a/p) exp(b/T-c)

$CH_4 .nH_2O:$
$\quad\quad a = 1.617x10^9\ kPa$
$\quad\quad b = -1414.909\ ^0C$
$\quad\quad c = -105.250\ ^0C$

$CO_2 .nH_2O:$
$\quad\quad a = 3.1289x10^9\ kPa$
$\quad\quad b = -1406.607\ ^0C$
$\quad\quad c = -94.460\ ^0C$

$H_2O+CH_4.nH_2O+CH_4(g)$
$H_2O+CO_2.nH_2O+CO_2(g)$
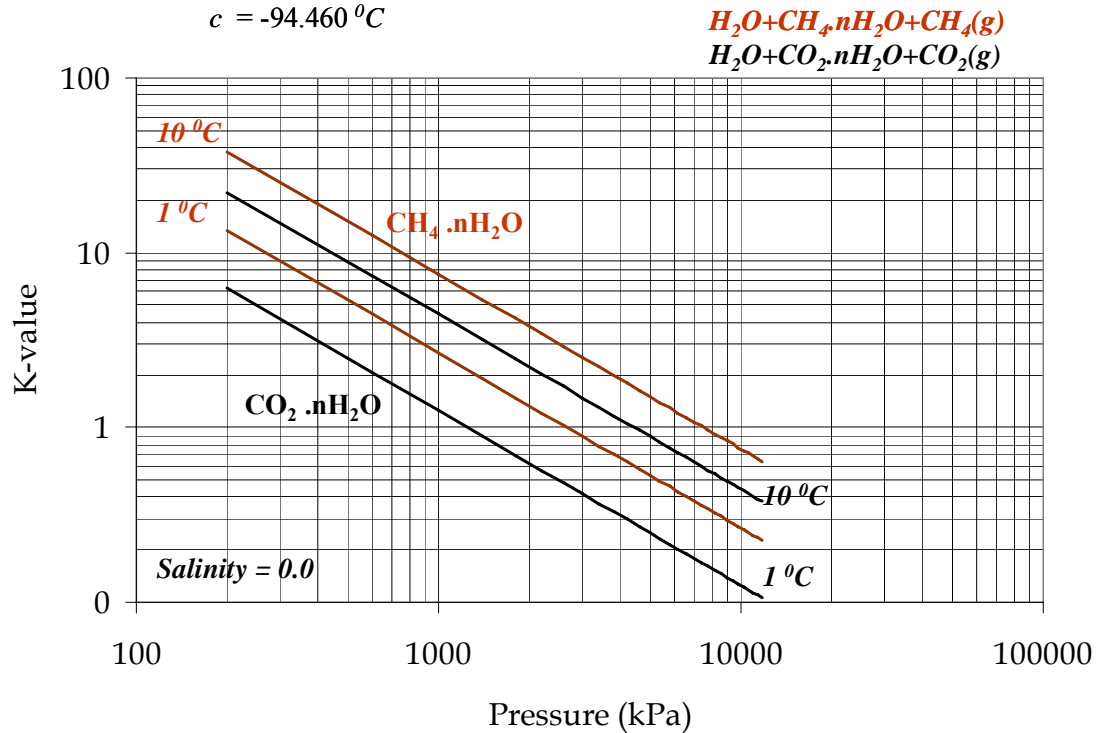
Figure 3: *K*-value curves for CH_4- and CO_2 hydrates stability at temperatures 1 and 10 ^0C for above freezing point *(water-hydrate-gas system)* (K (p, T) = p_e/p, p_e = hydrate equilibrium pressure) (Depending on grid cell *pressure-temperature-salinity-gas composition*, the gas hydrate model interpolates *K value* from the prescribed gas hydrate stability curves)

Advanced Numerical Simulation of CO₂ Hydrate Formation
In Geological Reservoirs by Injection of CO₂ Gas   [34]
May, 2006

ALBERTA
RESEARCH
COUNCIL
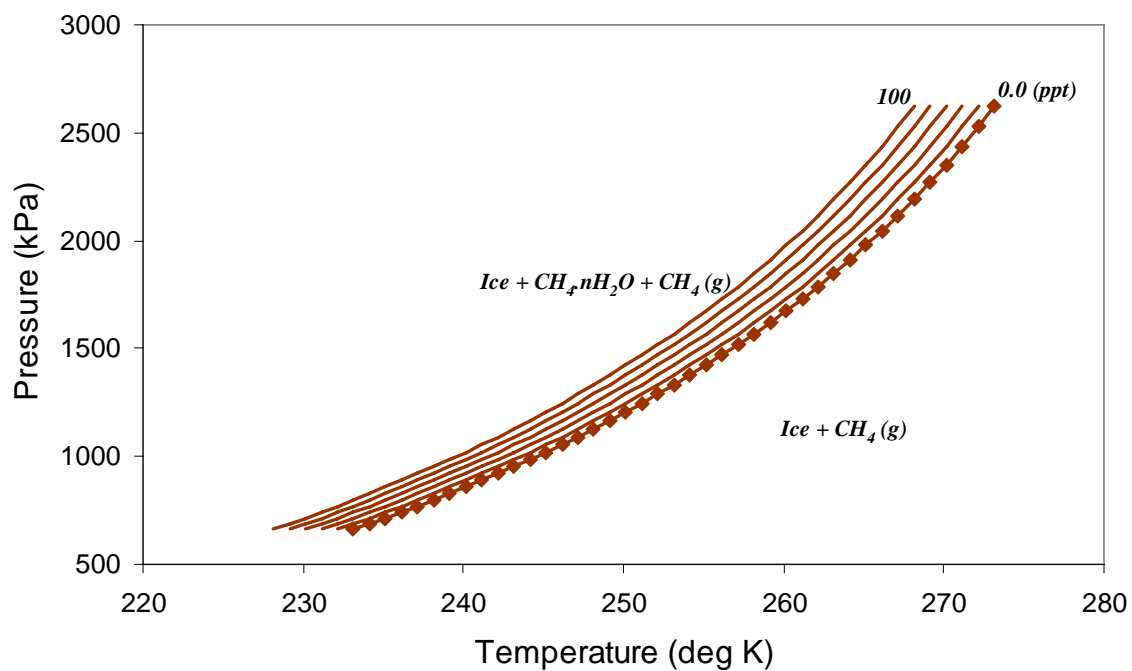
Figure 4: **CH$_4$ gas stability curves for below freezing point** *(ice-hydrate-gas system)* **(Pore-water salinity in parts per thousand (*ppt*))**
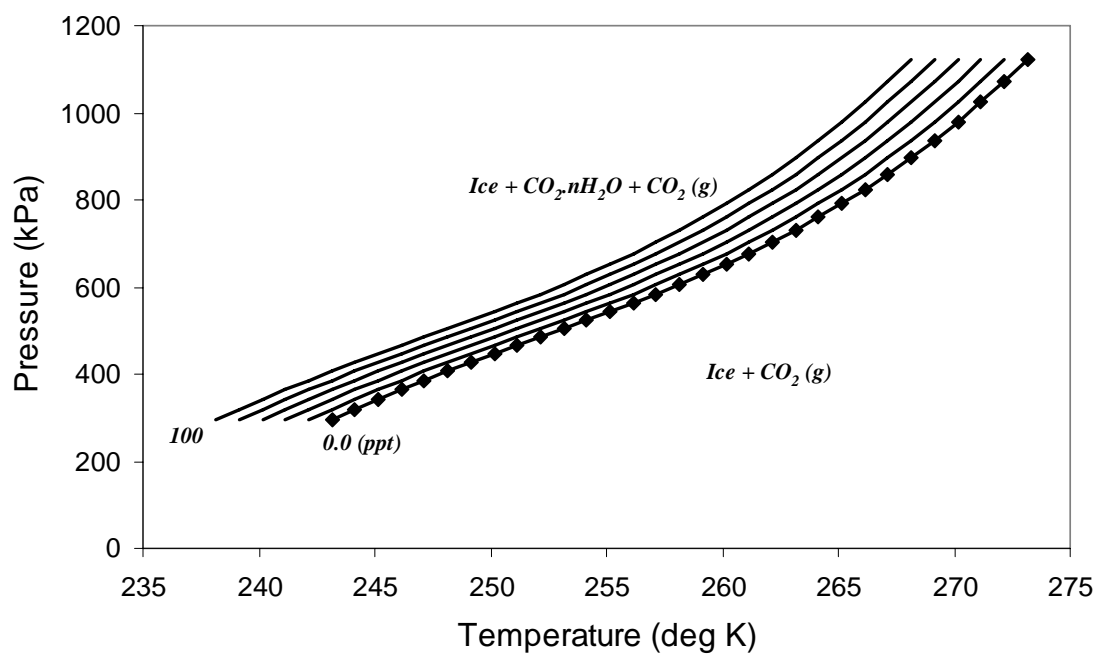
Figure 5: **CO$_2$ gas stability curves for below freezing point** *(ice-hydrate-gas system)* **(Pore-water salinity in parts per thousand (***ppt***))**
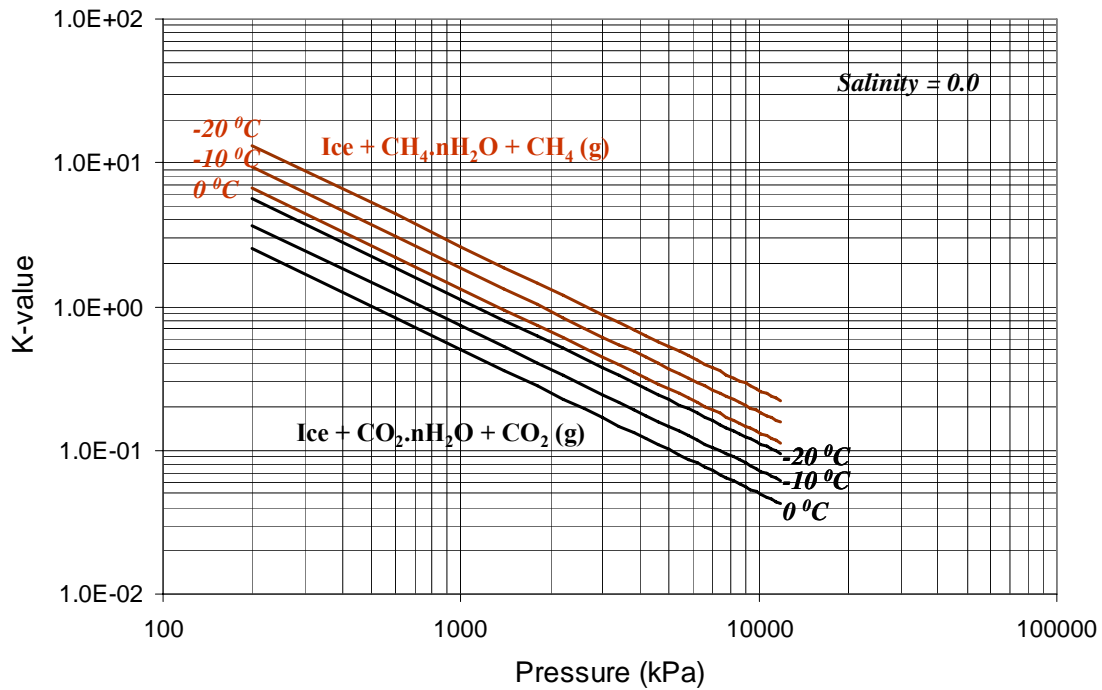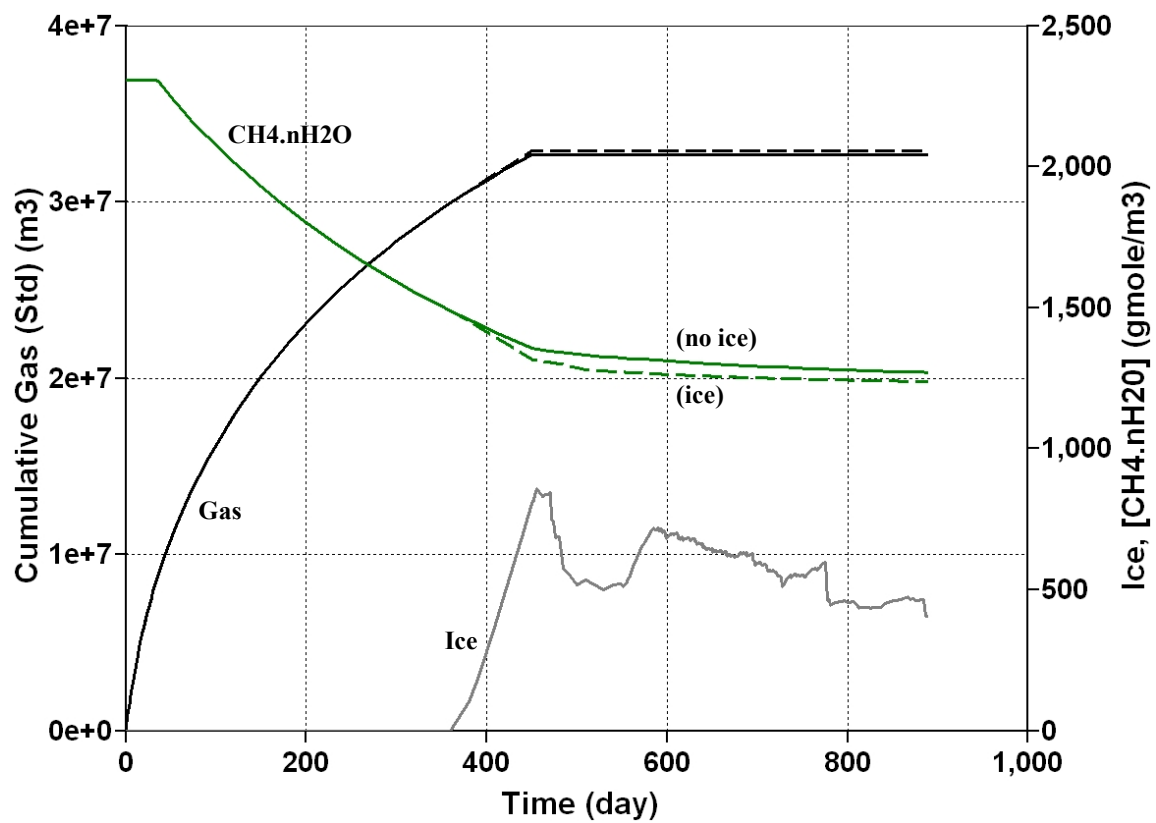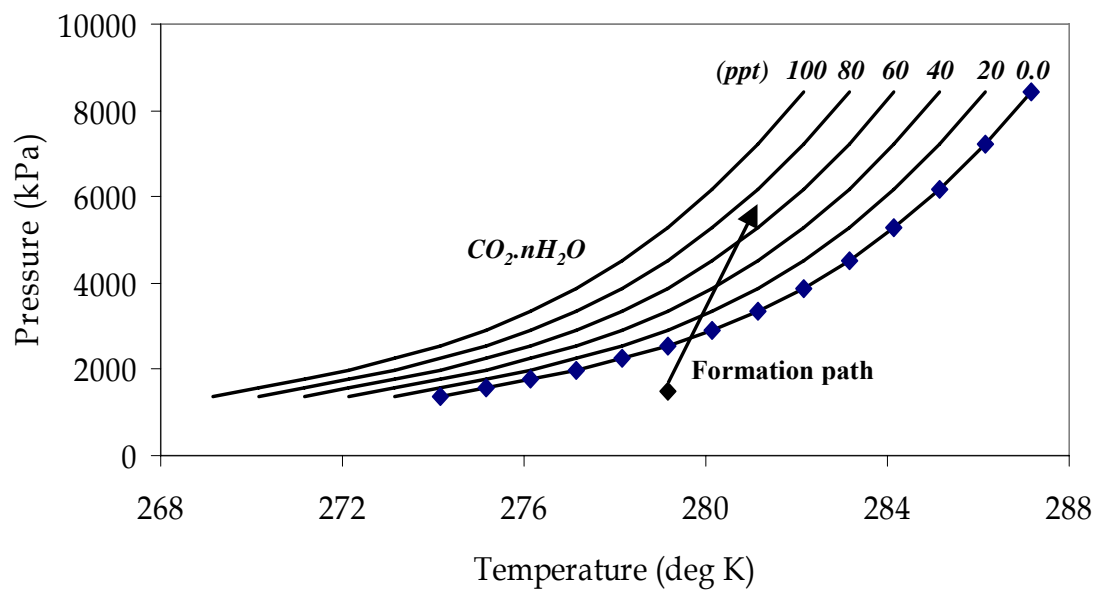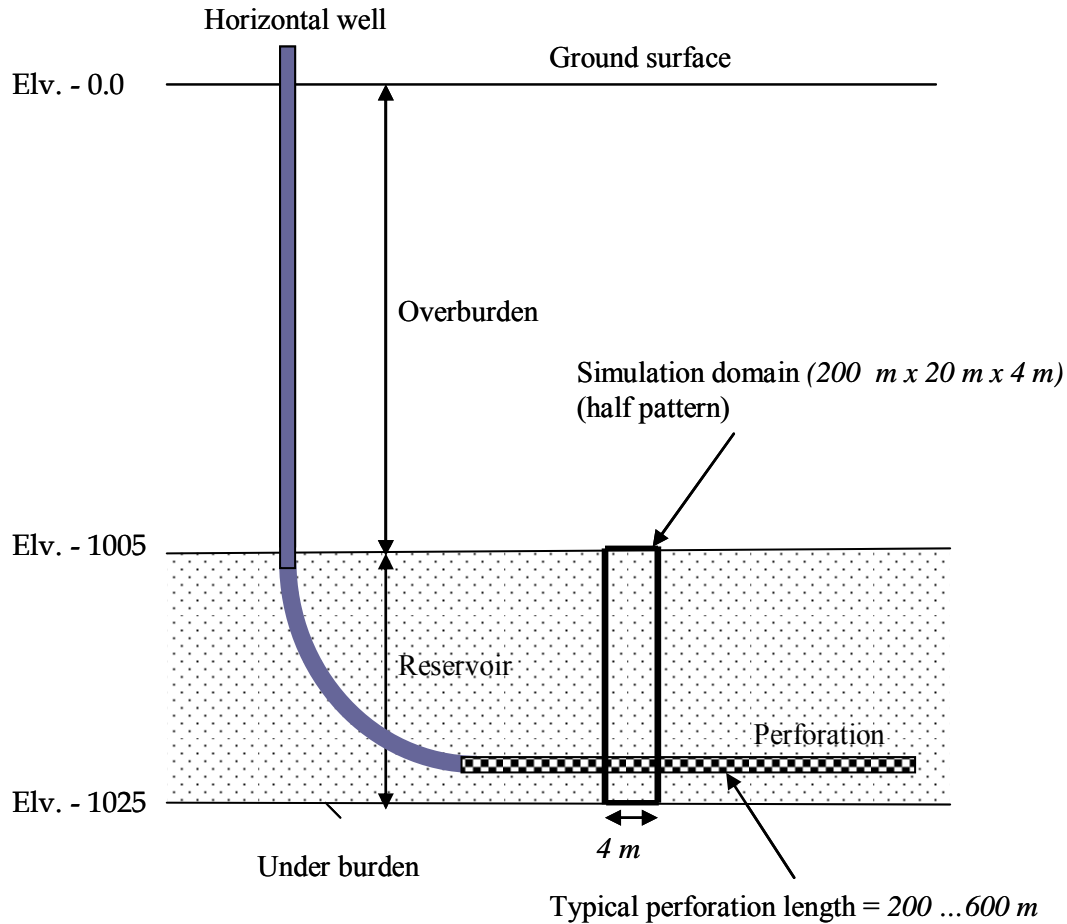
Figure 6: *K*-value curves for CH_4- and CO_2 hydrates stability at temperatures 0, -10 and -20 ^0C for below freezing point *(ice-hydrate-gas system)* $(K\ (p,\ T) = p_e/p,\ p_e =$ hydrate equilibrium pressure) (Depending on grid cell *pressure-temperature-salinity-gas composition*, the gas hydrate model interpolates *K value* from the prescribed gas hydrate stability curves)

Advanced Numerical Simulation of CO_2 Hydrate Formation
In Geological Reservoirs by Injection of CO_2 Gas   [37]
May, 2006

ALBERTA
RESEARCH
COUNCIL

Figure 7:   History Plots for Methane-Hydrate Decomposition with Ice Formation (Prototype Radial Model)

Figure 8: **CO₂ hydrate stability curves** *(water-hydrate-gas system)* **and hydrate formation path (CO₂ hydrate formation induced by the injection of CO₂ gas)**

Figure 9: Setup numerical flow system *(200 m x 20 m x 4 m)* - CO_2 hydrate formation in the 20 *m* thick generic reservoirs by injecting CO_2 gas

Numerical Setup:
1)   *Half pattern – 200 m x 20 m x 4 m*
2)   *Grid blocks – 200 x 40 x 4*

Numerical Studies:
1)   *Well bore modeling*
2)   *Overburden – under burden heat transfer*
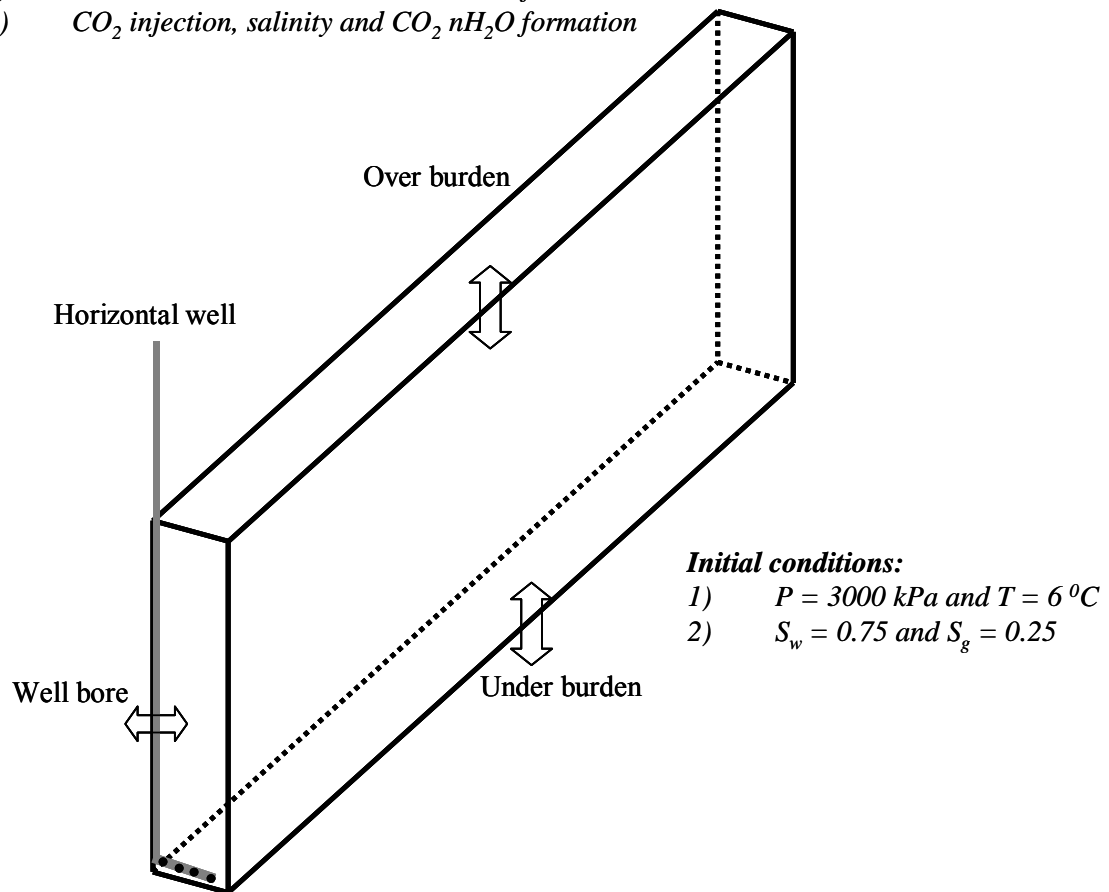3)   *CO_2 injection, salinity and CO_2 nH_2O formation*

Figure 10: Half pattern *(200 m x 20 m x 4 m)* numerical flow system – Initial and boundary conditions
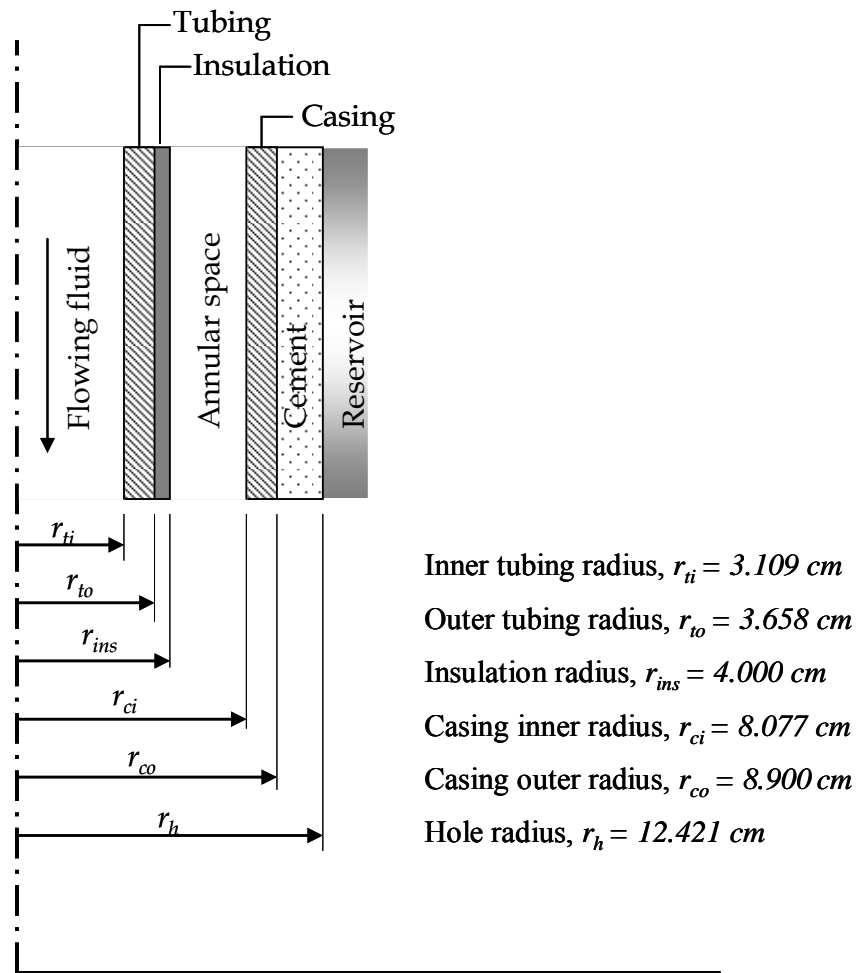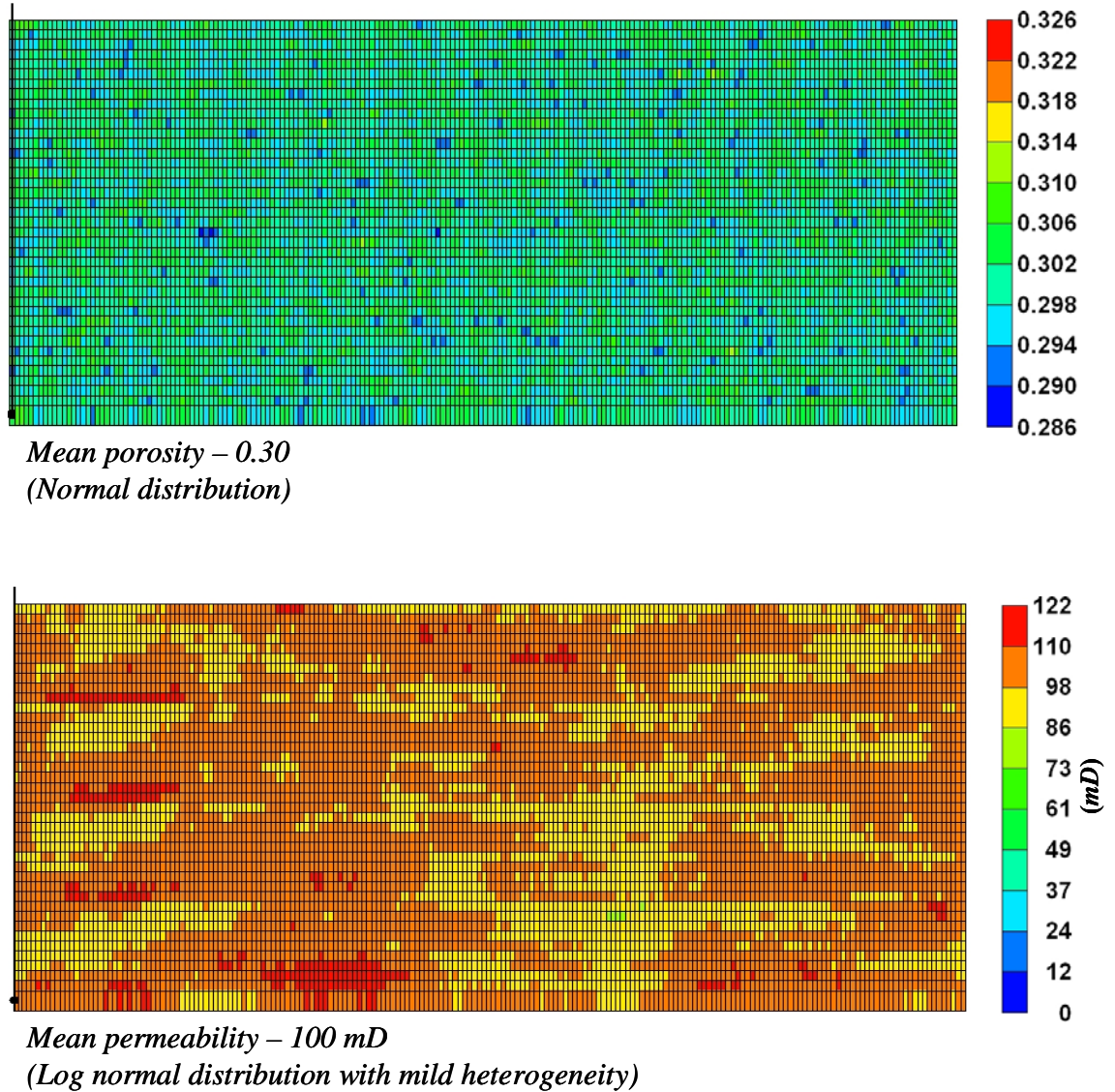
Inner tubing radius, $r_{ti} = 3.109\ cm$

Outer tubing radius, $r_{to} = 3.658\ cm$

Insulation radius, $r_{ins} = 4.000\ cm$

Casing inner radius, $r_{ci} = 8.077\ cm$

Casing outer radius, $r_{co} = 8.900\ cm$

Hole radius, $r_h = 12.421\ cm$

Figure 11: Well bore data

Generic Reservoir – I
Half pattern – 200 m x 20 m x 4 m

Mean porosity – 0.30
(Normal distribution)

Mean permeability – 100 mD
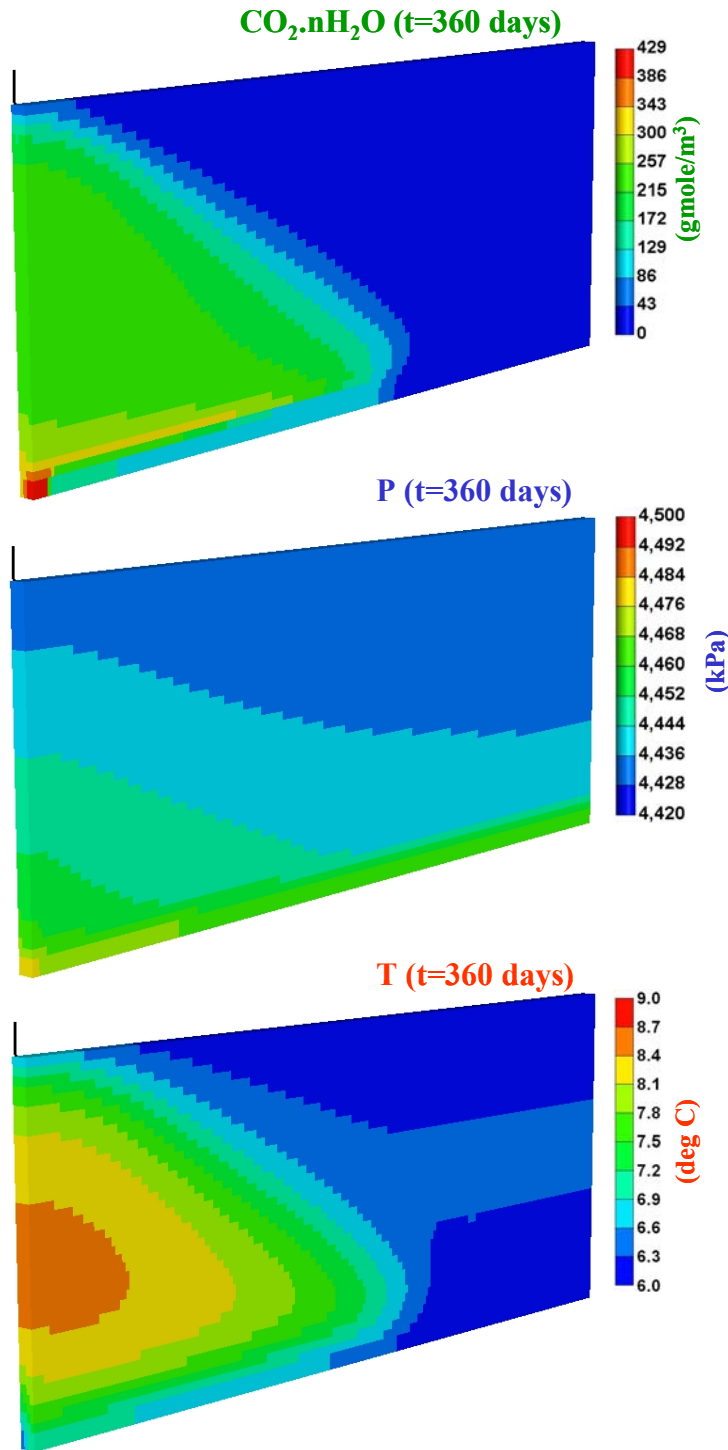*(Log normal distribution with mild heterogeneity)*

Figure 12: Porosity and permeability distributions for generic reservoir I: Mallik silt, mean permeability, k_0 = 100 mD and mean porosity, ϕ = 0.30 (Permeability is log-normally distributed with mild heterogeneity, porosity is normally distributed)
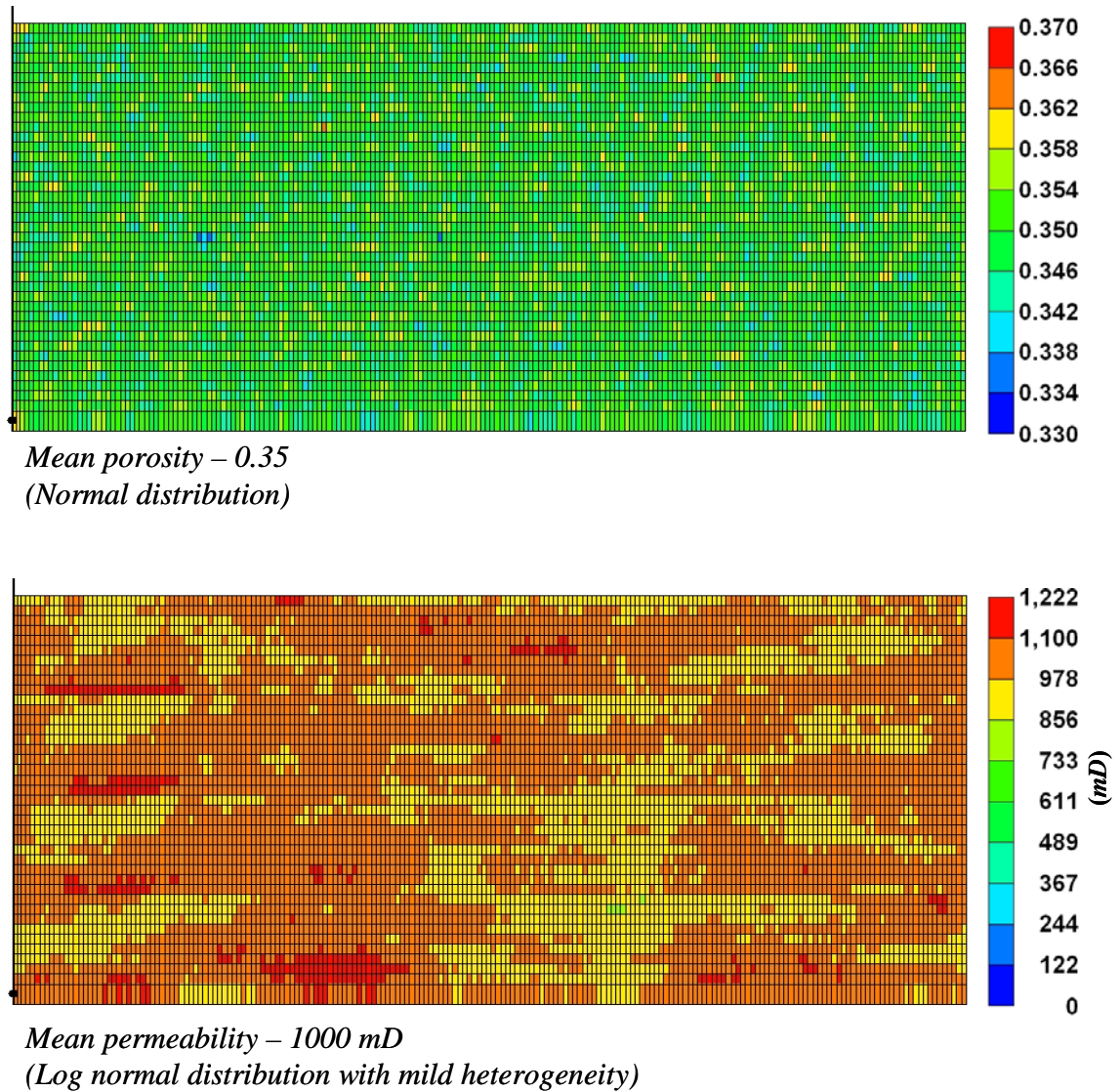
ALBERTA
RESEARCH
COUNCIL
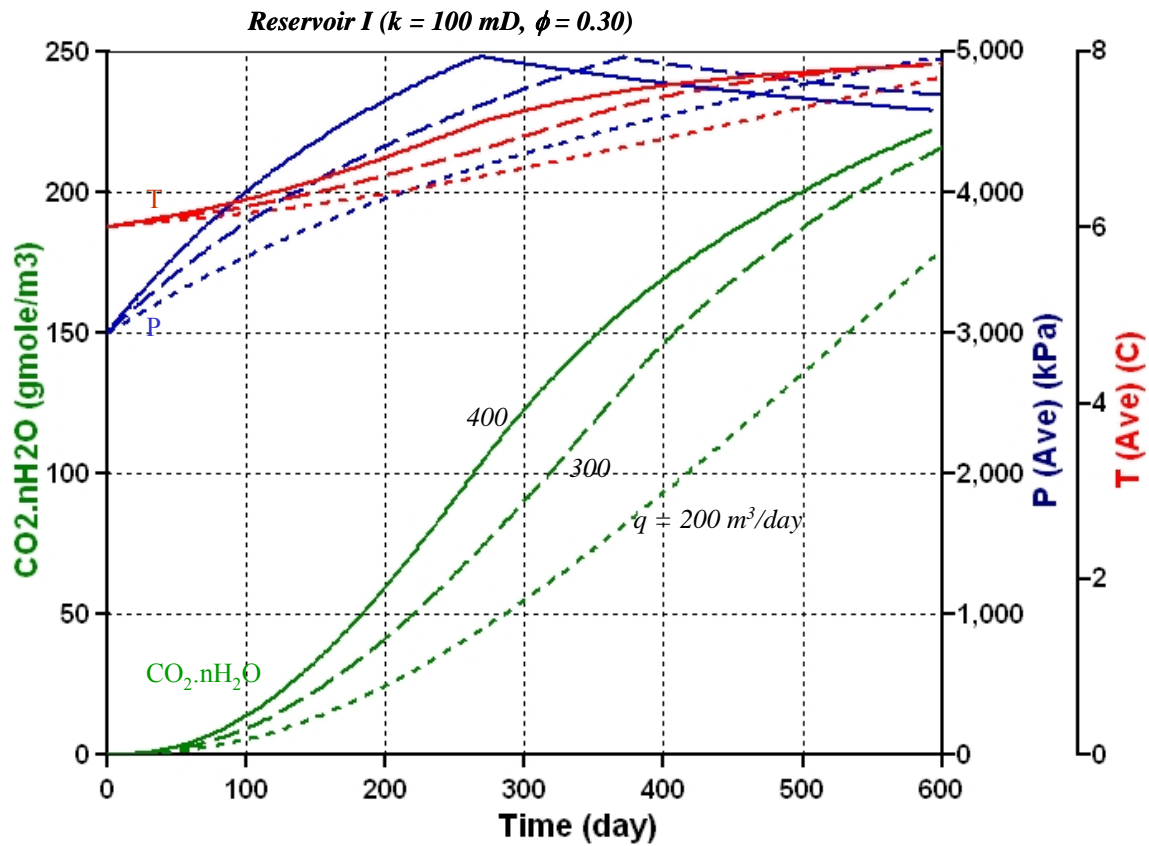
Figure 13: *Sensitivity of gas injection rate:* **Average field pressure (P), temperature (T) and CO₂ hydrate concentration (CO₂.nH₂O) at the CO₂ vapor injection rates, q = 200, 300 and 400 m^3/day (std) with a maximum bottom hole pressure constraint of 5000 kPa (Reservoir I: Mallik silt, mean permeability, k_0 = 100 mD, mean porosity, ϕ = 0.30, salinity = 0.0) (Hydrate saturation, S_H = Concentration (c_h)/Volumetric mole density (ρ))**
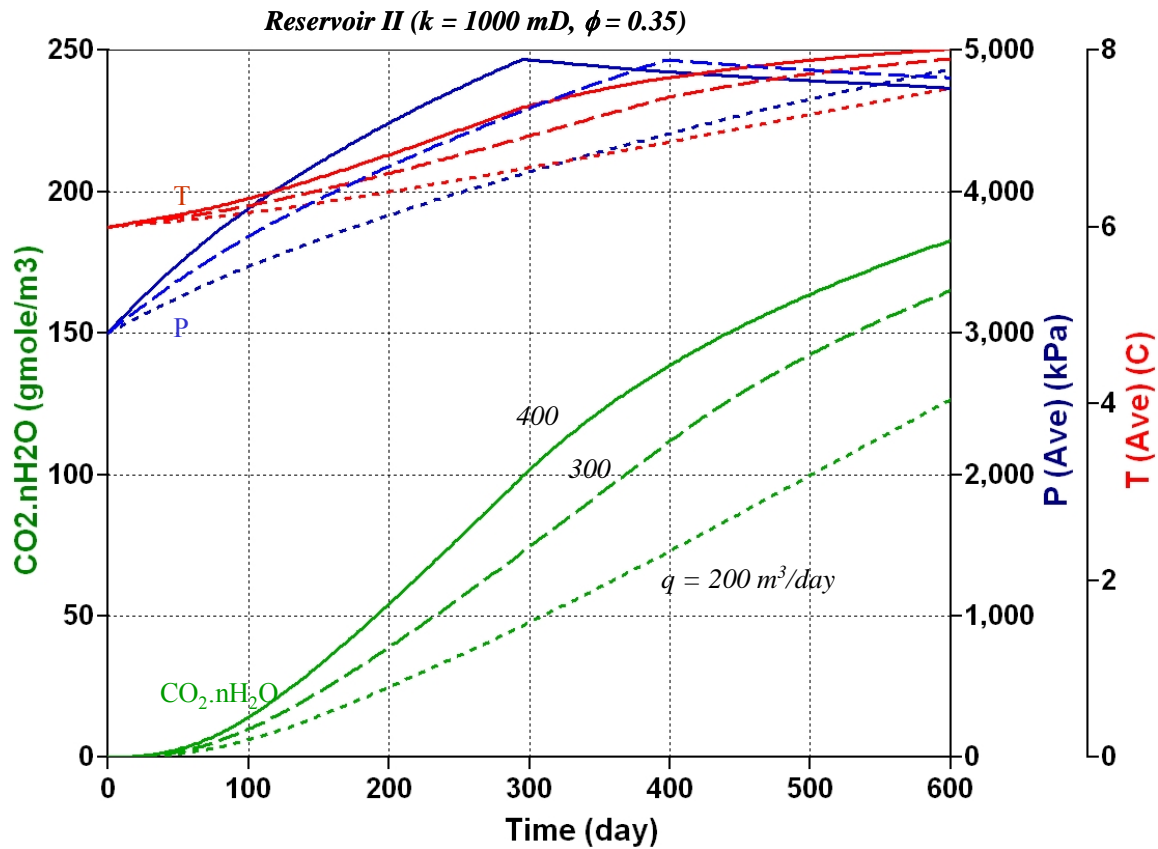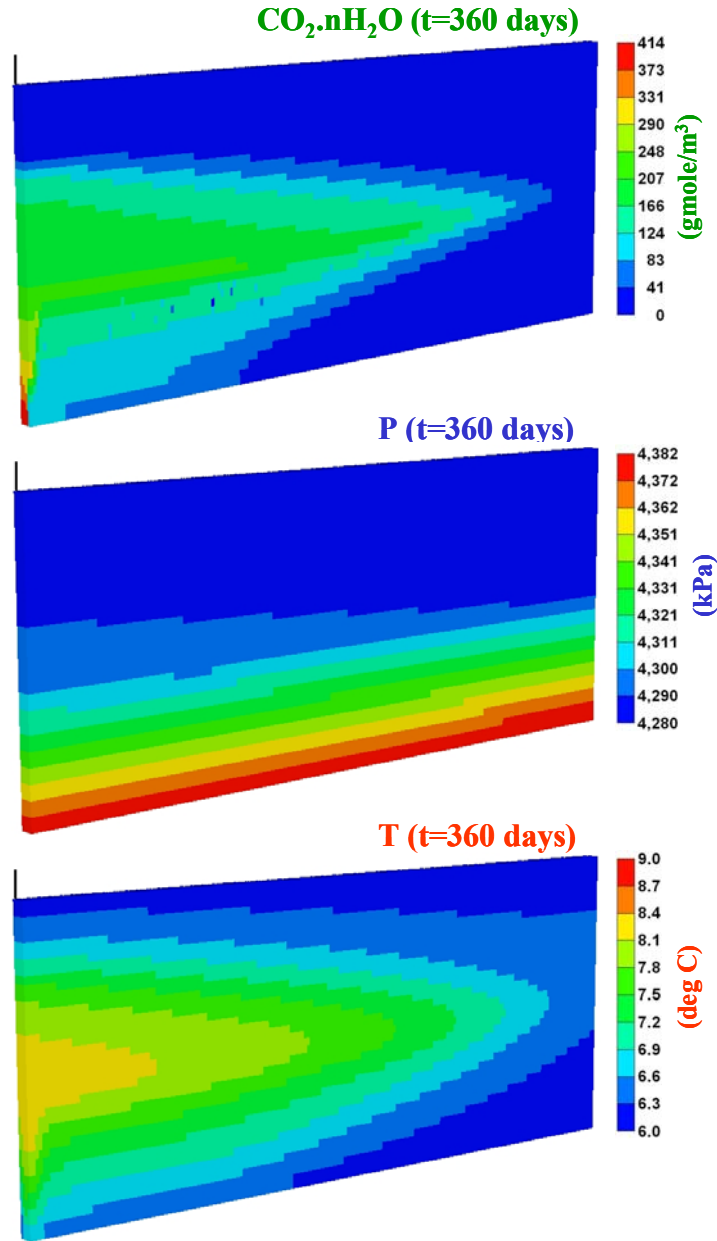
Figure 14: *Spatial variation*: **Average CO₂ hydrate concentration** *(CO₂.nH₂O)* **and pressure-temperature conditions at the end of time,** *t* **= 360** *days* **for CO₂ vapor injection rates,** *q* **= 200** *m³/day (std)* **(Reservoir I: Mallik silt, mean permeability,** *k₀* **= 100** *mD***, mean porosity,** *ϕ* **= 0.30, salinity = 0.0) (Hydrate saturation,** *S_H* **= Concentration** *(c_h)***/Volumetric mole density** *(ρ)***)**

Advanced Numerical Simulation of CO₂ Hydrate Formation
In Geological Reservoirs by Injection of CO₂ Gas   [45]
May, 2006

ALBERTA
RESEARCH
COUNCIL

Generic Reservoir – II
Half pattern – 200 m x 20 m x 4 m

Mean porosity – 0.35
(Normal distribution)

Mean permeability – 1000 mD
(Log normal distribution with mild heterogeneity)

Figure 15: Porosity and permeability distributions for generic reservoir II: Mallik sand, mean permeability, k_0 = 1000 mD and mean porosity, ϕ = 0.35 (Permeability is log-normally distributed with mild heterogeneity, porosity is normally distributed)

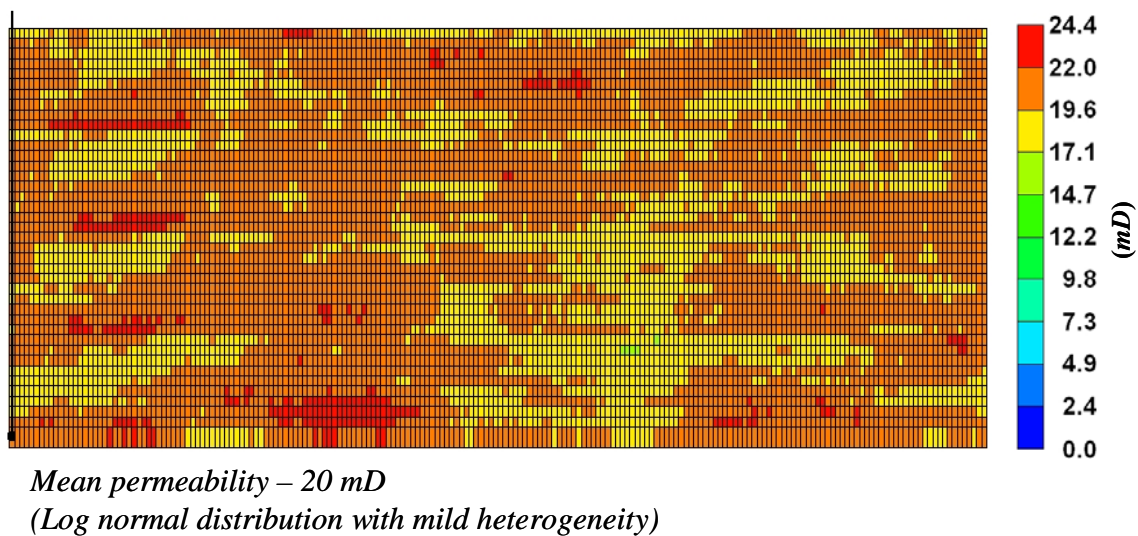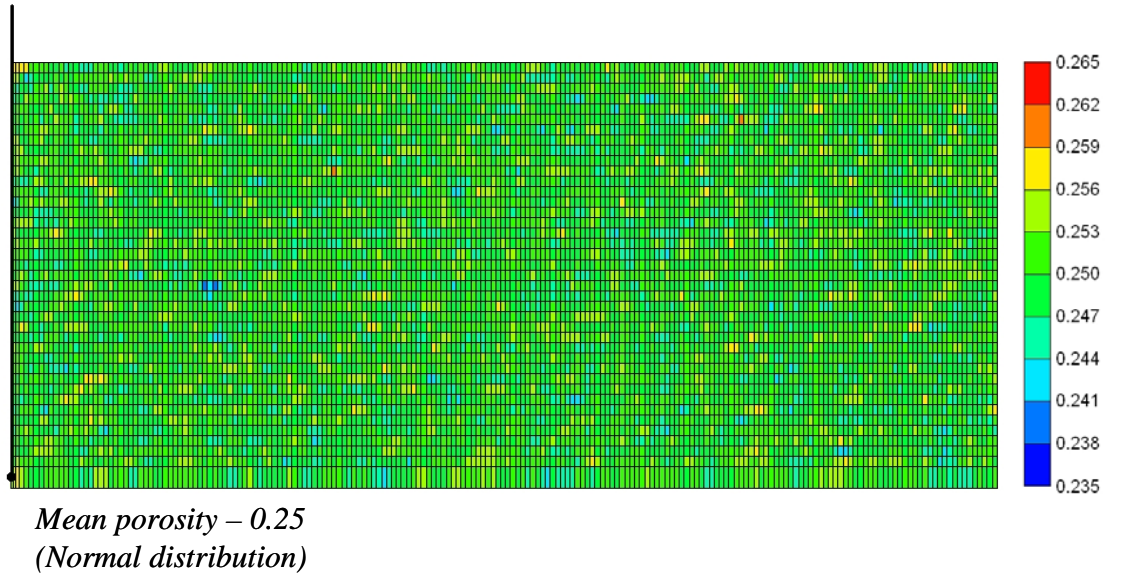**Figure 16***: Sensitivity of gas injection rate:* **Average field pressure** *(P)*, **temperature** *(T)* **and CO₂ hydrate concentration** *(CO₂.nH₂O)* **at the CO₂ vapor injection rates, q = 200, 300 and 400** *m³/day (std)* **with a maximum bottom hole pressure constraint of 5000** *kPa* **(Reservoir II: Mallik sand, mean permeability,** k_0 **= 1000** *mD*, **mean porosity,** ϕ **= 0.35, salinity = 0.0) (Hydrate saturation,** S_H **= Concentration** (c_h)/**Volumetric mole density** (ρ)**)**

Advanced Numerical Simulation of CO₂ Hydrate Formation
In Geological Reservoirs by Injection of CO₂ Gas   [47]
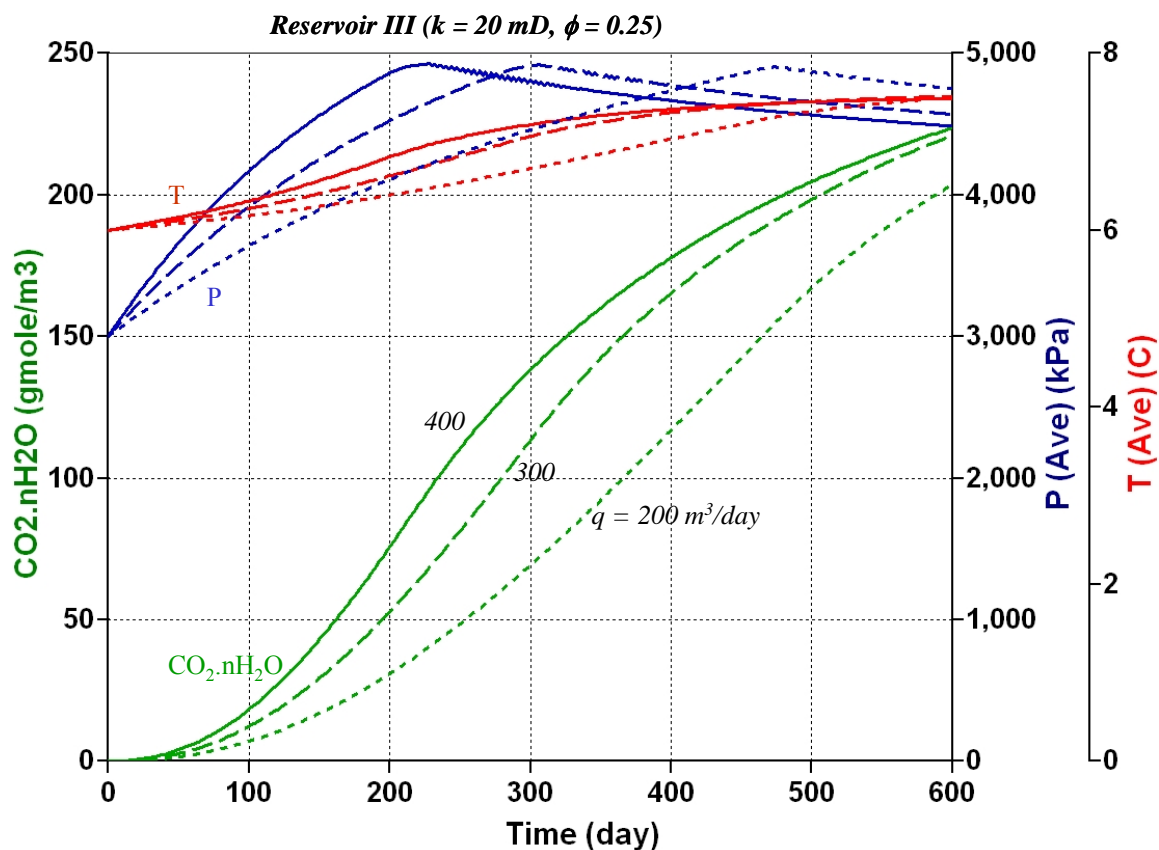May, 2006

ALBERTA
RESEARCH
COUNCIL

Figure 17: *Spatial variation*: **Average CO_2 hydrate concentration $(CO_2.nH_2O)$ and pressure-temperature conditions at the end of time, t = 360 *days* for CO_2 vapor injection rates, q = 200 *m³/day (std)* with maximum bottom hole pressure constraint of 5000 kPa (Reservoir II: Mallik sand, mean permeability, k_0 = 1000 *mD*, mean porosity, ϕ = 0.35, salinity = 0.0) (Hydrate saturation, S_H = Concentration (c_h)/Volumetric mole density (ρ))**
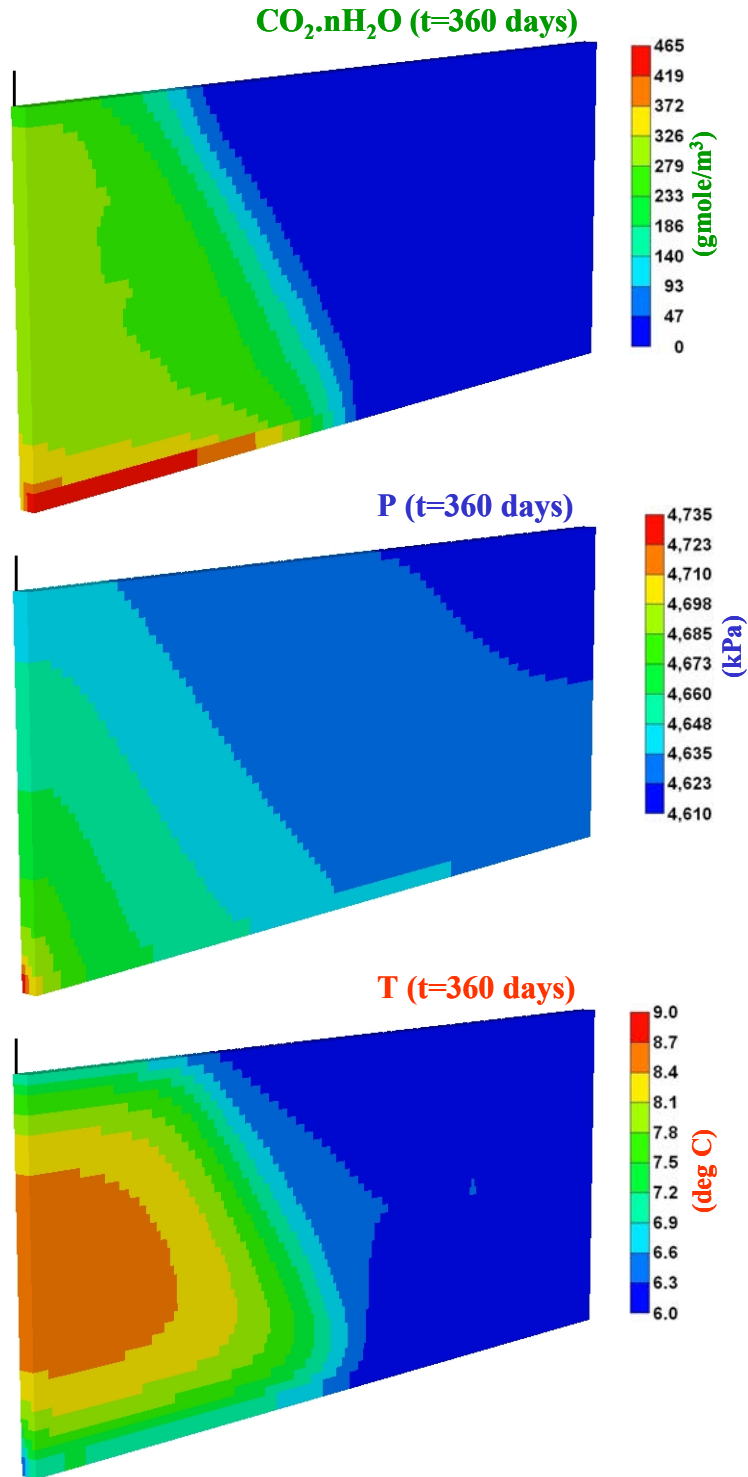
Advanced Numerical Simulation of CO_2 Hydrate Formation
In Geological Reservoirs by Injection of CO_2 Gas   [48]
May, 2006

ALBERTA
RESEARCH
COUNCIL

Generic Reservoir – III
Half pattern – 200 m x 20 m x 4 m

Mean porosity – 0.25
(Normal distribution)

Mean permeability – 20 mD
(Log normal distribution with mild heterogeneity)

Figure 18: Porosity and permeability distributions for generic reservoir III: Sandstone, mean permeability, $k_0 = 20$ mD and mean porosity, $\phi = 0.25$ (Permeability is log-normally distributed with mild heterogeneity, porosity is normally distributed)

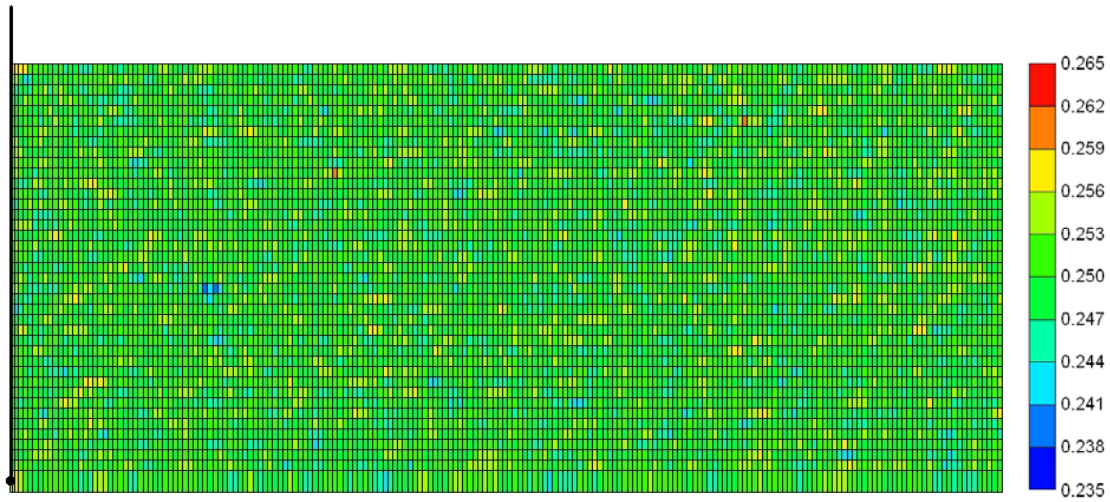Advanced Numerical Simulation of CO₂ Hydrate Formation
In Geological Reservoirs by Injection of CO₂ Gas   [49]
May, 2006

ALBERTA
RESEARCH
COUNCIL

Figure 19: *Sensitivity of gas injection rate:* **Average field pressure *(P)*, temperature *(T)* and CO₂ hydrate concentration *(CO₂.nH₂O)* at the CO₂ vapor injection rates, *q* = 200, 300 and 400 *m³/day (std)* with a maximum bottom hole pressure constraint of 5000 *kPa* (Reservoir III: Sandstone, mean permeability, k_0 = 20 *mD*, mean porosity, ϕ = 0.25, salinity = 0.0) (Hydrate saturation, S_H = Concentration *(cₕ)*/Volumetric mole density *(ρ)*)**

Advanced Numerical Simulation of CO₂ Hydrate Formation
In Geological Reservoirs by Injection of CO₂ Gas   [50]
May, 2006

ALBERTA
RESEARCH
COUNCIL

Figure 20: *Spatial variation*: **Average CO₂ hydrate concentration *(CO₂.nH₂O)* and pressure-temperature conditions at the end of time, *t* = 360 *days* for CO₂ vapor injection rates, *q* = 200 *m³/day (std)* with maximum bottom hole pressure constraint of 5000 *kPa* (Reservoir III: Sandstone, mean permeability, k_0 = 20 *mD*, mean porosity, ϕ = 0.25, salinity = 0.0) (Hydrate saturation, S_H = Concentration (c_h)/Volumetric mole density (ρ))**

Advanced Numerical Simulation of CO₂ Hydrate Formation
In Geological Reservoirs by Injection of CO₂ Gas   [51]
May, 2006

ALBERTA
RESEARCH
COUNCIL

Generic Reservoir – IV
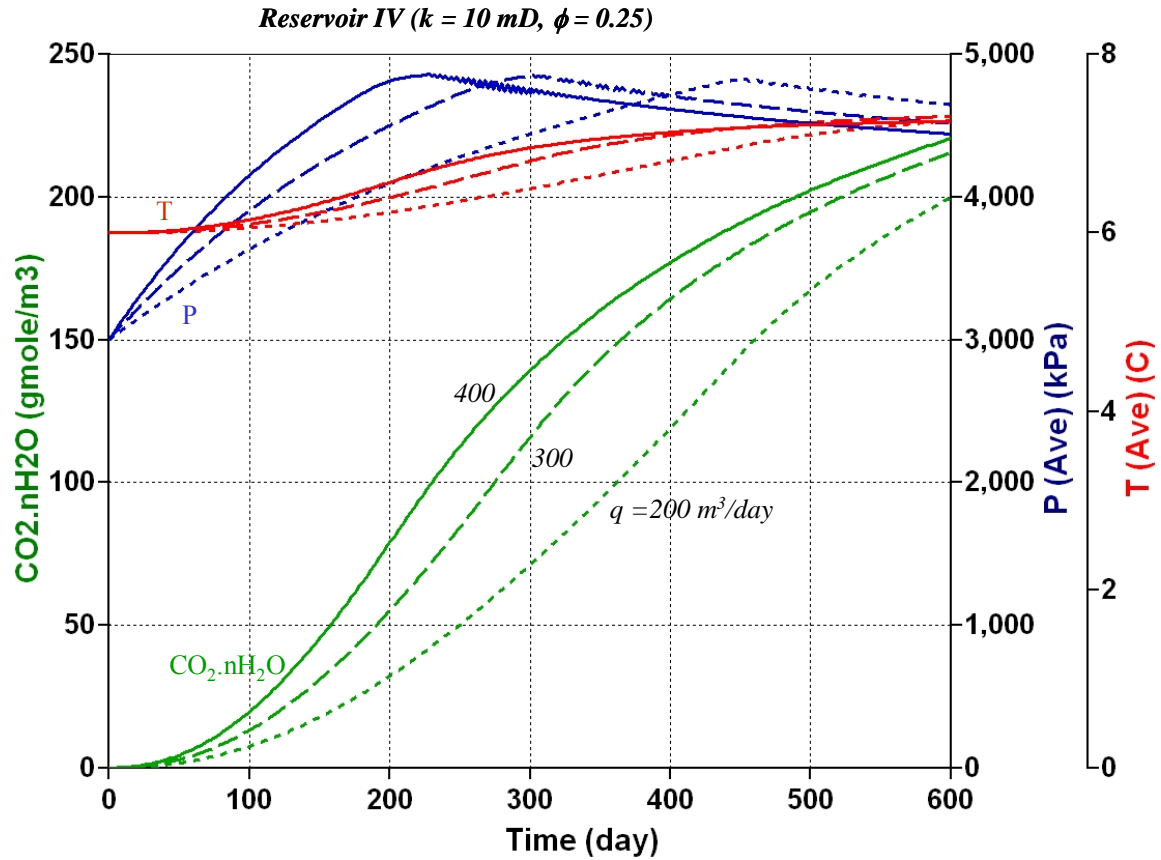*Half pattern – 200 m x 20 m x 4 m*

Mean porosity – 0.25
*(Normal distribution)*
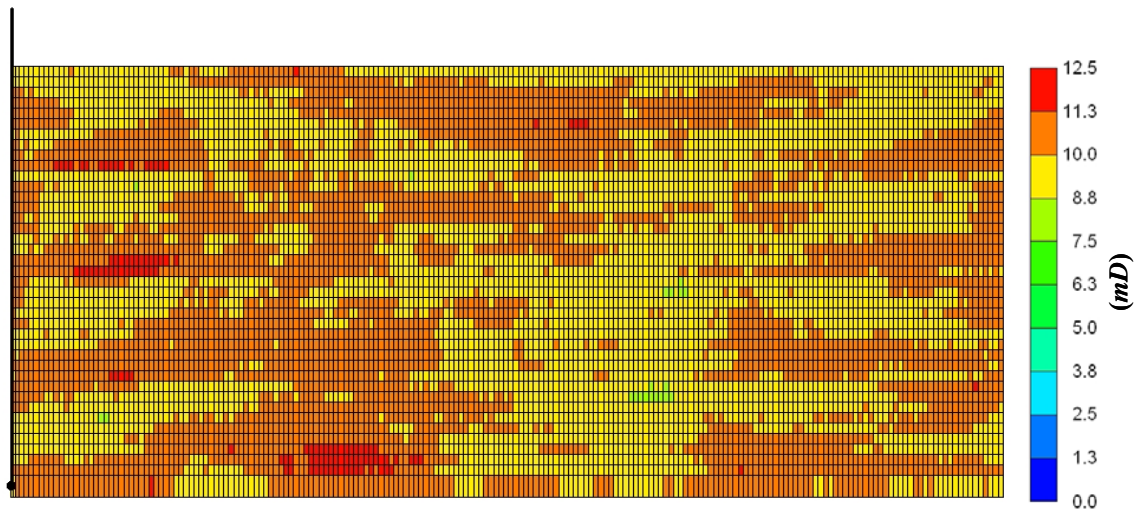
Mean permeability – 10 mD
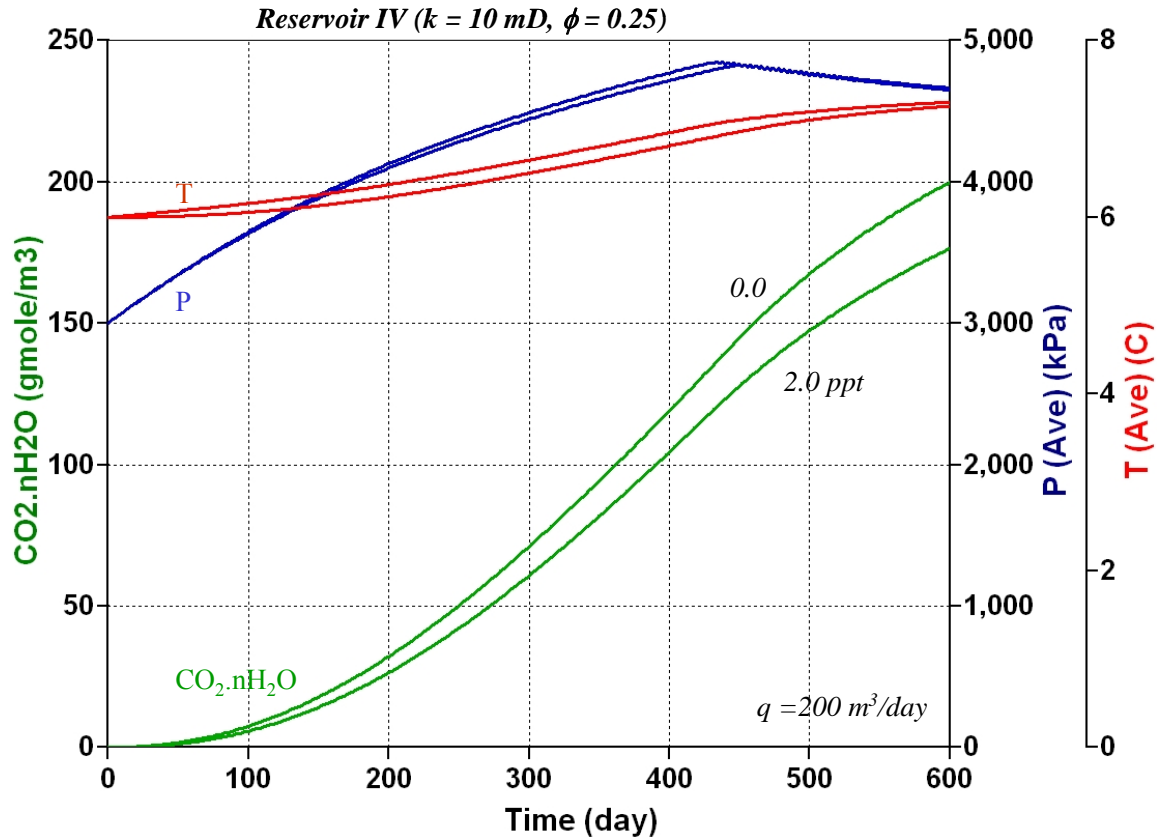*(Log normal distribution with mild heterogeneity)*

Figure 21: Porosity and permeability distributions for generic reservoir IV: Sandstone, mean permeability, k_0 = 10 *mD* and mean porosity, ϕ = 0.25 (Permeability is log-normally distributed with mild heterogeneity, porosity is normally distributed)

Advanced Numerical Simulation of CO₂ Hydrate Formation
In Geological Reservoirs by Injection of CO₂ Gas   [52]
May, 2006

ALBERTA
RESEARCH
COUNCIL

Figure 22: *Sensitivity of gas injection rate:* **Average field pressure** *(P)*, **temperature** *(T)* **and CO₂ hydrate concentration** *(CO₂.nH₂O)* **at the CO₂ vapor injection rates,** *q* **= 200, 300 and 400** *m³/day (std)* **with a maximum bottom hole pressure constraint of 5000** *kPa* **(Reservoir IV: Sandstone, mean permeability,** *k₀* **= 10** *mD*, **mean porosity,** *ϕ* **= 0.25, salinity = 0.0) (Hydrate saturation,** *S_H* **= Concentration** *(c_h)*/**Volumetric mole density** *(ρ)*)
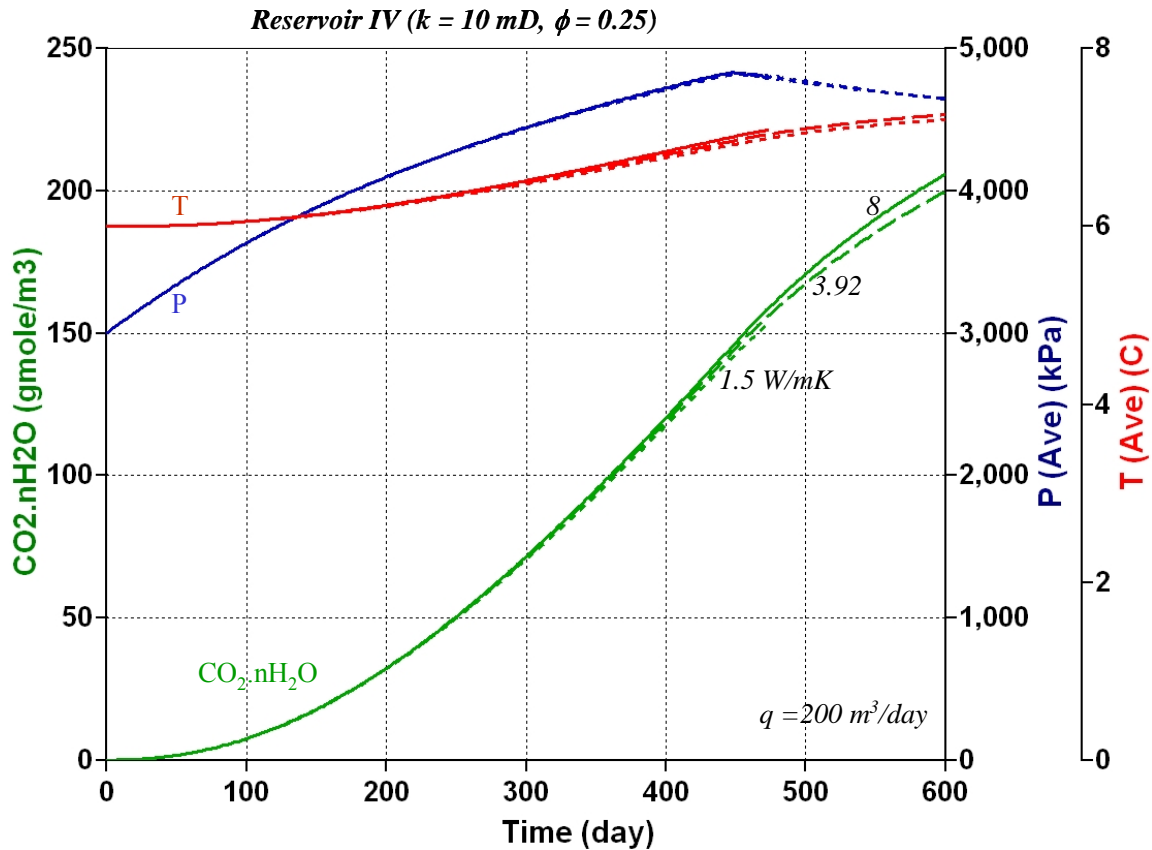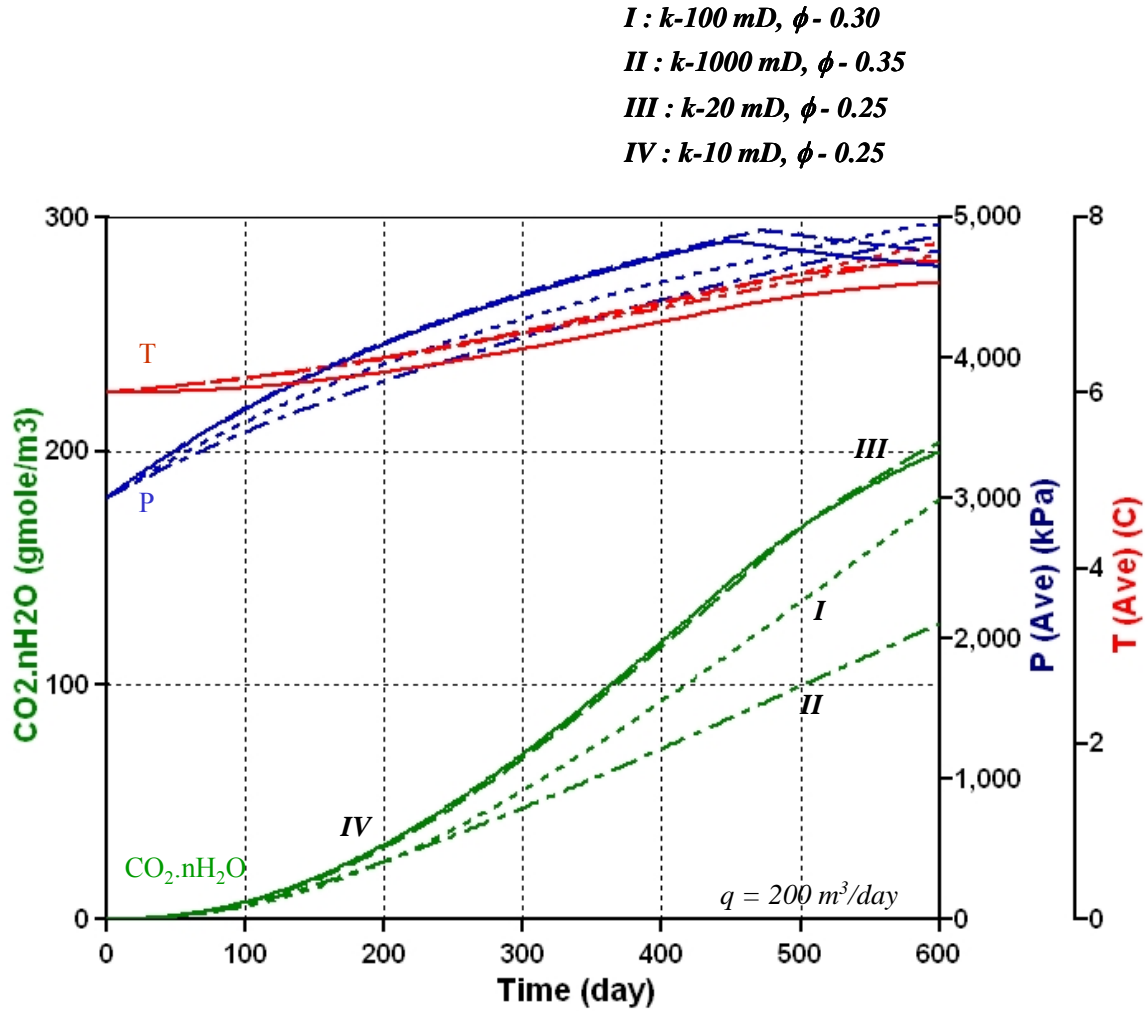
Figure 23: *Sensitivity of rock thermal conductivity:* **Average field pressure *(P)*, temperature *(T)* and CO_2 hydrate concentration *($CO_2.nH_2O$)* at the CO_2 vapor injection rate, *q* = 200 *m³/day (std)* with a maximum bottom hole pressure constraint of 5000 *kPa* (Reservoir IV: Sandstone, mean permeability, k_0 = 10 *mD*, mean porosity, ϕ = 0.25, salinity = 0.0) (Hydrate saturation, S_H = Concentration *(c_h)*/Volumetric mole density *(ρ)*)**
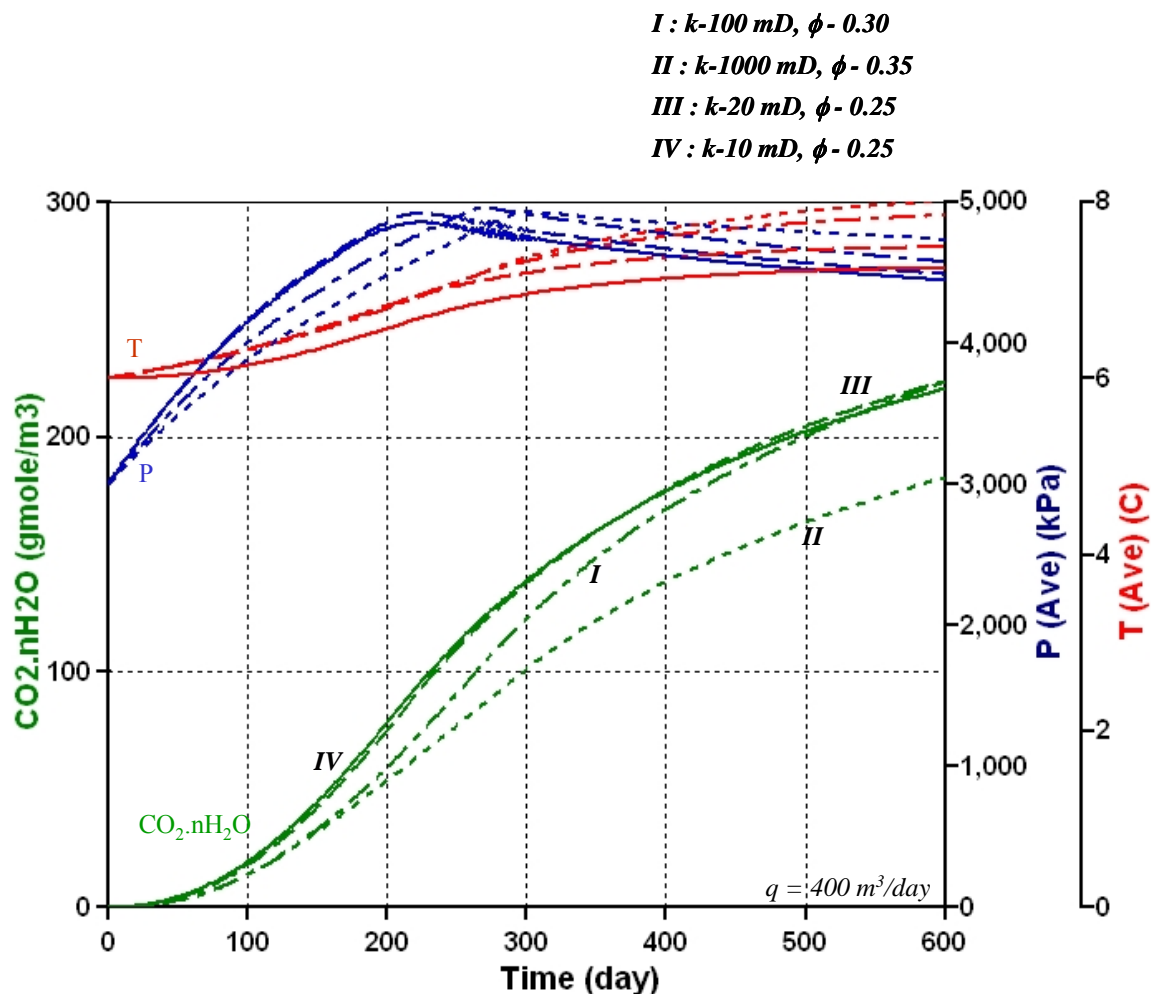
Advanced Numerical Simulation of CO₂ Hydrate Formation
In Geological Reservoirs by Injection of CO₂ Gas   [54]
May, 2006

ALBERTA
RESEARCH
COUNCIL

Figure 24: *Sensitivity of pore water salinity:* **Average CO₂ hydrate concentration *(CO₂.nH₂O)* at background salinity 0.0, and 2 *ppt* for CO₂ vapor injection rate, q = 200 *m³/day (std)* with a maximum bottom hole pressure constraint of 5000 *kPa* (Reservoir IV: Sandstone, mean permeability, k_0 = 10 *mD*, mean porosity, ϕ = 0.25) (Hydrate saturation, S_H = Concentration (c_h)/Volumetric mole density (ρ))**
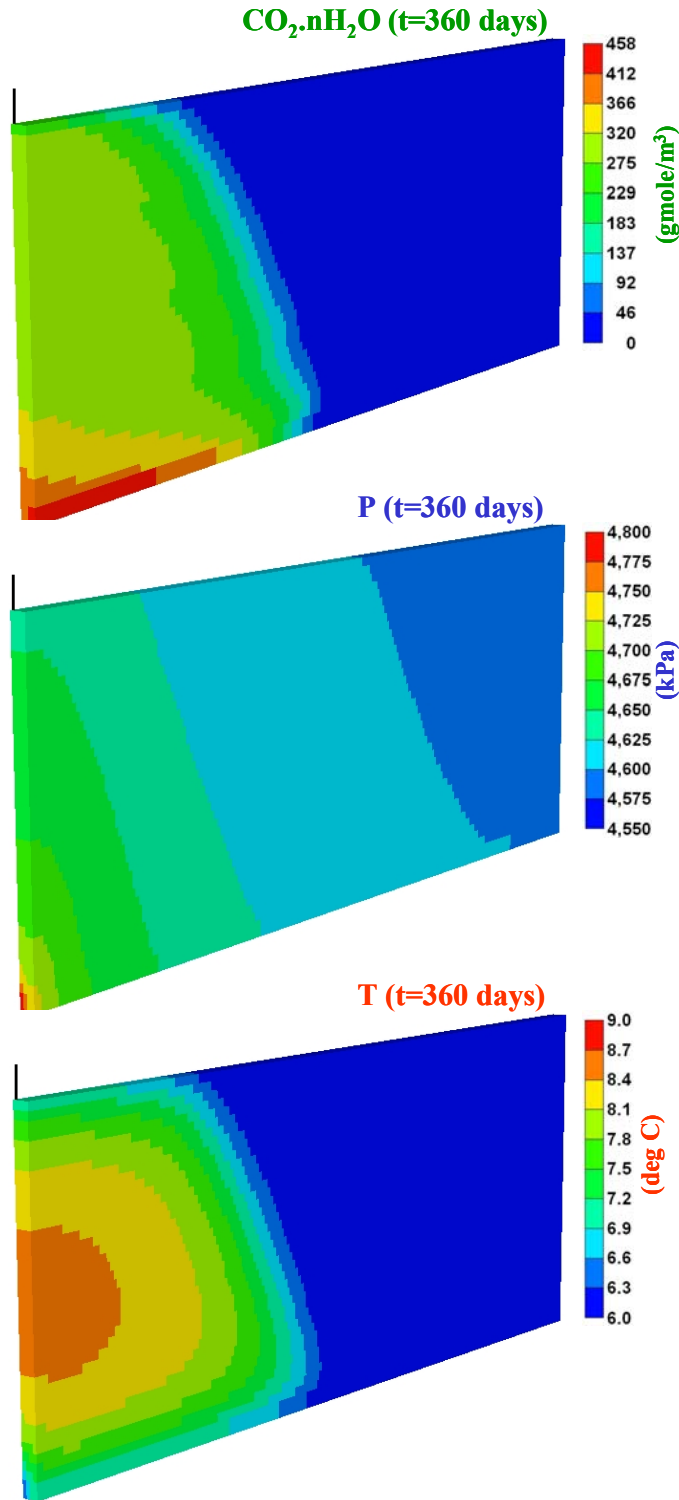
Figure 25: *Spatial variation:* **Average CO₂ hydrate concentration *(CO₂.nH₂O)* and pressure-temperature conditions at the end of time, *t* = 360 *days* for CO₂ vapor injection rates, *q* = 200 *m³/day (std)* (Reservoir IV: Sandstone, mean permeability, *k₀* = 10 mD, mean porosity, φ = 0.25, salinity = 0.0) (Hydrate saturation, *S_H* = Concentration *(c_h)*/Volumetric mole density (ρ))**

Advanced Numerical Simulation of CO₂ Hydrate Formation
In Geological Reservoirs by Injection of CO₂ Gas   [56]
May, 2006

ALBERTA
RESEARCH
COUNCIL

$I : k\text{-}100\ mD, \phi\text{-}0.30$

$II : k\text{-}1000\ mD, \phi\text{-}0.35$

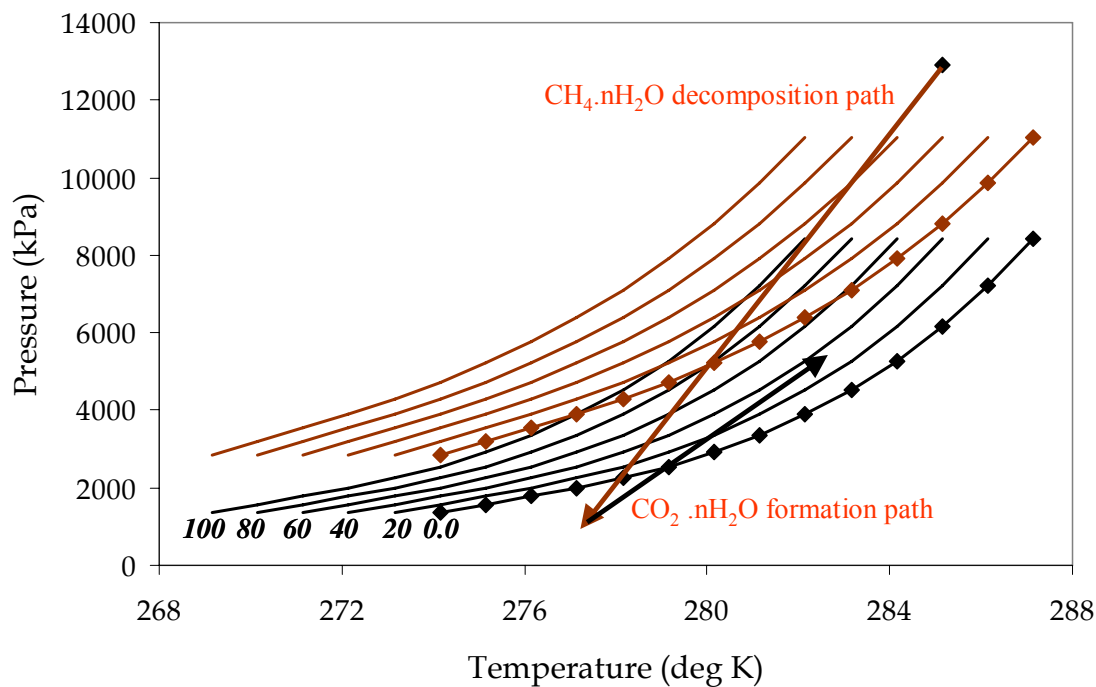$III : k\text{-}20\ mD, \phi\text{-}0.25$

$IV : k\text{-}10\ mD, \phi\text{-}0.25$

Figure 26: *Comparison results:* **Average field pressure (P), temperature (T) and CO_2 hydrate concentration ($CO_2.nH_2O$) at CO_2 vapor injection rate, q = 200 m^3/day (std) with a maximum bottom hole pressure constraint of 5000 kPa (Reservoir I, II, III and IV, salinity = 0.0) (Hydrate saturation, S_H = Concentration (c_h)/Volumetric mole density (ρ))**

Advanced Numerical Simulation of CO_2 Hydrate Formation
In Geological Reservoirs by Injection of CO_2 Gas   [57]
May, 2006

ALBERTA
RESEARCH
COUNCIL

Figure 27: *Comparison results:* **Average field pressure *(P)*, temperature *(T)* and CO₂ hydrate concentration *(CO₂.nH₂O)* at CO₂ vapor injection rate, *q* = 400 *m³/day (std)* with a maximum bottom hole pressure constraint of 5000 *kPa* (Reservoir I, II, III and IV, salinity = 0.0) (Hydrate saturation, S_H = Concentration *(c_h)*/Volumetric mole density *(ρ)*)**

Advanced Numerical Simulation of CO₂ Hydrate Formation
In Geological Reservoirs by Injection of CO₂ Gas   [58]
May, 2006

ALBERTA
RESEARCH
COUNCIL

Figure 28: CH₄- and CO₂ hydrate stability curves *(water-hydrate-gas system)* **and hydrate decomposition - formation paths (CH₄ hydrate decomposition by depressurization, CO₂ hydrate formation by injection of CO₂ gas**

Advanced Numerical Simulation of CO₂ Hydrate Formation
In Geological Reservoirs by Injection of CO₂ Gas   [59]
May, 2006

ALBERTA
RESEARCH
COUNCIL

Mallik Reservoir (5L-38)
CH_4nH_2O Zone (lower)
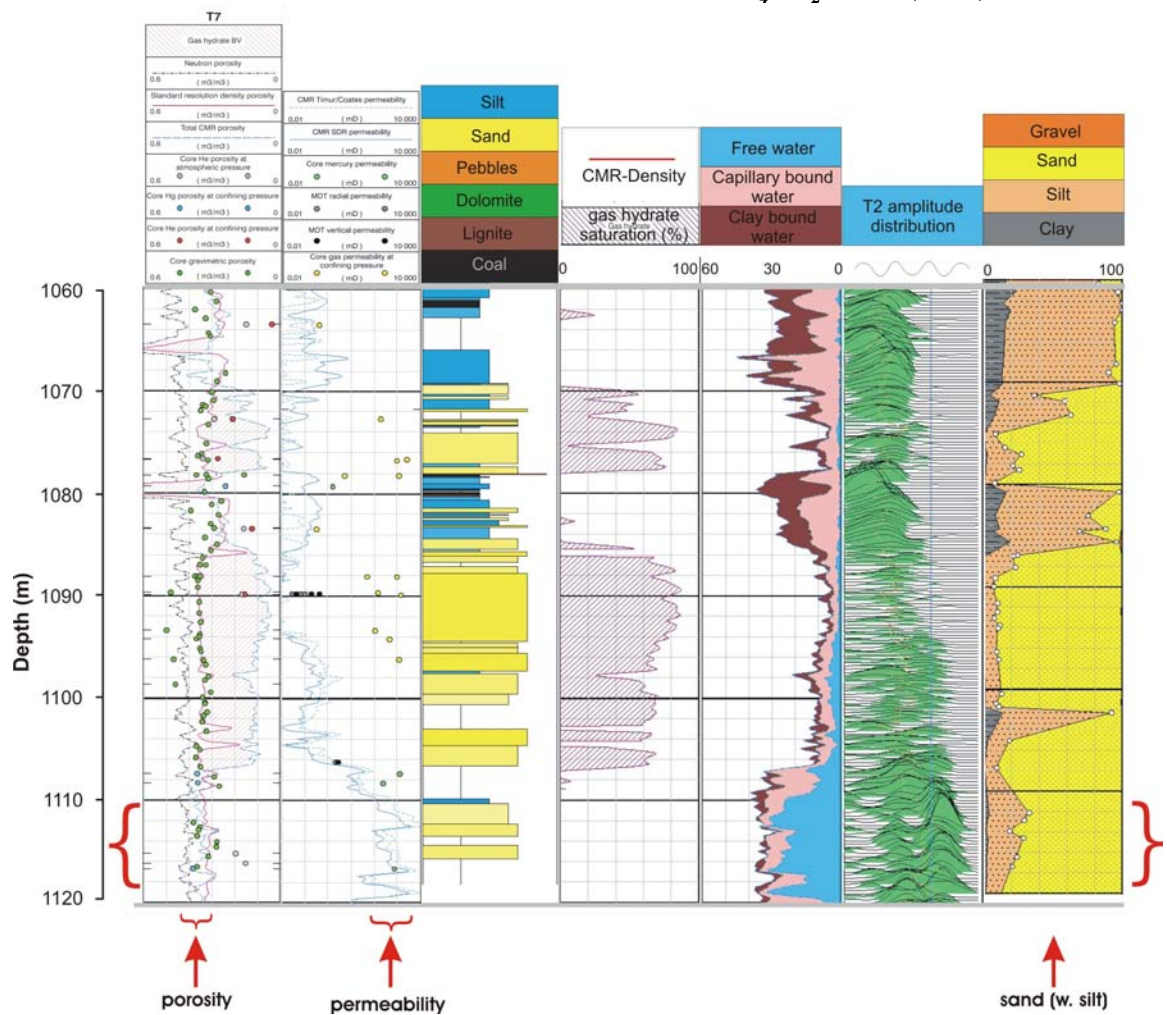
Figure 29: Mallik (5L-38) lower gas hydrate formation showing variation of porosity, permeability and gas hydrate saturation *(JAPEX/JNOC/GSC et al. Mallik gas hydrate production research well, Dallimore et al., 2005a,b)*

ALBERTA
RESEARCH
COUNCIL
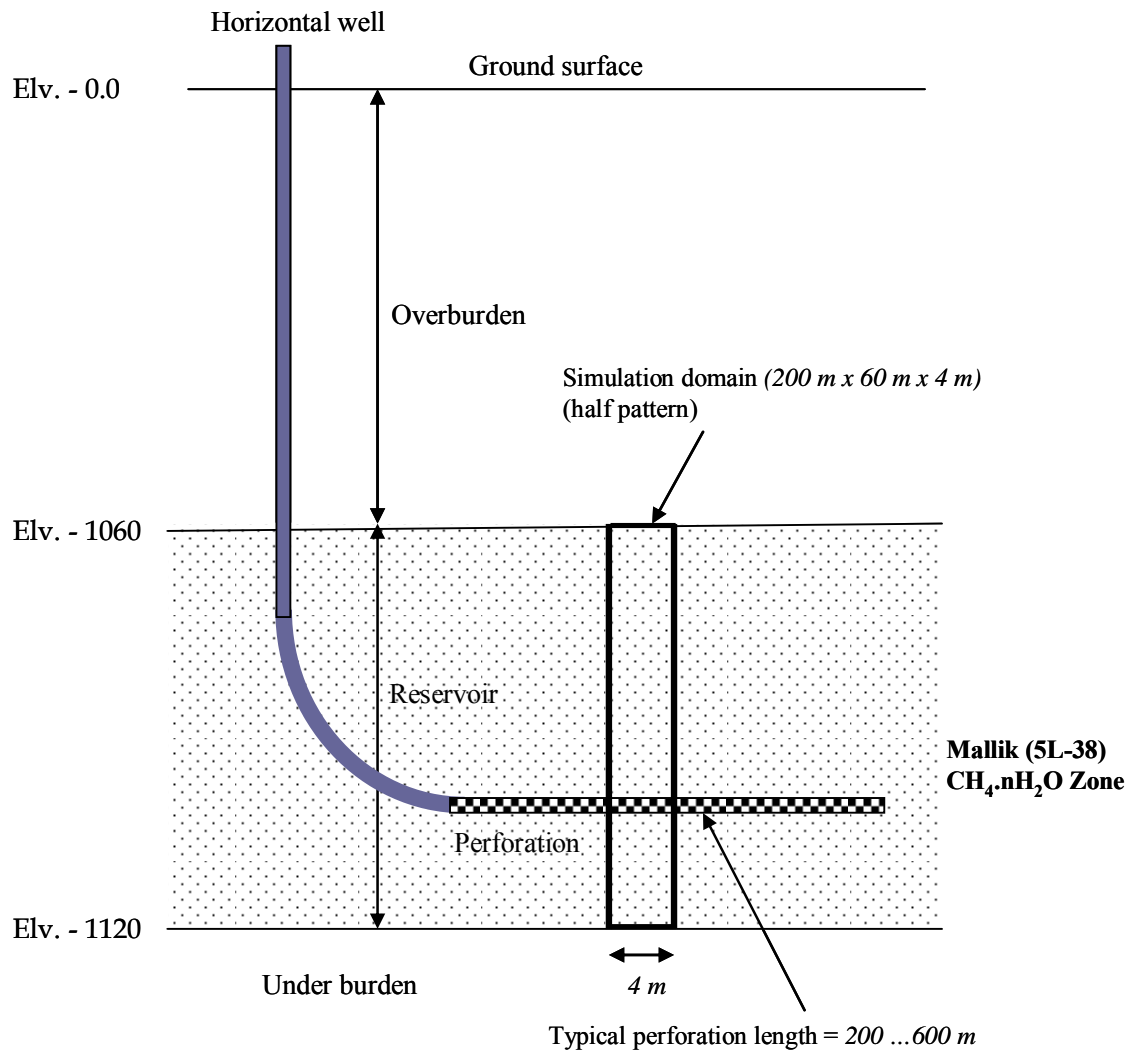
Field condition:
Suppose well perforation length $= 400\ m$
CO_2 injection rate, $q = 40{,}000\ m^3/day$

Simulation condition (4m wide half pattern):
Well perforation length $= 4\ m$
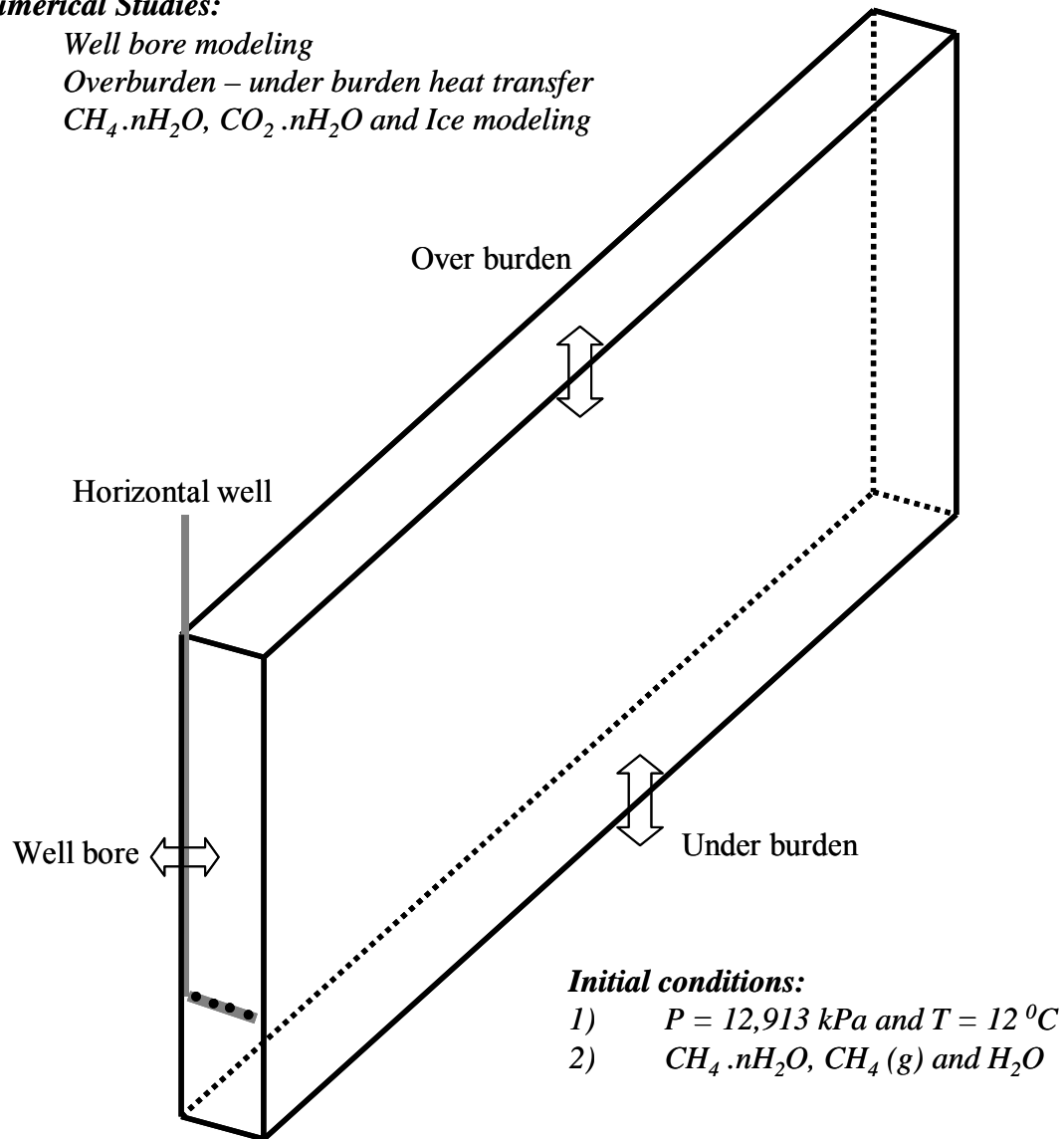CO_2 injection rate, $q = 0.5*(40{,}000*4/400) = 200\ m^3/day$

Figure 30: Setup numerical flow system *(200 m x 60 m x 4 m)* – CH₄ hydrate decomposition with pressure drawdown and CO₂ hydrate formation by injecting CO₂ gas

Numerical Setup:
1)   *Half pattern – 200 m x 60 m x 4 m*
2)   *Grid blocks – 200 x 60 x 4*

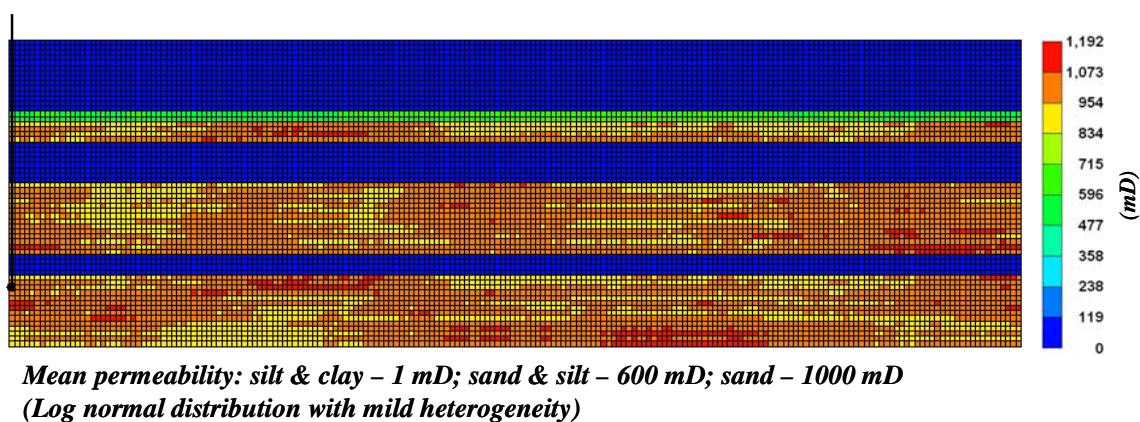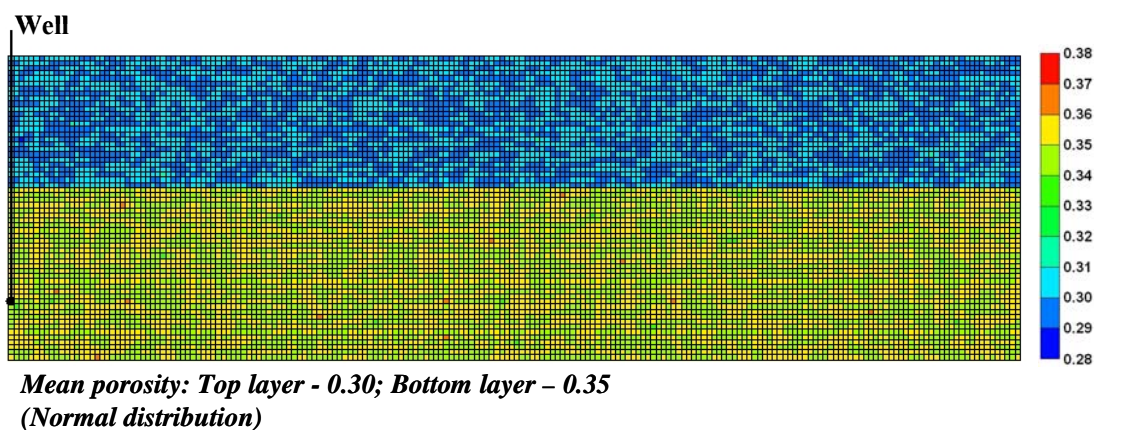*Numerical Studies:*
1)   *Well bore modeling*
2)   *Overburden – under burden heat transfer*
3) $CH_4 .nH_2O$, $CO_2 .nH_2O$ and Ice modeling

Over burden

Horizontal well

Well bore

Under burden

Initial conditions:
1)   *P = 12,913 kPa and T = 12 ^0C*
2)   *$CH_4 .nH_2O$, $CH_4 (g)$ and H_2O*

Figure 31: Half pattern *(200 m x 60 m x 4 m)* numerical flow system – Initial and boundary conditions

Advanced Numerical Simulation of CO₂ Hydrate Formation
In Geological Reservoirs by Injection of CO₂ Gas   [62]
May, 2006

ALBERTA
RESEARCH
COUNCIL

Mallik Reservoir (5L - 38)
Half pattern – 200 m x 60 m x 4 m

Well

Mean porosity: Top layer - 0.30; Bottom layer – 0.35
(Normal distribution)

Mean permeability: silt & clay – 1 mD; sand & silt – 600 mD; sand – 1000 mD
(Log normal distribution with mild heterogeneity)

Figure 32: **Porosity and permeability distributions in the numerical grid cells for the Mallik *(5L-38)* lower hydrate bearing formation**
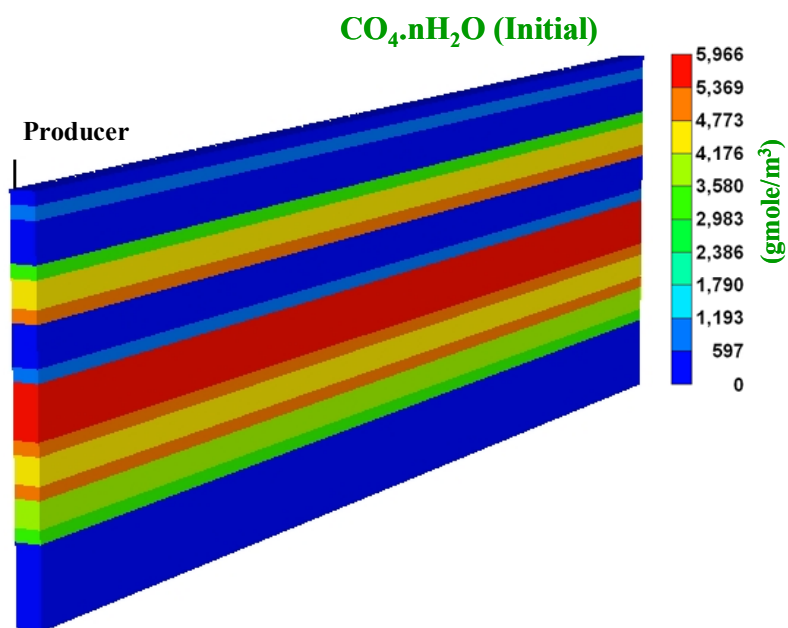
$CO_4.nH_2O$ (Initial)

Producer

(gmole/m^3)

5,966
5,369
4,773
4,176
3,580
2,983
2,386
1,790
1,193
597
0

Figure 33: Initial CH$_4$ hydrate concentration (Numerical representation for Mallik (5L-38) well log data in *Figure 29*)
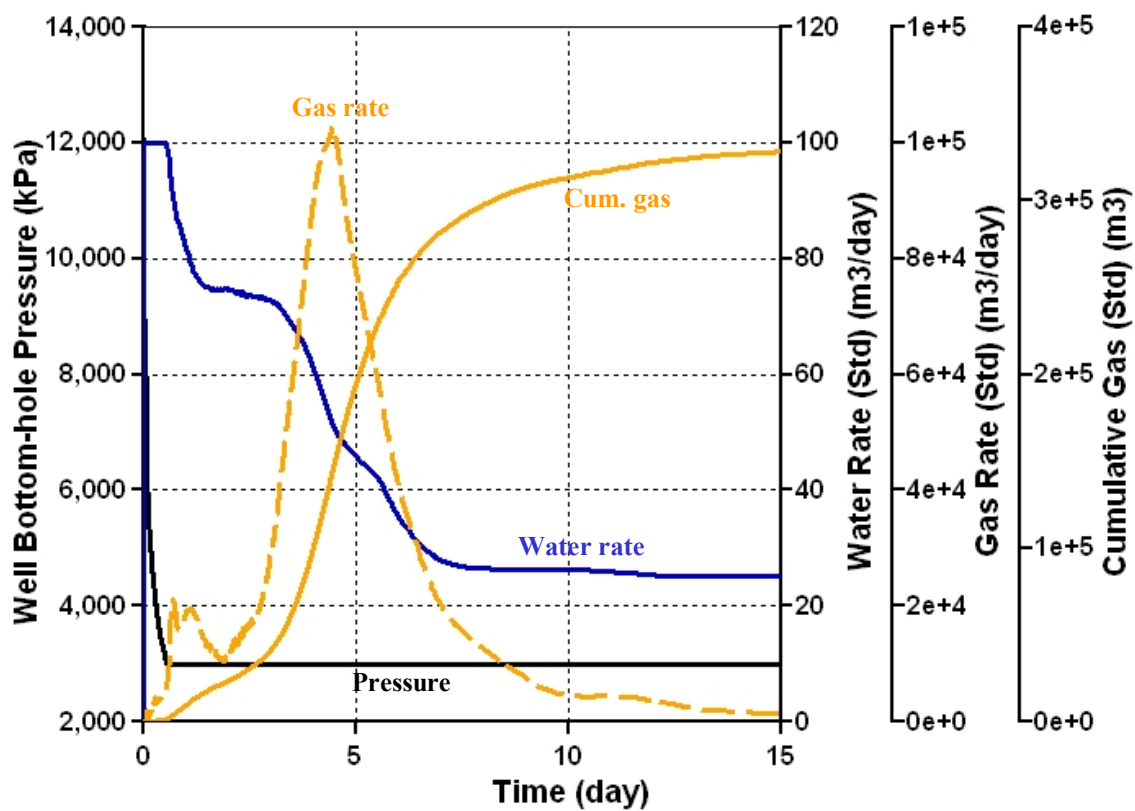
Advanced Numerical Simulation of CO$_2$ Hydrate Formation
In Geological Reservoirs by Injection of CO$_2$ Gas   [64]
May, 2006

ALBERTA
RESEARCH
COUNCIL

Figure 34: **Simulated production and pressure data,** *(i)* **gas** *(cumulative and rate)*, *(ii)* **water** *(rate)*, *(iii)* **well bottom hole pressures (Numerical domain** *(200 m x 4 m x 60 m)* **with horizontal well) (Mallik** *5L-38* **lower hydrate bearing formation)**
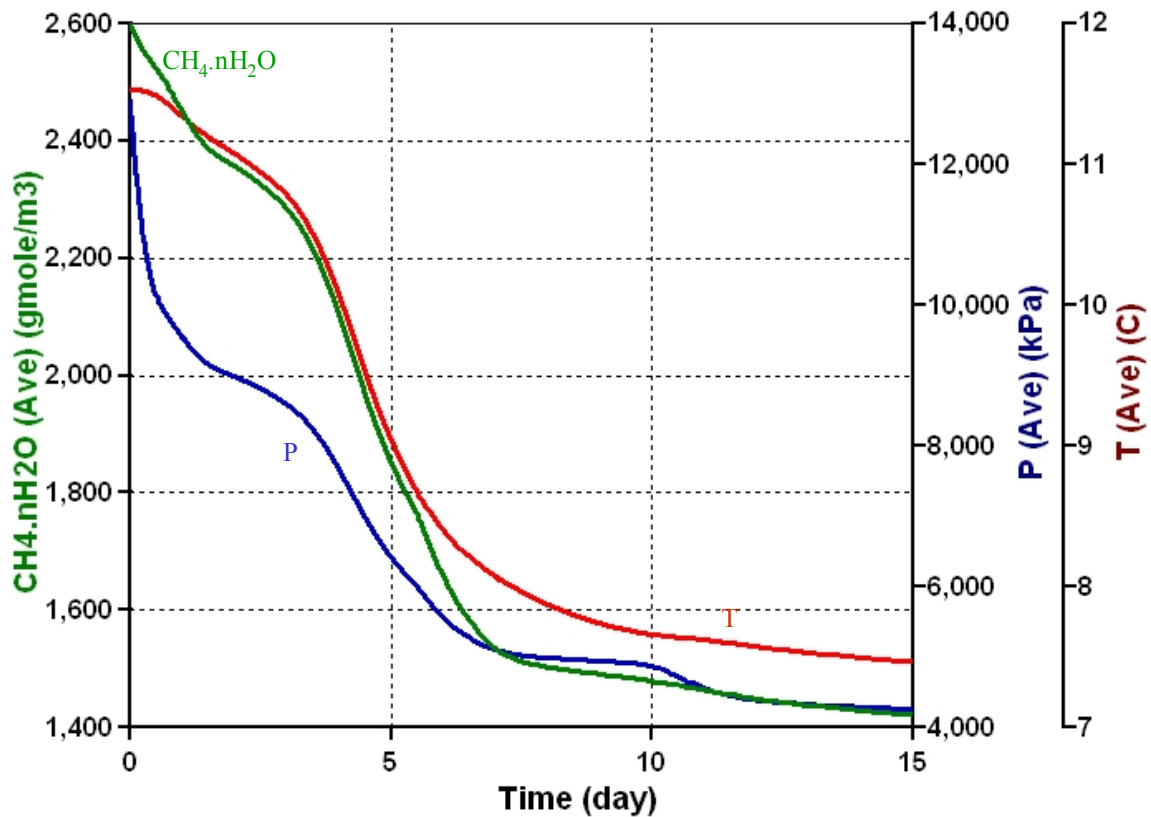
Advanced Numerical Simulation of CO₂ Hydrate Formation
In Geological Reservoirs by Injection of CO₂ Gas   [65]
May, 2006

ALBERTA
RESEARCH
COUNCIL

Figure 35: Average field pressure *(P)*, temperature *(T)* and CH₄ hydrate concentration *(CH₄.nH₂O)* (Hydrate saturation, S_H = Concentration (c_h)/Volumetric mole density (ρ)) (Numerical domain *(200 m x 4 m x 60 m)* with horizontal well) (Mallik *5L-38* lower hydrate bearing formation)

Advanced Numerical Simulation of CO₂ Hydrate Formation
In Geological Reservoirs by Injection of CO₂ Gas   [66]
May, 2006

ALBERTA
RESEARCH
COUNCIL
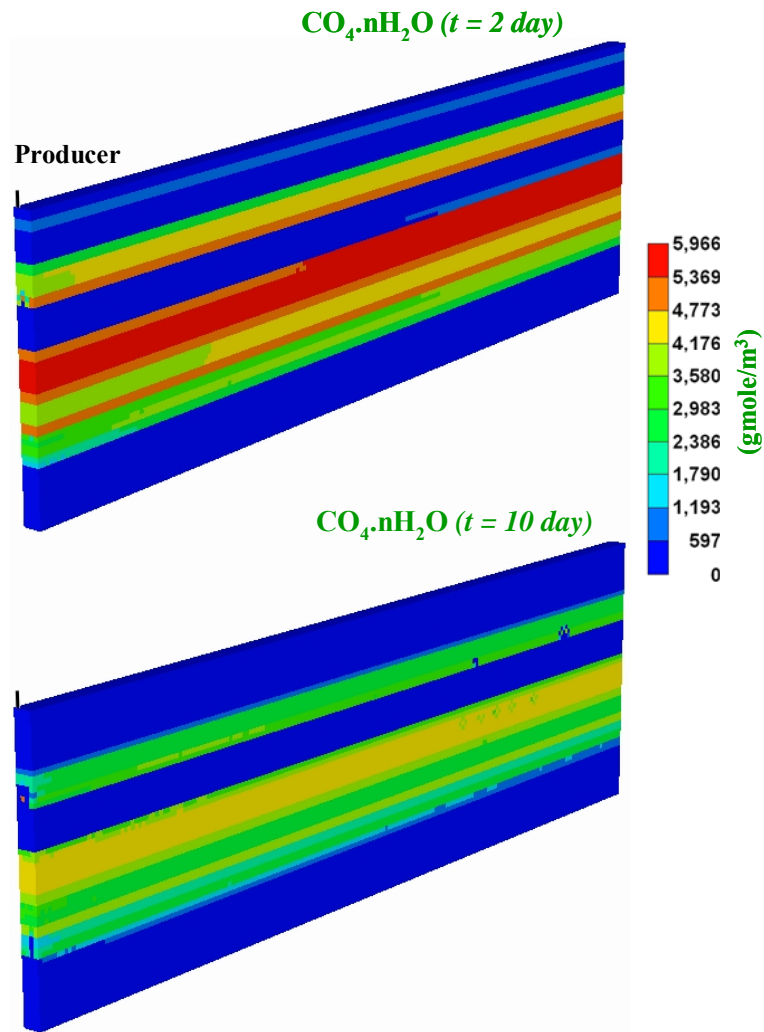
Figure 36: The average CH₄ hydrate *(CH₄.nH₂O)* concentrations at the end of *2 days* and *10 days* simulation times (Hydrate saturation, S_H = Concentration (c_h)/Volumetric mole density (ρ)) (Numerical domain *(200 m x 4 m x 60 m)* with horizontal well) (Mallik *5L-38* lower hydrate bearing formation)
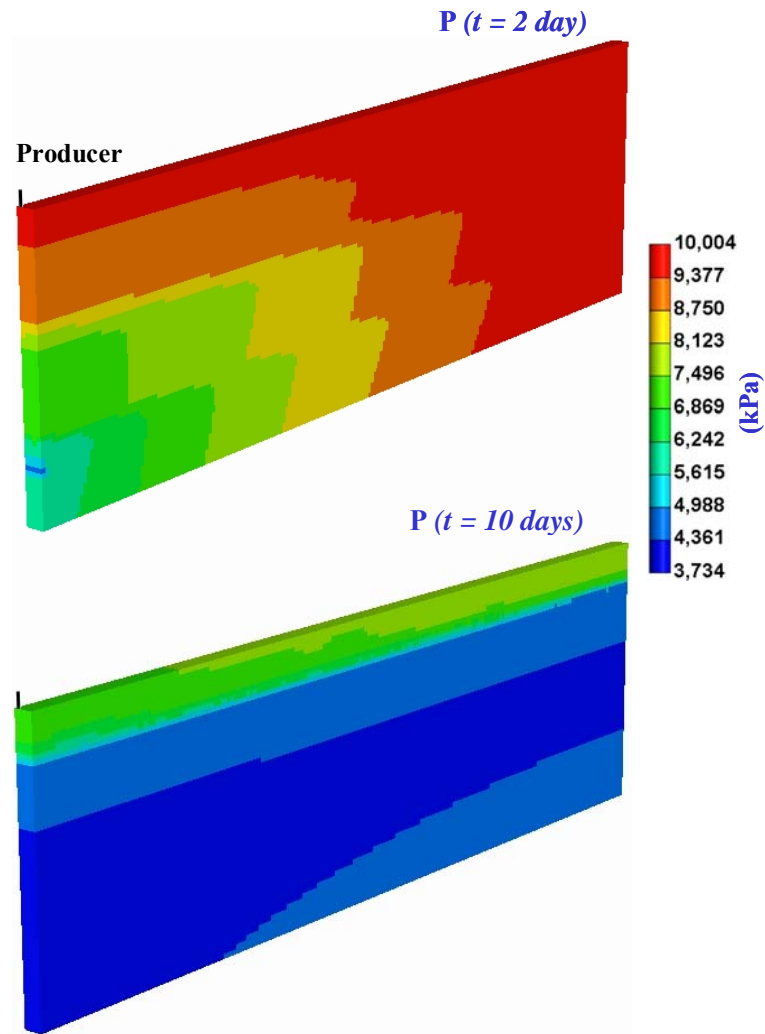
Figure 37: Average field pressures at the end of *2 days* and *10 days* simulation times (Numerical domain *(200 m x 4 m x 60 m)* with horizontal well) (Mallik *5L-38* lower hydrate bearing formation)
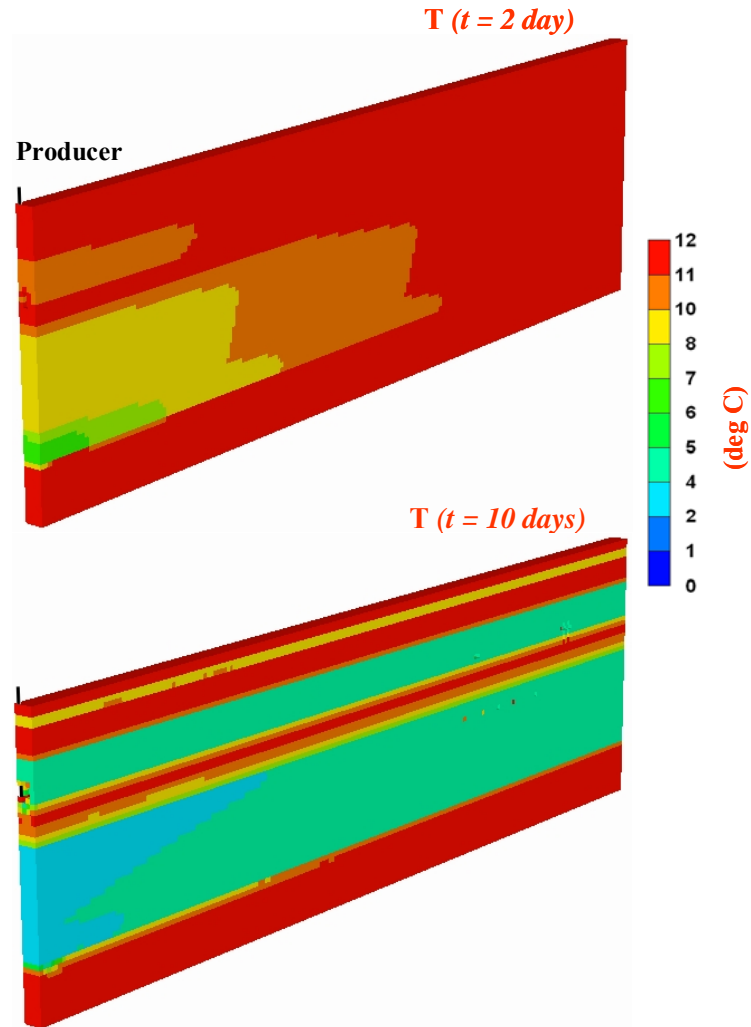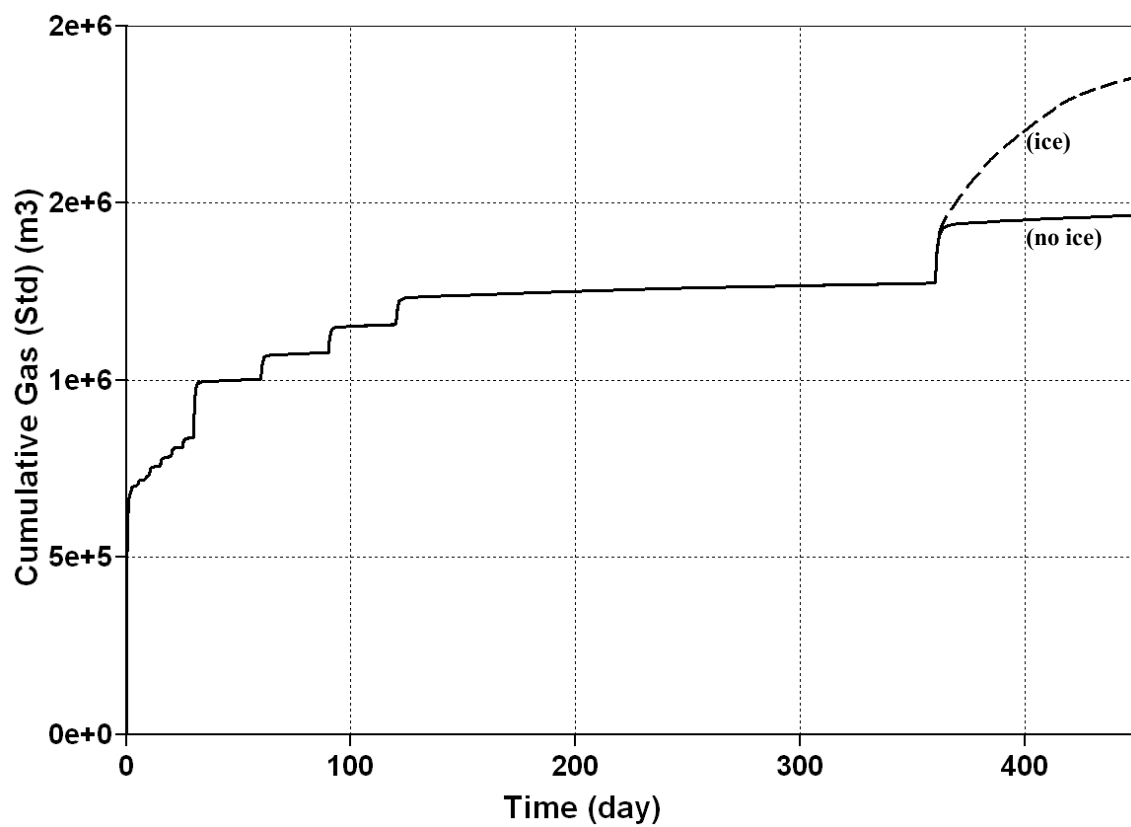
Figure 38: Average field temperatures at the end of *2 days* and *10 days* simulation times (Numerical domain *(200 m x 4 m x 60 m)* with horizontal well) (Mallik *5L-38* lower hydrate bearing formation)
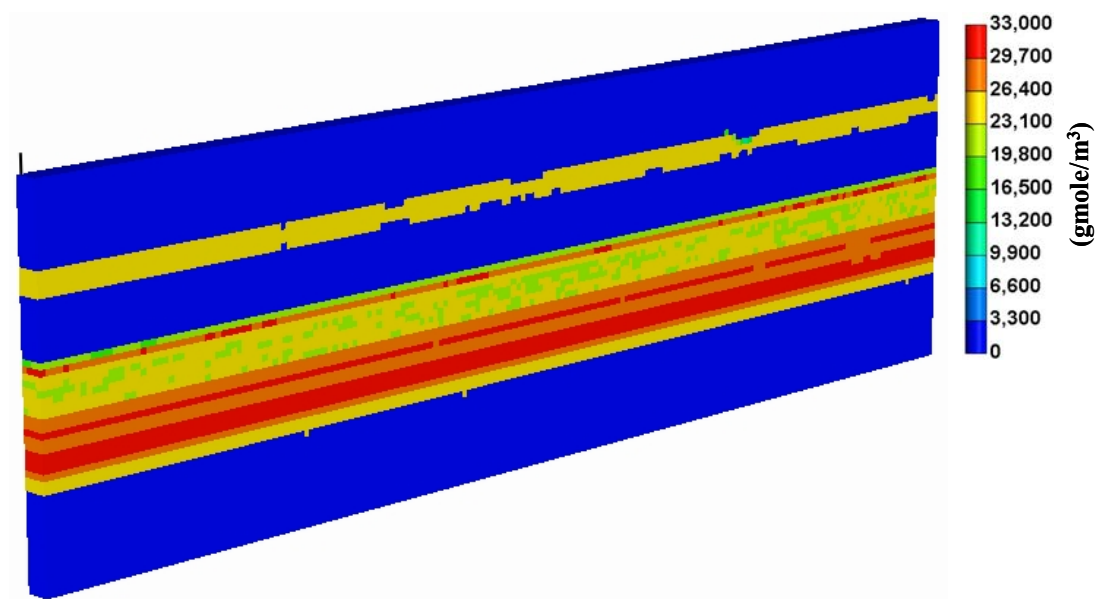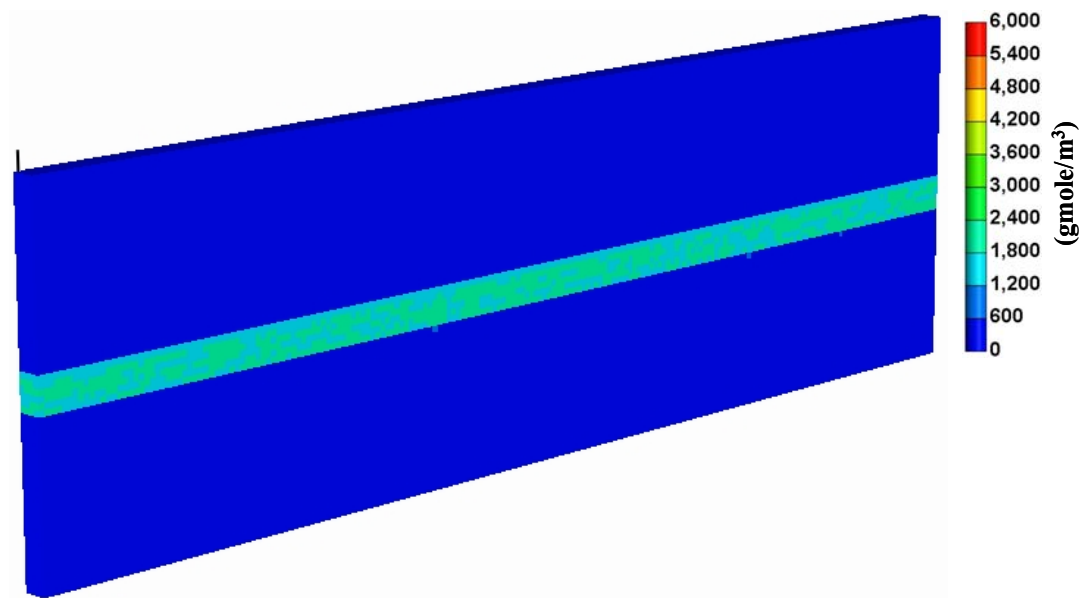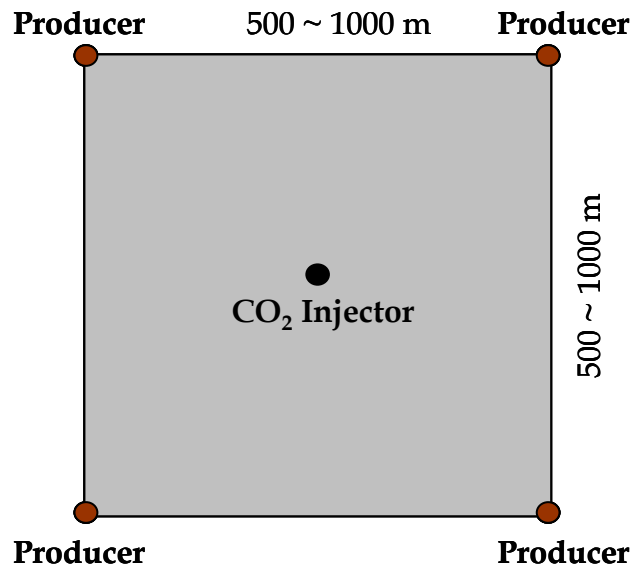
Figure 39: History Plots for Methane-Hydrate Decomposition with Ice Formation (Mallik Model)
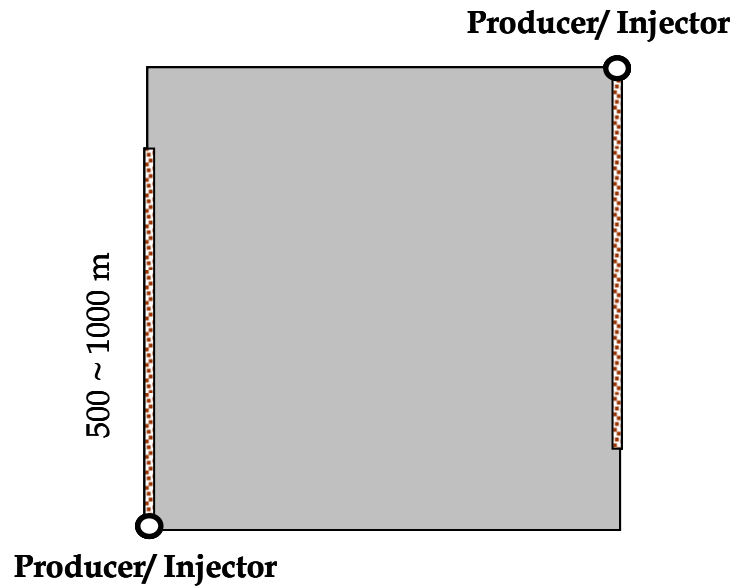
Figure 40: Ice Distribution at 500 days (Mallik Model)

Figure 41: Methane-Hydrate Distribution at 500 days (Mallik Model)

I. Vertical well system
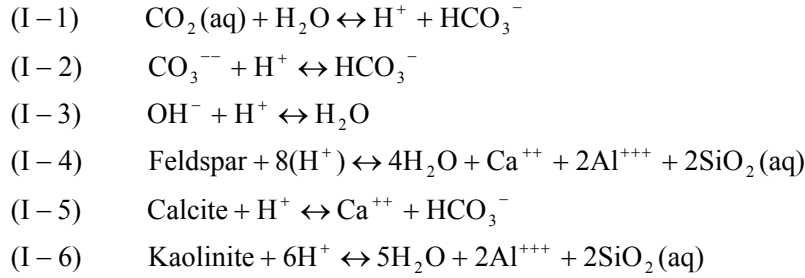
II. Horizontal well system

Figure 42: Mallik field simulation strategies for CH_4 hydrate decomposition and CO_2 hydrate formation (Strategy I: vertical well system, Strategy II: horizontal well system)

The most common hydro-geochemical reactions in hydrate bearing formation can be identified as:

(I – 1) $CO_2(aq) + H_2O \leftrightarrow H^+ + HCO_3^-$

(I – 2) $CO_3^{--} + H^+ \leftrightarrow HCO_3^-$

(I – 3) $OH^- + H^+ \leftrightarrow H_2O$

(I – 4) $Feldspar + 8(H^+) \leftrightarrow 4H_2O + Ca^{++} + 2Al^{+++} + 2SiO_2(aq)$

(I – 5) $Calcite + H^+ \leftrightarrow Ca^{++} + HCO_3^-$

(I – 6) $Kaolinite + 6H^+ \leftrightarrow 5H_2O + 2Al^{+++} + 2SiO_2(aq)$

where, Feldspar, Calcite and Kaolinite are the minerals and all other species are dissolved in the aqueous phase.

The chemical equilibrium reaction can be governed by the following equation:

(I – 7) $K_{eq} = \prod_{i=1}^{n} a_k^{v_i}$

The mineral dissociation and precipitation reaction rate can be calculated from Transition State Theory (TST). The reaction rate is:
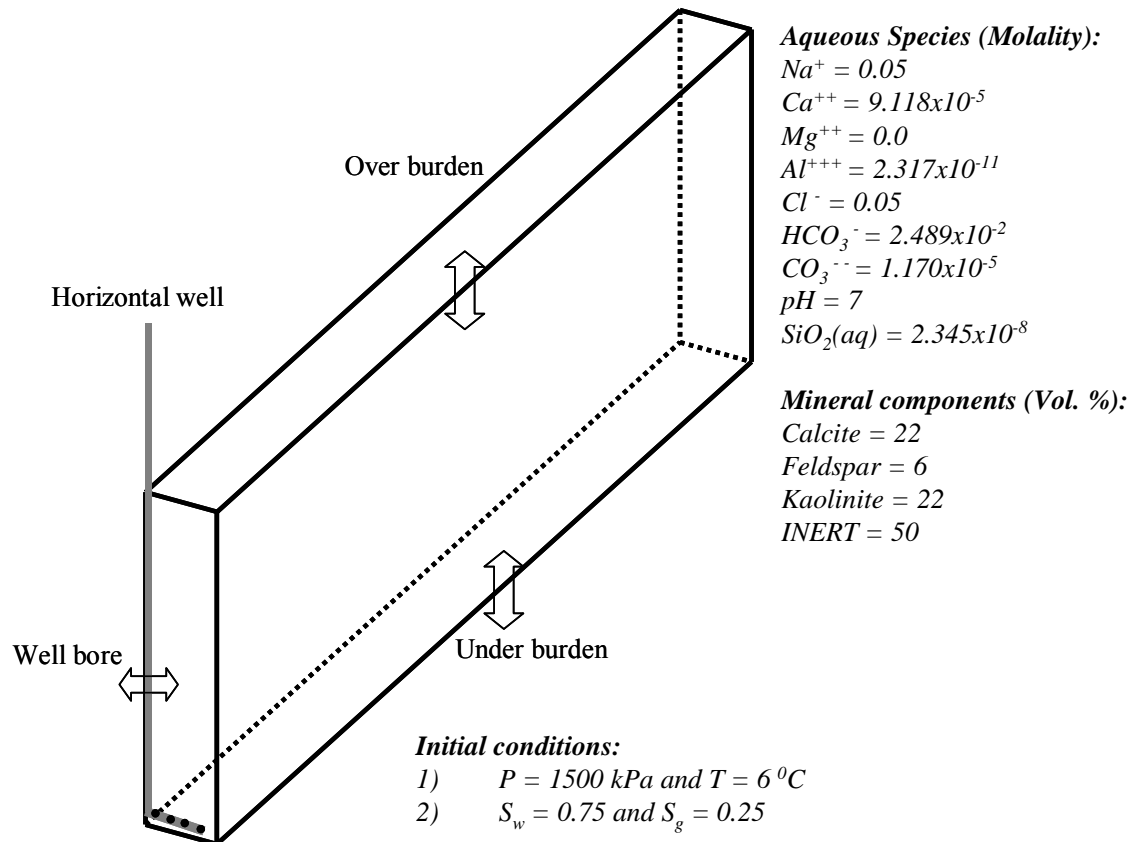
(I – 8) $K_{eq} = \prod_{i=1}^{n} a_k^{v_i}$

Advanced Numerical Simulation of CO₂ Hydrate Formation
In Geological Reservoirs by Injection of CO₂ Gas   [74]
May, 2006

ALBERTA
RESEARCH
COUNCIL

Numerical Setup:
1)   *Half pattern – 200 m x 20 m x 4 m*
2)   *Grid blocks – 200 x 40 x 4*

Numerical Studies:
1)   *Geochemical modeling*
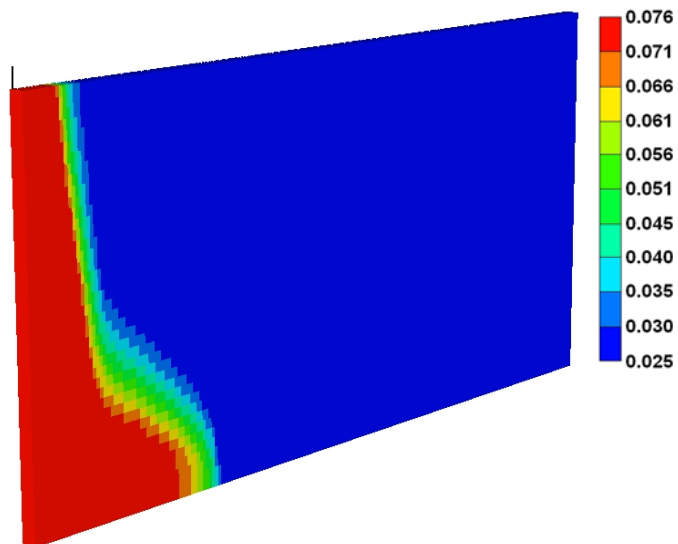

Over burden

Horizontal well

Well bore

Under burden

Aqueous Species (Molality):
$Na^+ = 0.05$
$Ca^{++} = 9.118x10^{-5}$
$Mg^{++} = 0.0$
$Al^{+++} = 2.317x10^{-11}$
$Cl^- = 0.05$
$HCO_3^- = 2.489x10^{-2}$
$CO_3^{--} = 1.170x10^{-5}$
$pH = 7$
$SiO_2(aq) = 2.345x10^{-8}$

Mineral components (Vol. %):
Calcite = 22
Feldspar = 6
Kaolinite = 22
INERT = 50

Initial conditions:
1) $P = 1500\ kPa\ and\ T = 6\ ^0C$
2) $S_w = 0.75\ and\ S_g = 0.25$

Figure A-I-1:   Half pattern *(200 m x 20 m x 4 m)* numerical flow system – Initial and boundary conditions

Advanced Numerical Simulation of CO₂ Hydrate Formation
In Geological Reservoirs by Injection of CO₂ Gas   [75]
May, 2006

ALBERTA
RESEARCH
COUNCIL
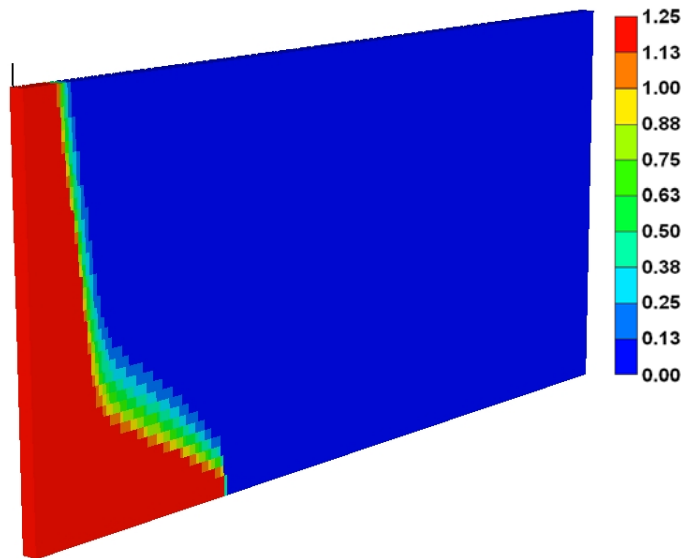
(a) CO₂ molality

(b) HCO₃ molality

Figure A-I-2: *CO₂* and *HCO₃* ⁻ molality at the end of 6 years

Advanced Numerical Simulation of CO₂ Hydrate Formation
In Geological Reservoirs by Injection of CO₂ Gas   [76]
May, 2006

ALBERTA
RESEARCH
COUNCIL
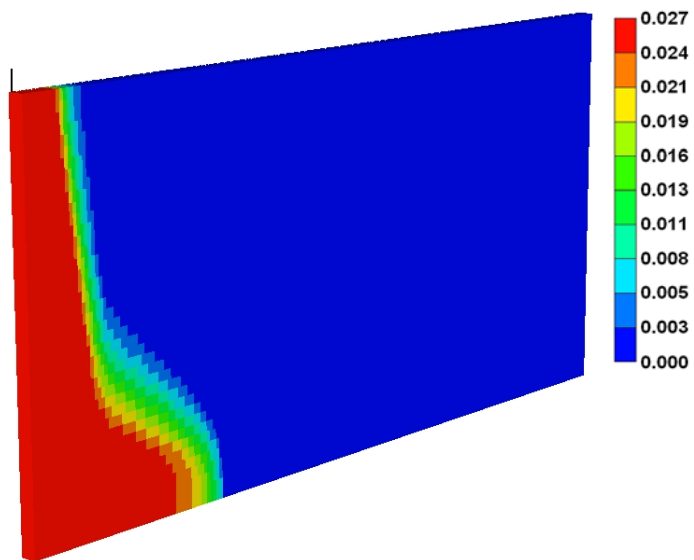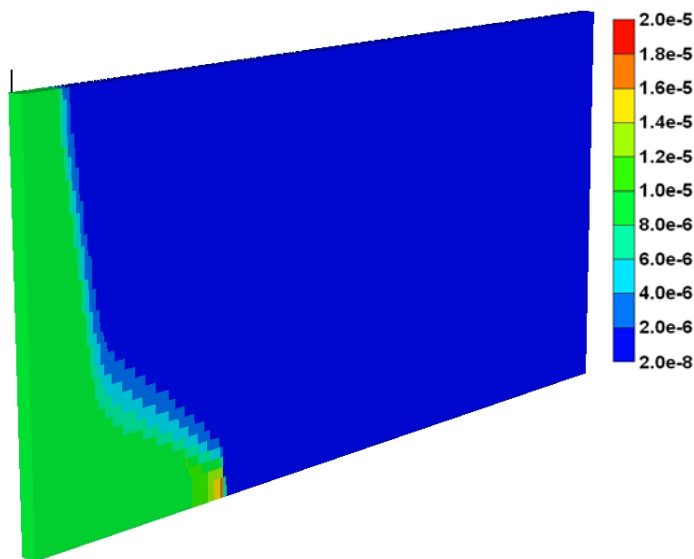
(a) Ca⁺⁺ molality

(b) pH

Figure A-I-3: *Ca⁺⁺* molality and *pH* condition at the end of 6 years

In this geo-mechanical model, tangential modulus as well as bulk modulus varies with minimum principle effective stress σ_3' and temperature. Poisson's ratio in this model is, thus, also varied. The model has a loading path and an unloading-reloading path which are distinguished by the reference shear stress criteria. In this model, the Mohr-Coulomb failure criterion is used for the material failure due to shear stress to compute the stress level. The stress level is also limited by one so that the shear stress can not exceed the shear failure of the Mohr-Coulomb model. More details on this model can be seen in related references.
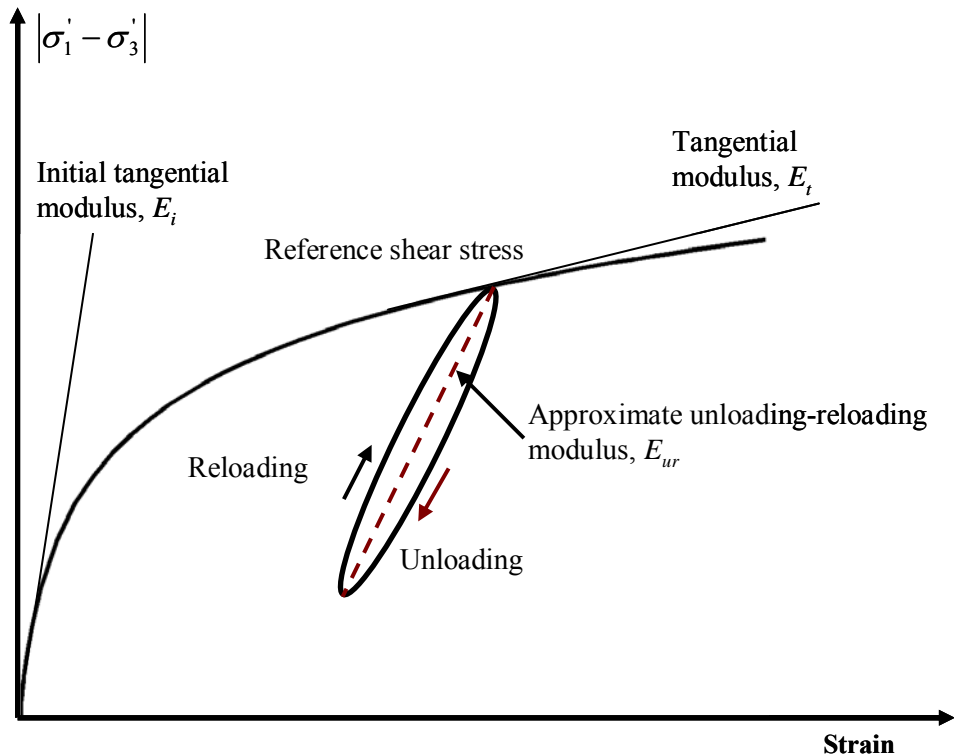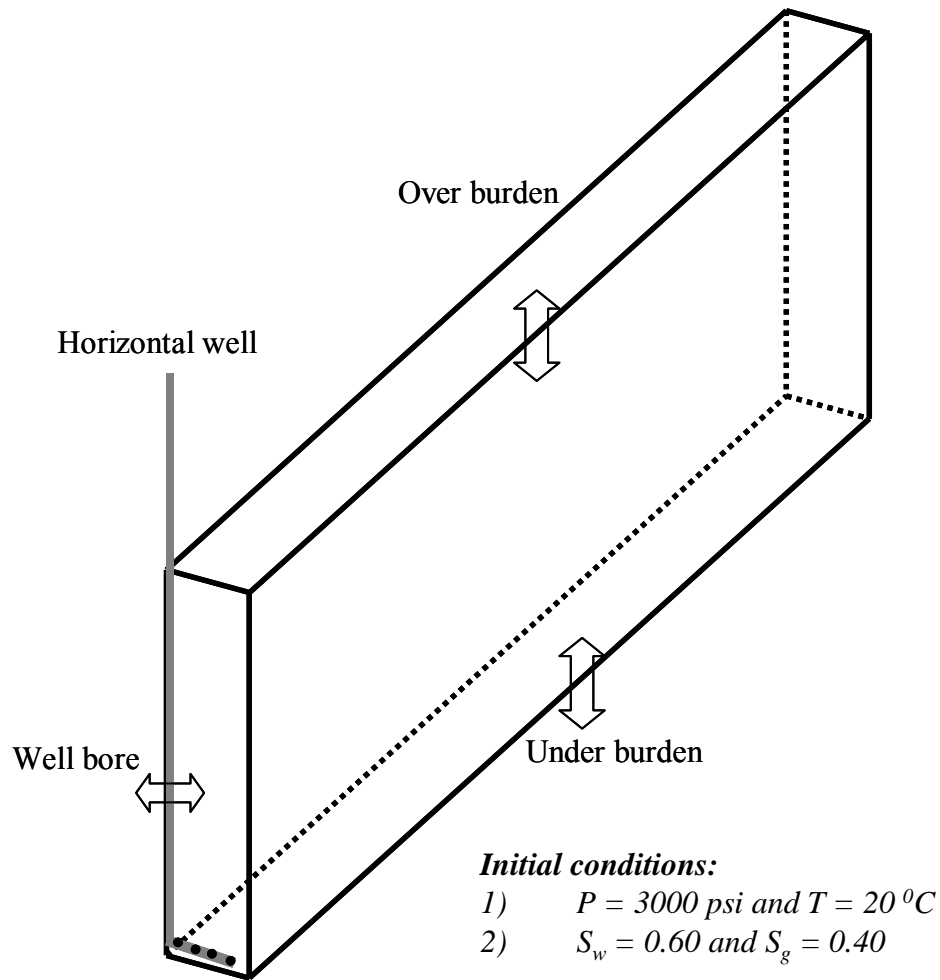

Figure A-II-1: Stress – strain diagram (Mathematical representations for the modulus (E_i, E_t **and** E_{ur}) **can be found in** *CMG STARS* **manual)**

Numerical Studies:
1)   Geo-mechanical

Over burden

Horizontal well

Well bore

Under burden

Initial conditions:
1)   P = 3000 psi and T = 20 ^0C
2) S_w = 0.60 and S_g = 0.40

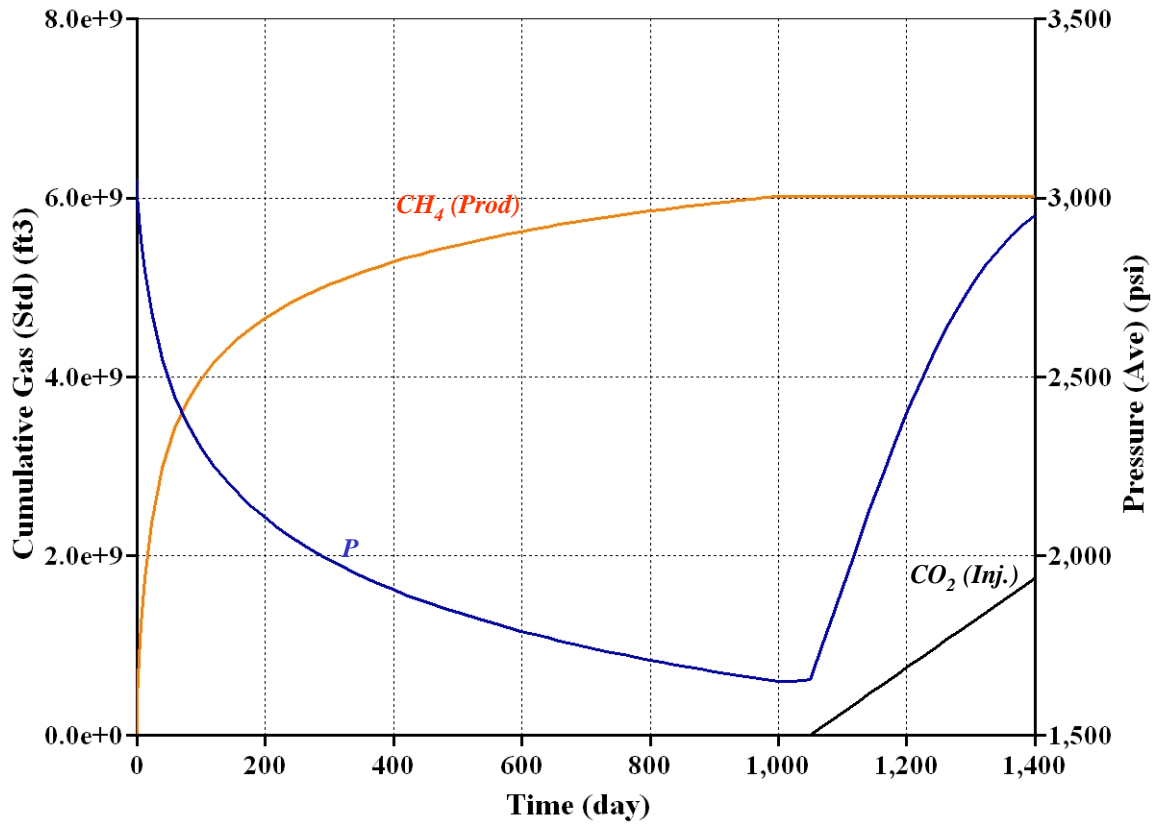**Figure A-II-2: Half pattern numerical flow system – Initial and boundary conditions**

Figure A-II-3: Pressure response with CH₄ gas production and CO₂ injection

Advanced Numerical Simulation of CO₂ Hydrate Formation
In Geological Reservoirs by Injection of CO₂ Gas
[80]
May, 2006

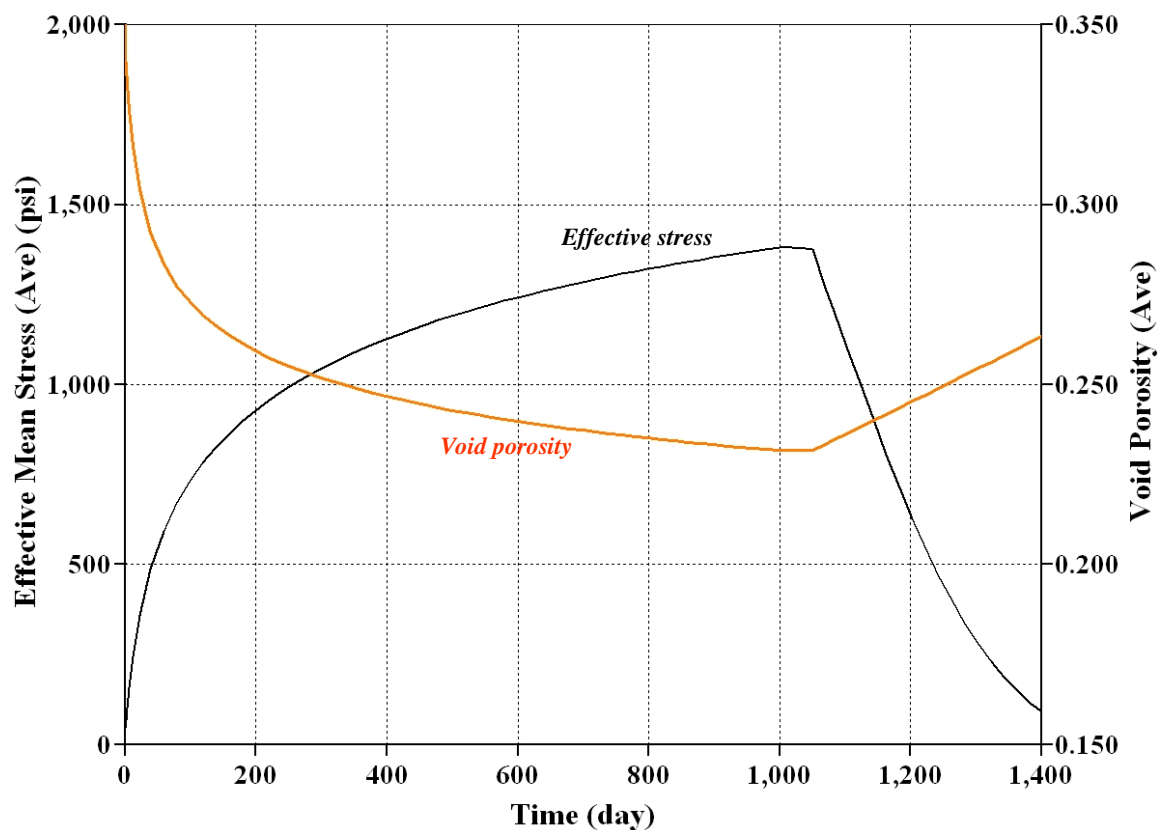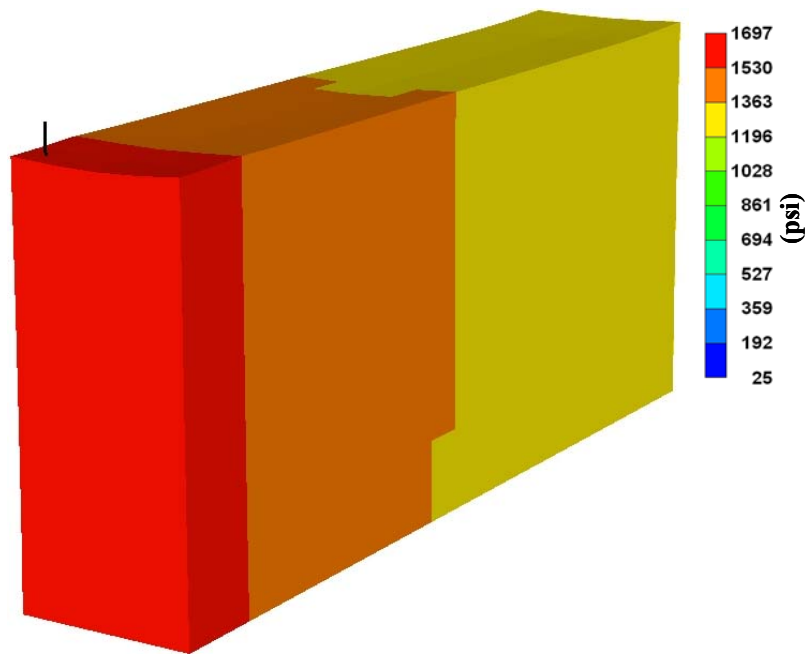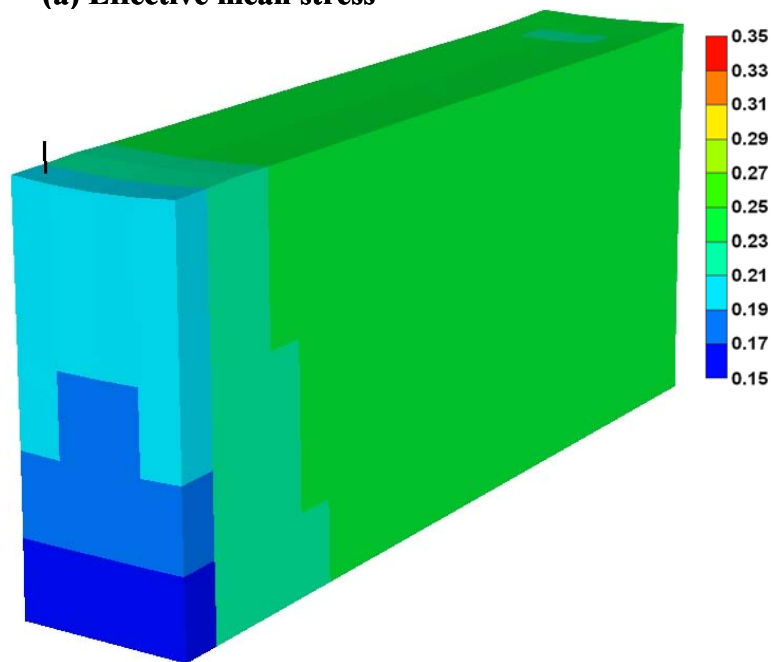ALBERTA
RESEARCH
COUNCIL

Figure A-II-4: Effective stress and void porosity during production – injection cycle

(a) Effective mean stress

(b) Effective void porosity

Figure A-II-5: **Effective stresses effective void porosity t the end of production cycle (***t = 1000 days***)**